10-5-2017

Lightweight Metal/Polymer/Metal Sandwich Composites for Automotive Applications

Federico Ferrari
University of Windsor

Lightweight Metal/Polymer/Metal Sandwich Composites

for Automotive Applications

By

Federico Ferrari

A Thesis

Submitted to the Faculty of Graduate Studies
through the Department of **Mechanical, Automotive and Materials Engineering**
in Partial Fulfillment of the Requirements for
the Degree of **Master of Applied Science**
at the University of Windsor

Windsor, Ontario, Canada

2017

Lightweight Metal/Polymer/Metal Sandwich Composites

for Automotive Applications

by

Federico Ferrari

APPROVED BY:

_____

R. Riahi
Department of Mechanical, Automotive & Materials Engineering

_____

J. Johrendt
Department of Mechanical, Automotive & Materials Engineering

_____

A. Edrisy, Advisor
Department of Mechanical, Automotive & Materials Engineering

08/29/2017

DECLARATION OF ORIGINALITY

I hereby certify that I am the sole author of this thesis and that no part of this thesis has been published or submitted for publication.

I certify that, to the best of my knowledge, my thesis does not infringe upon anyone's copyright nor violate any proprietary rights and that any ideas, techniques, quotations, or any other material from the work of other people included in my thesis, published or otherwise, are fully acknowledged in accordance with the standard referencing practices. Furthermore, to the extent that I have included copyrighted material that surpasses the bounds of fair dealing within the meaning of the Canada Copyright Act, I certify that I have obtained a written permission from the copyright owner(s) to include such material(s) in my thesis and have them available upon request.

I declare that this is a true copy of my thesis, including any final revisions, as approved by my thesis committee and the Graduate Studies office, and that this thesis has not been submitted for a higher degree to any other University or Institution.

ABSTRACT

Sandwich composites are becoming increasingly popular in the automotive sector as they are lightweight and facilitate noise attenuation. However, given that sandwich composites are relatively new in the sector, there are questions as to whether they can effectively replace monolithic metals and damping patches without compromising mechanical performance. Quiet Aluminum®, a sandwich composite produced by Material Sciences Corporation (MSC), employs as skins two aluminum alloys that are common in automotive manufacturing: 5754-O and 6061-T4. The current study examines and compares the mechanical properties of Quiet Aluminum® with the main Fiat Chrysler Automobiles (FCA) requirements for laminates with non-structural loads. The adhesion mechanism between the layers of the sandwich composites received was examined through: T-Peel test, roughness measurements and metallographic cross sectioning technique. The current study then employed tensile tests with different treatments applied to the sandwich materials, a Self-Piercing Riveting (SPR) joining evaluation, and hardness tests on the core section of the aluminum skins. The samples, which presented rolling mill-finish surface roughness R_a range of $0.46 - 0.56\ \mu m$, met the FCA adhesion requirements with adhesive failure mode even after the paint bake-cycle simulation ($20\ min$ at 185℃) and the hardening treatment applied on the sandwich with AA6061-T4 skin ($1h$ at 200℃). The tensile properties, computed simulating stamping process (2% pre-applied strain), the paint-bake cycle and the hardening treatment were comparable to the monolithic ones. Finally, SPR technique, evaluated through lap shear test and macro-graphic measurements, successfully joined Quiet Aluminum® samples ($1.06\ mm$ thickness) with structural High Strength Low Alloy steel ($HSLA$, $1.8\ mm$ thickness and $340\ MPa$ minimum yield strength).

DEDICATION

A Voi, che siete sempre al mio fianco, che sempre mi lasciate libero di scegliere, sbagliare e vivere pienamente. Non potrei chiedere di meglio. Grazie, Allegra Famiglia Ferrari

ACKNOWLEDGEMENTS

This thesis has been developed with the collaboration of two universities, Politecnico di Torino and University of Windsor, as well as FCA, one of the biggest automotive manufacturers in the world. I want to express my deepest gratitude to this project and whoever is involved, in particular: Prof. Belingardi from Politecnico, Prof. Johrendt from the University of Windsor, Edoardo Rabino from FCA Italy and Mohammed Malik from FCA Canada. I further want to thank Material Sciences Corporation (MSC) and Stanley Engineered Fastening for their disposability and professionalism, during the project development.

My deepest appreciation goes to my academic advisors: Prof. Edrisy from the University of Windsor, Prof. Belingardi and Prof. Settineri from Politecnico di Torino for their important suggestions and guidelines, allowing me to choose and work autonomously. I am very thankful to my industrial advisors, Michele Maria Tedesco and Jugraj Singh, and my committee members, Prof. Riahi and Prof. Johrendt who helped me throughout the project, sharing their knowledge and experience. I also want to mention the staff at the University, in particular Matthew Bondy, Olufisayo Gali, Douglas Boudreau, Matthew St. Louis, Andrew Jenner and Gang Li because of their sincere help during the experiments phase.

Huge thanks to my family, always by my side regardless of the distance and to Camilla, who never gave up supporting me through the whole year.

Finally, thanks to my second family: Agostino, Angela, Benedetto, Simone and Wenzhou. Thank you for sharing the best experience of my life.

TABLE OF CONTENTS

LIST OF TABLES

LIST OF FIGURES

LIST OF EQUATIONS

LIST OF ABBREVIATIONS/SYMBOLS

FCA	Fiat Chrysler Automobiles
NVH	Noise, Vibration and Harshness
SPR	Self-Piercing Riveting
CO_2	Carbon dioxide
MIT	Massachusetts Institute of Technology
EPA	US Environment Protection Agency
FTP-75	Federal Test Procedure
HWFET	Highway Fuel Economy Test
WRB	Warm Roll Bonding
FLD	Forming Limit Diagram
PP	Polypropylene
PU	Polyurethane
STL	Sound Transmission Loss
HSLA	High Strength Low Alloy
ASTM	American Society for Testing and Materials
RD	Rolling Direction
CAD	Computer-Aided Design
UTS	Ultimate Tensile Strength
UE	Uniform Elongation
UYP	Upper Yield Point

LYP	Lower Yield Point
HSLA	High Strength Low Alloy Steel

NOMENCLATURE

σ_y	Yield strength
ε_s	Atoms mismatch parameter
C	Solute concentration
σ_c	Flow stress of the composite
σ_α	Flow stress of general phase α
σ_β	Flow stress of general phase β
V_α	Volume fraction of phase α
V_β	Volume fraction of phase β
α_s	Peel strength
P	Average Load
w	Specimen width
R_a	Surface roughness
ω	Rolling speed
t_r	Thickness reduction
T	Temperature
t_p	Polymer core thickness
t_1	Thickness of the one aluminum sheet in the sandwich
t_2	Thickness of the other aluminum sheet in the sandwich
t_{tot}	Total thickness
HV	Vickers Hardness

$\bar{d}$	Average diagonal length of the indentation
$\dot{e_e}$	Strain rate in the elastic region
$\dot{e_p}$	Strain rate in the plastic region
V_c	Cross-head speed
l_0	Initial gauge length
e	Engineering strain
$R_{p0.2}$	Yield stress with 0.2% strain offset
k_f	Flow stress
K	Strength hardening coefficient
ε	True strain
n	Strain hardening exponent
N	Number of data pairs for strain hardening exponent
r	Plastic strain ratio
S_p	Maximum height within the defined area
S_v	Absolute value of the largest pit within the defined area
S_z	Maximum profile height
t_{bottom}	Thickness of the bottom layer in SPR joints
t_{top}	Thickness of the upper layer in SPR joints
i_{sx}	Interlocking on the left side
i_{dx}	Interlocking on the right side
i_{min}	Minimum interlocking required by FCA

r_t	Residual thickness
F_{peak}	Maximum force sustained by the SPR joint
$n_{4-6\%}$	Strain hardening exponent computed in 4-6% strain range
$k_{4-6\%}$	Strength hardening coefficient computed in 4-6% strain range
$n_{10-20\%/UE}$	Strain hardening exponent in 10-20% or UE strain range
$k_{10-20\%/UE}$	Strength hardening coefficient computed in 10-20% or UE strain range

1. INTRODUCTION AND MOTIVATION

1.1 Background

All over the world, the upcoming emission regulations (Figure 1-1) are forcing automotive manufacturers to develop and use lighter materials. It is well known that composite materials are raising interests in many applications and in particular in automotive, aerospace and marine sectors due to lightweight and high specific mechanical properties of composites concerning bulk materials. Indeed, many automakers declared that light weighting is the main strategy for meeting 2025 standards [1].

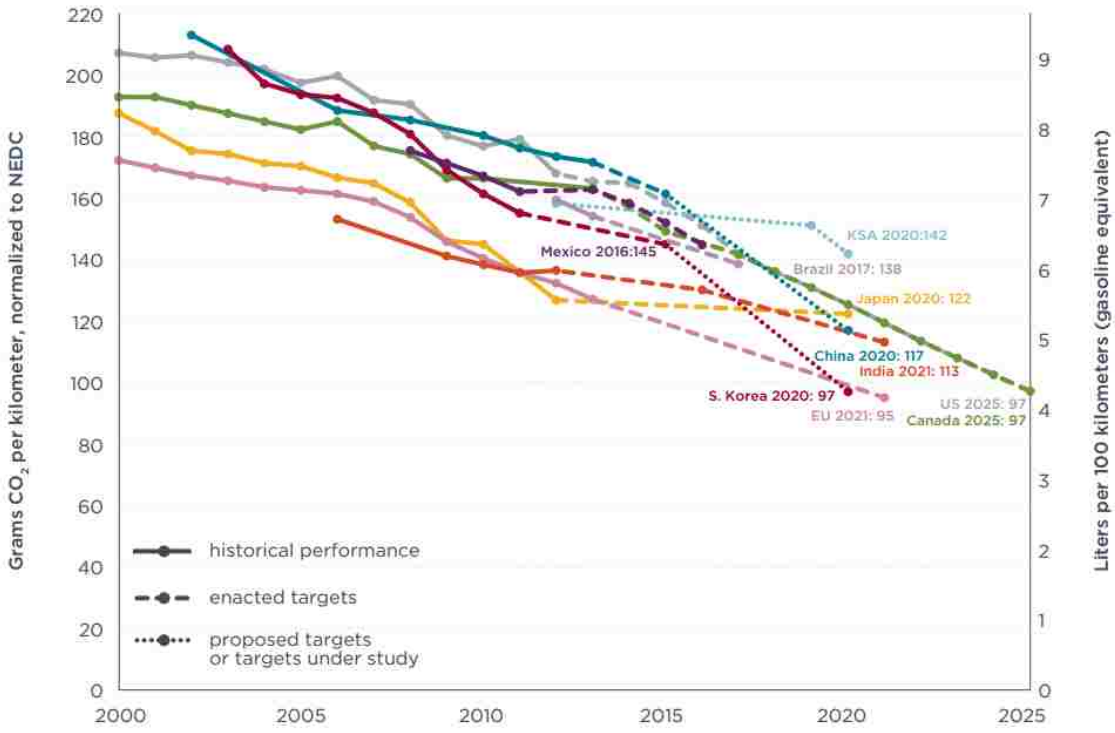

Figure 1-1: Comparison of light-duty vehicle efficiency standards (passenger cars only, light-duty trucks excluded) [1].

In general, steep decrement in the emissions is going to be applied in the next few years. In particular, the most challenging emission regulations are: 97 $\frac{gCO_2}{km}$ in 2020 in Korea, 95 $\frac{gCO_2}{km}$ in 2021 in Europe and 97 $\frac{gCO_2}{km}$ in 2025 for United States and Canada.

Lighter materials, according to the Massachusetts Institute of Technology (MIT) study [2], can reduce the fuel consumption, and so the emissions, up to about 7% per 10% of reduced weight. The authors studied the fuel consumption performance on a new average passenger car and a new average light truck, simulating the gasoline internal combustion engine consumption based on the both city (Federal Test Procedure FTP-75) and highway (Highway Fuel Economy Test HWFET) drive cycle. They also used the same correcting factors used by the Environmental Protection Agency to better estimate the on-road performance.

It is also important to highlight that, the use of lighter materials does not always have consequent higher costs and, if they do, they are well below the government predictions (rulemaking line in Figure 1-2) [3].

Indeed, design improvement can lead to weight reduction not only without adding, but even saving money (dark purple curve in Figure 1-2). The net costs range in Figure 1-2 (red line) refers to the hypothesis that, aluminum will take into account only one third of the upcoming strategies to reach light weight, so that feasible weight reduction can occur at even less than half of the rulemaking estimation.

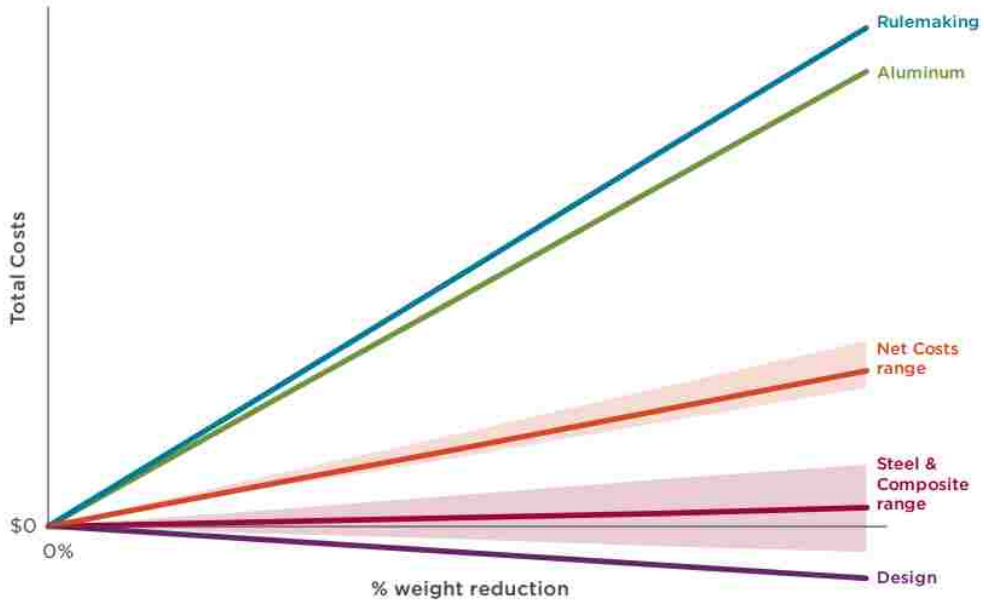

Figure 1-2 Total cost as a function of percent vehicle weight reduction. Note that composites include plastics, but not carbon fiber [3].

For these reasons, automakers are implementing larger use of lighter materials on the vehicle body such as aluminum, high strength steel and composite materials. For example, a large percentage of conventional steel is going to be replaced mainly with High/Medium Strength Steel, Polymer/Composites, Aluminum and Magnesium alloys (Figure 1-3) [4].

Nevertheless, it is well known that other safety, comfort is one of the main parameters through which customers estimate the quality of the vehicle. Among the several parameters that influence comfort in a vehicle, Noise, Vibration and Harshness (NVH) play a significant role. Moreover, prolonged vibrations and noise induce fatigue to the driver, with consequents safety impacts. Automotive manufacturers are making tremendous efforts to reduce NVH issues and testing the whole vehicle to assess the comfort inside the cabin. Focusing on the high frequency range, noise can be transmitted in different ways, but mainly through the wind, the transmission and the powertrain, as well as through the road [5].

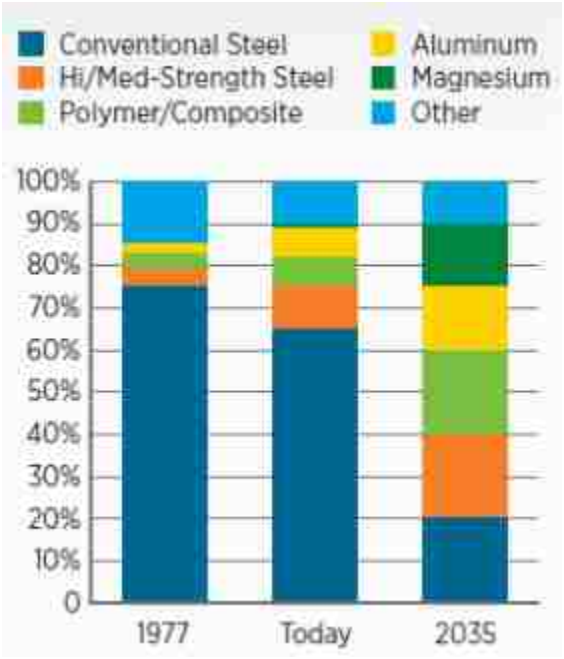

Figure 1-3: Material usage trend in automotive industry [4].

Figure 1-4: Damping patches location in the vehicle [6].

Mastic damping patches, sealants, butyls and cork tape are some of the most common solutions used by automakers to reduce NVH. Figure 1-4 gives an idea about the significant amount of damping patches used inside the vehicle. The damping layers are applied on panels like the firewall, floor panels, trunk compartment panels, wheel arches, roof, doors and hatches. Unfortunately, these solutions add considerable weight to the vehicle and also increase the cycle time of the assembly line. Consequently, it is clear that NVH attenuation has great margins for improvement.

Composites are promising solutions for the issues stated above. Indeed, they are becoming more and more important in automotive industry due to their tailor ability, the property of being suitable and flexible for many different applications. There are several types of composites, among these, laminates are raising most of the interests. Usually laminates are three-layer materials formed by two metal skins and a polymer core, recalling the same idea of a sandwich, from which they get the name sandwich composites. Thanks to the metal alloy skin, chosen based on the different application, the structure gains flexural stiffness and high mechanical properties, whereas the polymer leads to lightweight, as well as damping

performance. Sandwich composites are considered promising solutions also because of their sustainable manufacturing costs and continuous production [7]. Moreover, composites with sandwich structure could avoid the usage of damping patches, decreasing the total weight on the vehicle, easing the assembly procedures and reducing the relative costs.

1.2 Statement of Purpose

The possible applications for sandwich composites are various, since they can potentially replace every panel in the vehicle. For example, seat-storage tub, wheel house, dash panel, cowl plenum, front and rear floor panels are possible solutions that can be easily implemented in the assembly line due to low mechanical requirements [8].

The objective of this study is to determine the main mechanical properties of Quiet Aluminum® sandwich composites and evaluate, comparing their performance with FCA requirements, the implementation of the materials in automotive industry as panels with non-structural loads. Since the sound-deadening characteristics of Quiet Aluminum® were already tested by the manufacturer, the comprehensive testing performed in the current study focused on determining the mechanical properties of Quiet Aluminum® necessary to replace the monolithic panels in the vehicle.

In order to reach the objective, targeted tests were performed: adhesion strength between the layers, tested through T-peel test, roughness and metallographic analysis on the cross section, tensile properties (anisotropy and strain hardening exponent included), as well as an evaluation on Self-Piercing Riveting technique for joining the sandwich composite together with a structural HSLA steel.

2. LITERATURE REVIEW

In this section, the literature work used to build a complete background on aluminum alloys and sandwich composites properties is presented.

2.1 5xxx and 6xxx Aluminum Alloys

In the automotive industry, the use of 5xxx and 6xxx aluminum alloys is common especially for body panels such as doors, firewall and floor panels or ceiling ones. Indeed, these alloys present high formability and corrosion resistance together with good mechanical properties [9]. 5xxx Aluminum alloys contain Magnesium (Mg) as a primary alloying element, which is exploited for solid solution hardening. The yield strength of an aluminum alloy changes when it is subjected to solution heat treatment. Indeed, yield strength σ_y is proportional to the solute concentration and depends on the "mismatch" between solute and solvent atoms as explained in Equation 1:

Equation 1: Yield strength relation with solute concentration and mismatch between solute and solvent [10].

$$\sigma_y \, \alpha \, \varepsilon_s^{\frac{3}{2}} C^{\frac{1}{2}}$$

where ε_s expresses the "mismatch" between solute and solvent atoms and C is the solute concentration. As expected, a bigger solution concentration and badly matched atoms obstruct more efficiently the dislocation movements, enhancing plastic deformation. In case of a 5xxx Aluminum alloy, Magnesium is put into solution and then rapidly quenched to room temperature.

Instead, 6xxx aluminum alloys have Magnesium and Silicon as major alloying elements and are Heat-Treatable alloys. Since their phase diagrams have a steep decrement in the solid solubility with the decreasing temperature, precipitation hardening phenomena can be exploited [10]. In fact, precipitation of the intermetallic compound Mg_2Si provides hardening, with considerably relevant gains in yield strength [11]. Figure 2-1, gives an overview on the obtainable yield strength as a function of time and temperature for the aluminum alloy 6061, highlighting the influence of the variables on the precipitation hardening process. Aging stage is done at low temperatures for longer times to obtain higher process control.

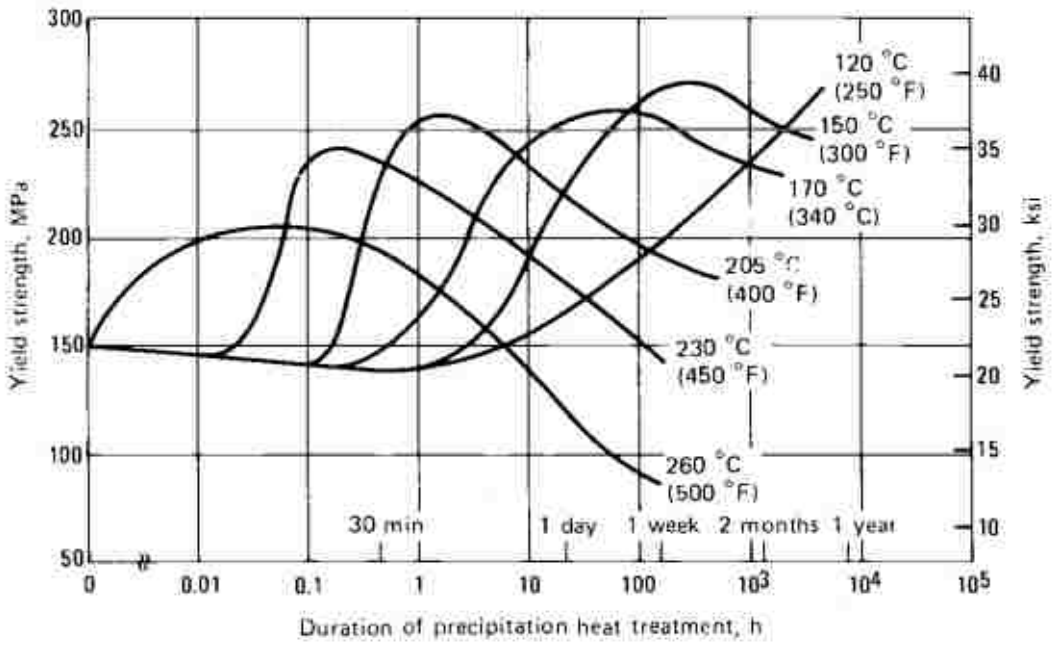

Figure 2-1: Precipitation heat treatment or artificial aging curves for solution heat-treated aluminum alloy 6061 [12].

Figure 2-2 and Figure 2-3 instead, show the typical stress-strain curves for respectively 5xxx and 6xxx aluminum alloys with specimens tested under $0°, 45°, 90°$ to the rolling direction.

The latter are also called non-heat treatable alloys, but can be hardened with cold working. As previously said, they have good mechanical performance and high ductility, especially in annealed condition. Nevertheless, Lüders bands are common in Magnesium-containing aluminum alloys as well as serrated stress-strain curve, which is related to dynamic strain aging (Portevin-le-Chatelier effect) [13]. Since stretcher strains are visible even after polishing and painting, those alloys are preferred for internal body panels. Instead, since 6xxx Aluminum alloys are not subjected to stretcher strains, they are preferred for production of external body panels in automotive industry for obvious aesthetics reasons. Moreover, these two alloys exhibit high corrosion resistance using a thin aluminum oxide layer that forms on the skin when the material is exposed to the environment. The oxide layer prevents further oxidation and protects the aluminum from weathering as well as from many acids [14].

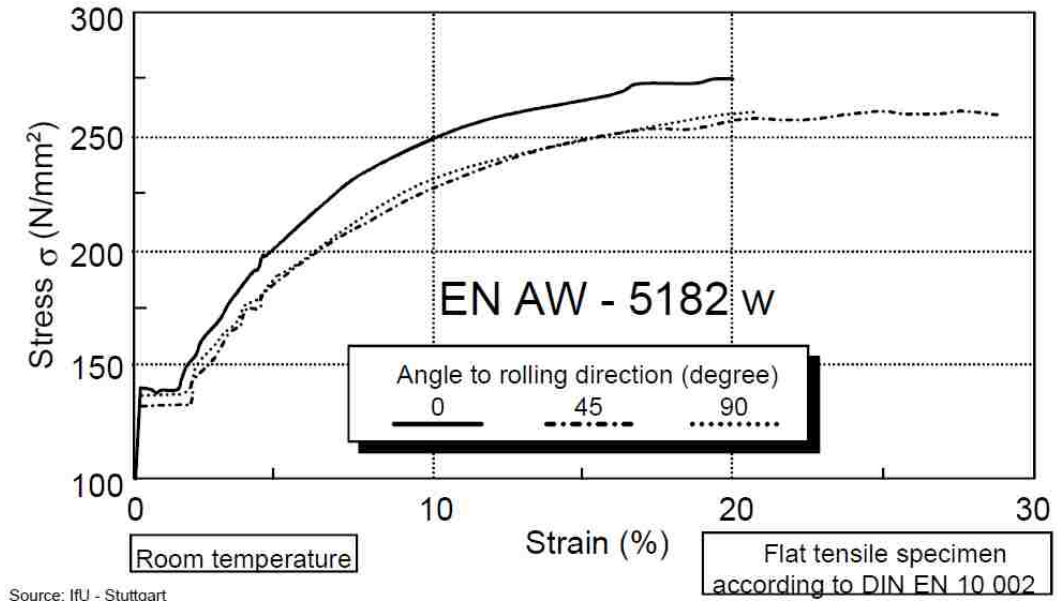

Figure 2-2: Stress-strain diagram for a Non-Heat-Treatable alloy [13].

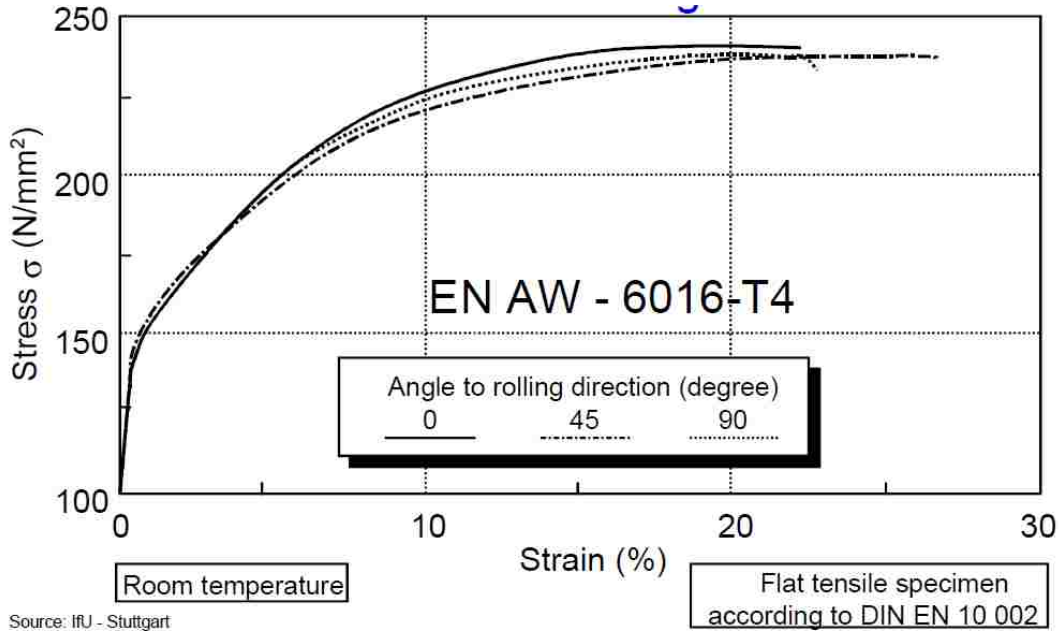

Figure 2-3: Stress-strain diagram for a Heat-Treatable alloy [13].

In this study, particular focus is given on 5754-O aluminum alloy (annealed condition) and 6061-T4 (naturally aged) since they are the alloys used as skins in the sandwich composites examined. Aluminum 6061-T4 has Magnesium and Silicon as main alloying elements, with about 1% Mg and 0.6% Si, whereas 5754-O presents a higher amount of Magnesium, about 3%, that is the main alloying element. 6061-T4 alloy also has a higher amount of Copper in its chemical composition than the counterpart. As far as the mechanical properties are concerned, density, Young modulus, strain hardening exponent and ductility of the two alloys can be considered almost equal, whereas AA5754-O presents lower Ultimate Tensile and Yield Strengths. Furthermore, the hardness values for the above mentioned alloys as well as the artificially aged aluminum 6061-T6 are shown in Table 2-3. It is clear that aluminum 6061-T6 presents the highest hardness ($HV = 107$), whereas the non-heat treatable alloy is the softest ($HV = 62$).

Table 2-1: Chemical composition for AA6061-T4 and 5754-O [15].

Chemical composition	Al [%]	Mg [%]	Si [%]	Mn [%]	Fe [%]	Cr [%]	Zn [%]	Cu [%]	Ti [%]	Res. [%]
AA5754-O	94.2 to 97.4	2.6 to 3.6	0 to 0.4	0 to 0.5	0 to 0.4	0 to 0.3	0 to 0.2	0 to 0.1	0 to 0.15	0 to 0.15
AA6061-T4	95.9 to 98.6	0.8 to 1.2	0.4 to 0.8	0 to 0.15	0 to 0.7	0.04 to 0.35	0 to 0.25	0.15 to 0.4	0 to 0.15	0.05 to 0.15

Table 2-2: Mechanical properties for AA6061-T4 and 5754-O [16].

Mechanical properties	Density $\left[\frac{g}{cm^3}\right]$	Young's modulus $[GPa]$	UTS $\left[\frac{N}{mm^2}\right]$	Yield strength (0.2% offset) $\left[\frac{N}{mm^2}\right]$	Elongation [%]	r-value @8.00-10.00%	n-value @10.00-20.00 [%]
AA5754-O	2.7	69	215	112	19	0.72	0.24
AA6061-T4	2.7	68	255	141	20	0.58	0.24

Table 2-3: Vickers Hardness reference values [16].

Monolithics	Al 5754-O	Al 6061-T4	Al 6061-T6
Vickers Hardness [HV]	62	75	107

2.2 Metal/Polymer/Metal Sandwich Composites

F.C Campbell stated "a composite material can be defined as a combination of two or more materials that results in better properties than those of the individual components used alone" [17]. Composites have a matrix and a reinforcement phase that provides stiffness and strength to the matrix according to the design requirements. However, the definition of composite is complex and sometimes discussed; indeed hybrid metal laminates are a special segment of composites usually composed by layers [18]. Here matrix and reinforcements are indistinguishable. The concept of three-layer hybrid metal laminates, more commonly called sandwich composites, is to combine high strength materials as metals on the outer side with light materials as polymer cores. With this combination, high flexural stiffness can be obtained with lightweight. Moreover, the large variety of existing composites allows exploiting their tailorable properties.

Therefore, sandwich composites can be divided into three main categories, based on the intended application: low-density laminates, sound-deadening laminates and clad sheets (Figure 2-4).

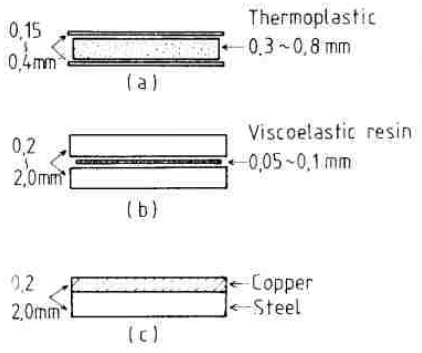

Figure 2-4: Schematic representation of the (a) low-density laminate, (b) sound-deadening laminate, (c) clad sheet. [19].

The first ones exploit thick polymer cores ($40 - 60\%$ polymer volume fraction) and metal skins to achieve high flexural stiffness and weight saving with respect to the monolithic panels. Sound-deadening laminates have a thin viscoelastic layer of about 20% or less of the total thickness, specifically designed for sound-damping. Clad sheets instead, are metal sandwich with usually different nature and thickness.

Sandwich composite with sound-deadening properties are very attractive to the automotive sector, but more in general wherever noise reduction is desired.

2.2.1 Mechanical Properties of Metal/Polymer/Metal Sandwich Composites

As previously stated, sandwich composites can be divided into mainly three categories: low-density laminates, sound-deadening laminates, and clad sheets. Nevertheless, in the literature few studies have been carried out on sound-deadening laminates. In fact, most of the works on sandwich mechanical properties are based on low-density laminates. For this reason, the work on Quiet Aluminum® sound-deadening laminates completed in this study has an even more relevant contribution to the research since it is a good starting point to study the properties of thin viscoelastic sandwich composites. The literature work cited refers mainly to conventional sandwich composites with thick polymer cores.

The simple structure of sandwich composites allows manufacturers to choose the aluminum alloy to be used as skin by looking at the mechanical properties required. Obviously, changing the metal alloy, the properties of the material change significantly. Stiffer sandwich composites can be obtained at the cost of formability; consequently, designers have to match the characteristics of the material by taking into account the relative requirements.

The usage of sandwich composites is also eased by a relatively simple and cheap manufacturing process. Indeed, several techniques to manufacture laminates are available; the most common ones are heat pressing, direct injection molding and roll bonding. The latest is found to be more efficient, since it allows continuous production and cost reduction [20].

The process consists of:

- pretreating the aluminum surfaces to remove the contaminated layers from the surface, especially the ones that will adhere with the polymer core. This operation usually involves degreasing with ethanol and then sanding.
- bonding the three components of the sandwich soon after the surfaces cleaning.
- rolling the sandwich through a pair of flat rollers under sufficient pressure, so that the deformation will ensure proper bonding.

When heat is involved in the process the technique is called Warm Roll Bonding (WRB). With this method the surfaces are heated up before the rolling process to increase the ductility and the strength of the bond. The process, shown in Figure 2-5, depends on many parameters: temperature of the pre-heating, pre-treatments of the surfaces, rolling speed, thickness reduction and post-rolling treatments.

In manufacturing sandwich composites, it is possible to have indirect adhesion (with glue agent) or a direct adhesion (the polymer itself behaves like an adhesive). Indirect adhesion is mostly used, even though direct adhesion between polymer and metals showed good bonding strength [21].

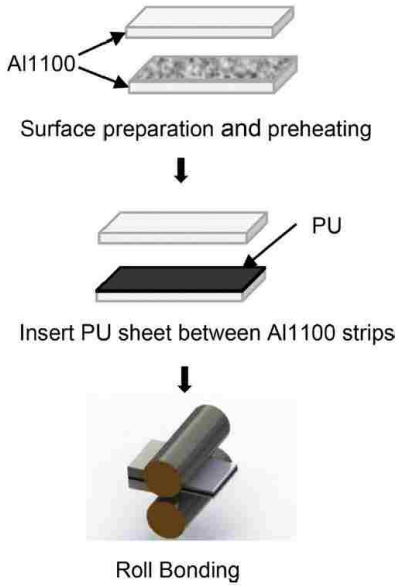

Figure 2-5: Schematic representation of the Warm Roll Bonding process [20].

As far as the tensile properties are concerned, it is quite simple to match the low tensile strength requirements for panels with non-structural loads.

It is well known that composites with hard particles follow the rule of mixtures (Equation 2):

Equation 2: Rule of mixtures [17].

$$\sigma_c = V_\alpha \sigma_\alpha + V_\beta \sigma_\beta$$

Where σ_c represents the flow stress of the composite, α and β are the two phases, V_α and V_β the volume fractions and σ_α and σ_β the flow stresses for the respective phases.

The rule of mixture can also be applied for sandwich composites; Liu and Xue [22] showed the good accordance between the predicted tensile behavior and the experimental results (Figure 1-1) on three different sandwiches made of two $0.5\,mm$ Al 5052 skin sheets and a polypropylene core (three different core thicknesses). Moreover, accordance between the rule of mixtures and experimental results was also found in Shin et alias' study [23]. Consequently, Equation 2 can be used for sandwich composites, where α and β are the two different materials, V_α and V_β the respective volume fractions and σ_α and σ_β the metal and polymer flow stresses.

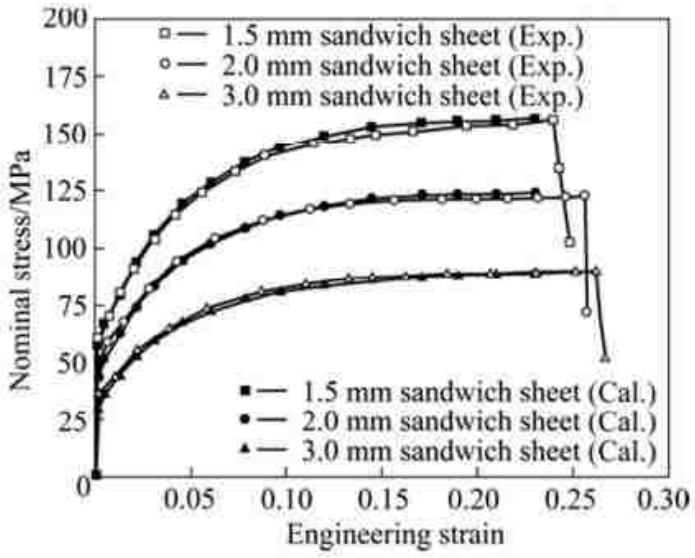

Figure 2-6: Nominal stress-engineering strain curves of sandwich sheets [22].

Based on the previous considerations, tensile strength requirement can be easily obtained by matching the volume fraction of the hard aluminum skin and the soft polymer core.

5xxx and 6xxx aluminum alloys are commonly used for panels in automotive industry due to their good formability and mechanical properties (tensile strength is more than 200 MPa), but these properties should be carefully taken into account when a polymer core is introduced between the two metal sheets. Many studies have been carried out on formability; it is found that sandwich composites can reach formability properties similar to the monolithic metals [24] [25].

Formability can be evaluated through different testing methods. One of them is the Erichsen Index (IE, depth of impression of a cup in millimeters required to obtain fracture). According to the Erichsen Cupping Test (DIN 50101) and deep drawing benchmark test, Palkoskwi et. Al [24] showed that the stretch formability of the sandwich manufactured in laboratory, composed of stainless steel AISI SS316L/polypropylene copolymer/AISI SS316L with a roll-bonding process by means of a 2-high 10" rolling mill, reached the monolithic steel one.

In Carrado' et al.'s paper [25], the formability of sandwich composites with different manufacturing processes, metal skins (austenitic steel, aluminum alloy), different cores and adhesives were evaluated (Figure 2-7). The experiments showed again similar behavior of the sandwich composite produced in laboratory (SRB1 in Figure 2-7, sandwich manufactured with roll bonding procedure) regarding the monolithic steel. Even the sandwich with aluminum alloy (SRB4 in Figure 2-7) reached the performance of its monolithic counterpart. Nevertheless, here again the sandwich was considerably thicker than the bare aluminum.

Forming Limit Diagram (FLD) shows the relationship between the limits of minor and major strains in the plane of the stretched sheet. Kim et al. compared, in their study [26], a $1.2\ mm$ thickness AA5182/Polypropylene/AA5182 sandwich composite concerning $0.2\ mm$ thickness AA5182 skin and $1\ mm$ AA5182 skin. They found an even better FLD for the sandwich composite (Figure 2-8), stating that the polymer presence can play a positive role, especially if the positive contribution due to its higher strain sensitivity is stronger than the negative contribution due to the lower strain hardening exponent.

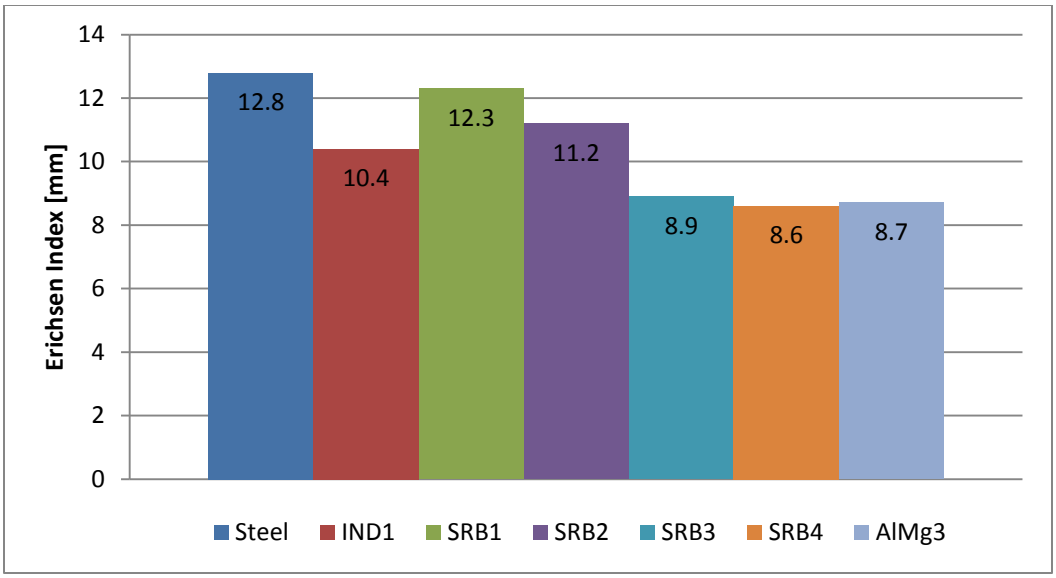

Figure 2-7: Averaged maximum index of five samples in Erichsen index. Adapted from [25].

Table 2-4: Skin layer composition and sandwich thicknesses. Adapted from [25].

	Specimen	Total thickness$[mm]$	Process
Steel	1.4404	1	-
IND1	H400 (1.4376; PP-PE)	1.6	Industrial
SRB1	1.4404/PP-PE/$AlMg3$	1.5	RB
SRB2	1.4404/PP-PE/ $AlMg3$	1.5	RB
SBR3	$AlMg3$/PP-PE/1.4404	1.5	RB
SBR4	$AlMg3$/PP-PE/ $AlMg3$	1.5	RB
Aluminum alloy	$AlMg3$	1	-

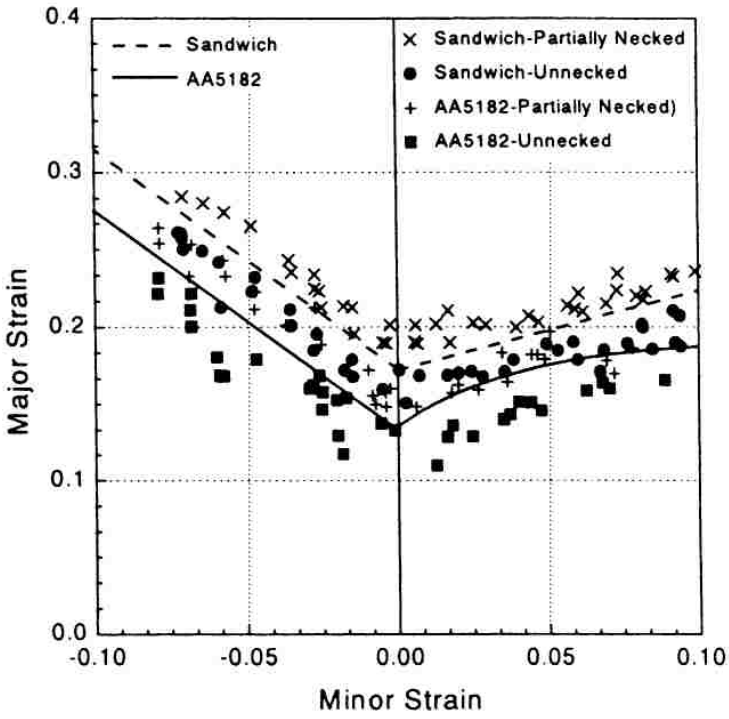

Figure 2-8: Measured FLD of the 0.2t AA5182 and 1.2t sandwich sheets [26].

2.3 Adhesion

Adhesion performance has major priority in sandwich composites. In fact, if the material is not able to maintain proper adhesion between the different layers, the detached layers are no longer acting as a unique component. Hence the sandwich composite loses its mechanical performance. For this reason, the main requirement for sandwich composites is sufficient adhesive bonding between the three layers.

2.3.1 Adhesion Mechanisms

Adhesion is a very complex and multi-disciplinary topic; in fact, it includes chemistry, thermodynamics and mechanics. For this reason, the adhesion phenomenon is explained through many theories, between these: adsorption theory, mechanical interlocking model,

electronic or electrostatic theory, weak boundary layer theory, diffusion or inter-diffusion theory, chemical bonding theory are the most adopted ones [27].

The thermodynamic theory or adsorption is the most accredited model and is based on the "wetting" phenomenon as well as on the interatomic and intermolecular forces between the adhesive and the adherend surface like primary and secondary bonds or acid-base interaction. Indeed, to have a strong adhesion, continuous contact between adhesive and the adherends surfaces is primary important. The so called "wetting" phenomenon occurs in a proper way when the adhesive is filling the valleys and crevices present in the substrate of adherends surfaces. Wetting is related to contact angle, which explains the configuration a droplet of liquid on a solid surface takes to minimize the energy of the system. Good wettability occurs when the surface tension (excess energy associated with the presence of a surface) of the liquid (adhesive) is lower than the critical surface energy of the solid, that is equal to the surface tension of a liquid which spread totally onto the solid (zero contact angle) [28]. This also enables to understand and anticipate the wettability between a solid applied by another in a liquid state, very common procedure in manufacturing sound-deadening laminates. Figure 2-9 shows an example of good and poor wettability between a liquid and a solid surface.

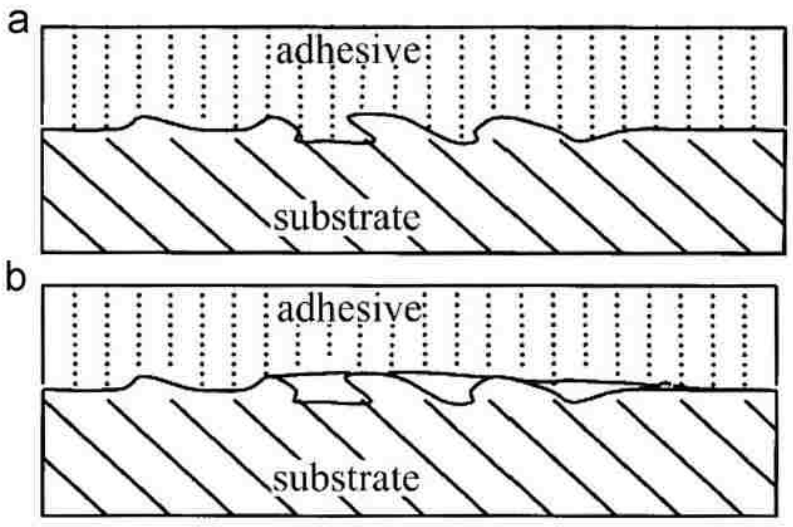

Figure 2-9: (a) Sufficient wetting and (b) Poor wetting [29]. After [27].

Obviously, good wetting is not sufficient to achieve strong adhesion between the surfaces and physical or chemical adsorption is needed through molecular attraction forces. The attraction forces just mentioned can have different nature, including:

- Secondary bonds: van der Waals forces, and hydrogen bonds.
- Primary bonds: covalent, Ionic, metallic and donor–acceptor interactions (acid–base interaction).

The mechanical interlocking model is one of the earliest theories and is based on the adhesive trapping into the irregularities or pores of the other material substrate. It is related to the ability of the adhesive to displace trapped air at the interface and the ability to enter substrate surface irregularities (pores, cavities and asperities). For this reasons, roughness and porosity of the substrate, assuming sufficient wettability, are very important parameters. However, mechanical interlocking does not act at molecular level and it is mainly a technical mean through which adsorption is enhanced [29]. Figure 2-10 represents a typical substrate with irregularities, in which mechanical interlocking occurs.

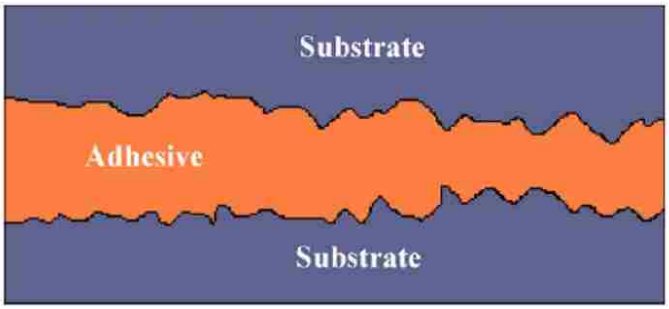

Figure 2-10: Illustration of mechanical coupling between two substrates [30].

The Diffusion model was firstly proposed by Voyutski [31] and is based on the inter-diffusion between polymers macromolecules at the interface. Figure 2-11 gives a schematization of the phenomenon. The diffusion between macromolecules leads to the replacement of the initial boundary with a gradual change between the characteristics of the adhesive and the substrate. Nevertheless, the model is limited by the fact that it is applicable just in polymer to polymer adhesion and welding of thermoplastics.

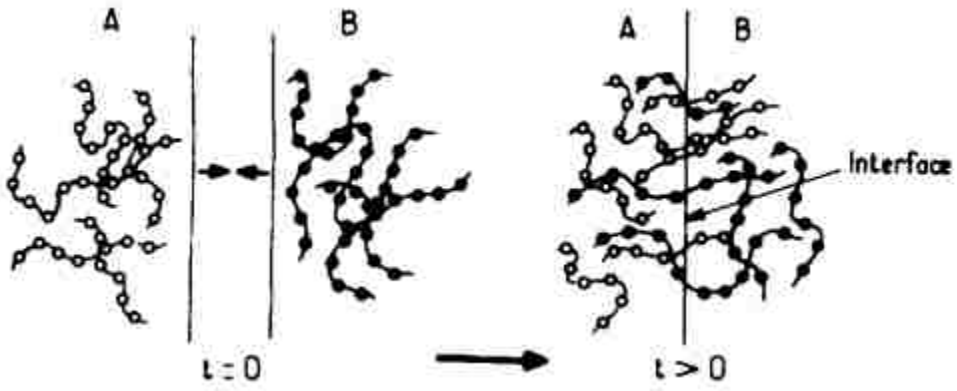

Figure 2-11: Inter-diffusion across the interface [27].

Instead, the electrostatic theory is based on the charge transfer across the interface adhesive/adherend. It is a parallel example of a capacitor whose plates are the two substrates into contact. The scheme in Figure 2-12 represents the capacitor, whose stored energy is equal to the work needed to break the adhesive bond [32].

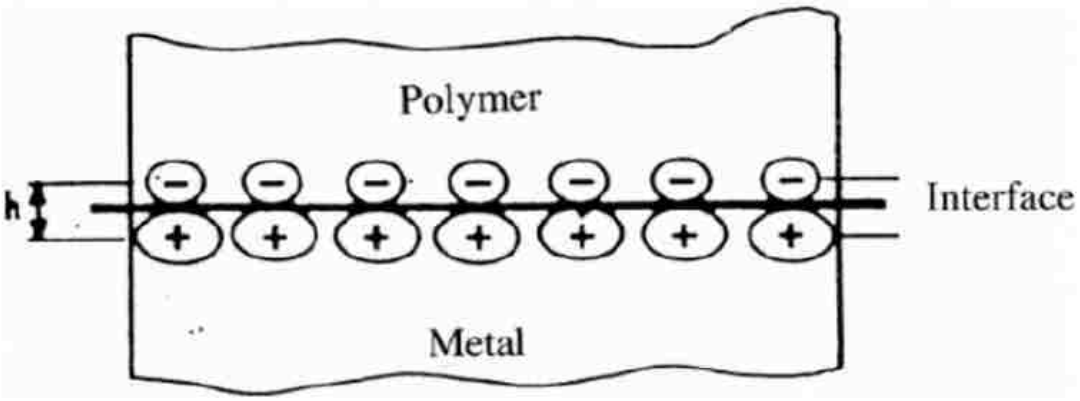

Figure 2-12: Electrical double layer at polymer-metal interfaces [27].

According to the weak boundary adhesion theory, it is improbable that an adhesive/adherend interface would fail [33], instead the failure depends only on the bulk properties of the two materials or it occurs due to the formation of a weak boundary creation between the two substrates [34].

Some of the reasons for weak boundary layer failure can be scaly oxide layers attached to the base metal, poor cleanliness of the surfaces and air trapped at the interface [34].

Those conditions are carefully taken into account in manufacturing laminates; indeed metal sheets undergo cleaning and surface activation processes in order to minimize the root causes of weak boundary layer failure.

The chemical or molecular bonding adhesion theory is related to the intermolecular forces (van der Walls and dipole-dipole interactions) and chemical interactions. A chemical bond is usually considered as primary bond for its superior strength than secondary bonds. If the adhesive and the substrate are sufficiently in intimate contact, a chemical bond is formed, with an energy range of $40 - 400 \frac{kJ}{mol}$. Consequently, promoter molecules can be used to exploit the chemical bonding in adhesion designing. Those molecules are also called coupling agents and are able to react with the metal substrate as well as with the polymer molecules, creating a strong chemical connection between the two sides [35].

2.3.2 Adhesion in Metal/Polymer/Metal Sandwich Composites

As previously mentioned, it is not possible to apply a universal adhesion theory for all circumstances. In adhesive bonding and especially in metal/polymer interfaces the failure modes are driven by the existing forces between adhesives and metal adherends. Those forces can be then divided into: adhesive forces and cohesive forces.

The former take place at the interface metal/polymer, whereas the latter act between the polymer molecules of the adhesive itself or within the metal substrate. Figure 2-13 shows a schematic representation of the concepts just explained. It is clear to understand that the overall bonding strength depends on the balance between the two acting forces. If the adhesive forces are weaker than the cohesive ones (or vice versa), the failure always occurs at the lower load.

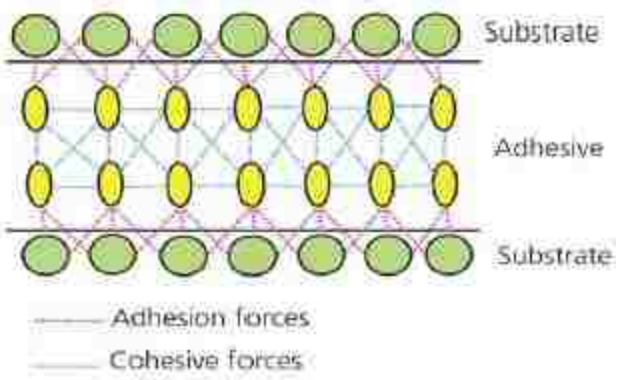

Figure 2-13: Schematic representation of adhesion and cohesive forces acting in adhesive bonds [36].

The failure modes in adhesive joints in laminates are three (Figure 2-14):

- Apparent adhesive failure (Figure 2-14-c), when the failure is at the interface between adhesive and the adherend substrate or at a boundary layer located in proximity of the interface. The term apparent derives from Bikermann's theory [33], which states a high improbability of pure adhesive failure, whereas failure is addressed to an inadequate surface preparation.
- Cohesive failure, when it is encountered within the polymer (Figure 2-14-a) or within the metal substrate (Figure 2-14-b).
- Mixed mode failure (Figure 2-14-d), when a combination between adhesive and cohesive failure takes place.

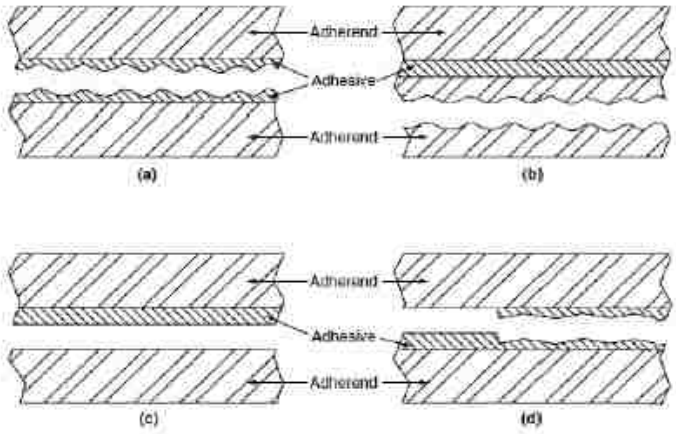

-

Figure 2-14: Adhesive bonds failure; a) cohesive failure inside the adhesive, b) cohesive failure inside the adherend, c) apparent adhesive failure, d) mixed mode failure [37].

One of the most common and reliable testing methods to evaluate the bonding strength of sandwich composites is the $90°$ peel test, also called T-peel test. This procedure can be performed with a universal tensile machine, in which two flexible substrates have been bonded together and placed into its grips, so that one substrate sticks up and the other sticks down forming a "T" shape together with the horizontally bonded area (Figure 2-15). The outcome of the test is the average peel strength $\alpha_s = \frac{P}{w}$, where P is the average load and w is the bond width.

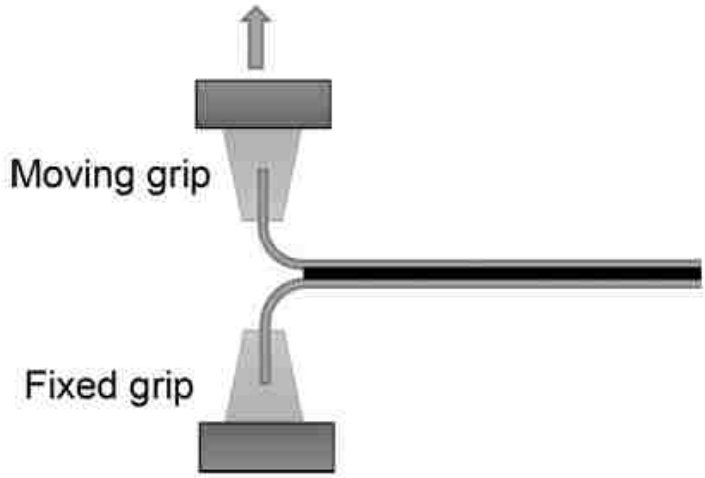

Figure 2-15: Schematic illustration of the T-peel test specimen position with respect to the grips [20].

In Mousa and Kim's study [20], parameters such as surface roughness, preheating temperature, rolling speed and thickness reduction were evaluated based on a Warm Roll Bonding (WRB) manufacturing process on a commercially pure aluminum (AL1100) skin and polyurethane (PU) core sandwich composite. The Al strips were cut into dimensions of $60\,mm \times 10\,mm \times 0.5\,mm$, and the PU sheets were cut into dimensions of $60\,mm \times 10\,mm \times 0.7\,mm$.

The results showed increasing bond strength with increasing roughness from the as-received material with $R_a = 0.6\,\mu m$ till reaching an optimum strength with $R_a = 5.83\,\mu m$, from which the peel strength starts decreasing (Figure 2-16) due to poor polymer penetration into the crevices and valleys.

Unfortunately, these results cannot be considered universally valid, since the adhesion mechanisms are complex and depend on several parameters such as chemical composition of adherends and adhesives, surface irregularities, roughness, surface topography and many

others. Indeed, it is not possible to build a simple model and every application must be evaluated basing on the characteristics of the two materials to be bonded.

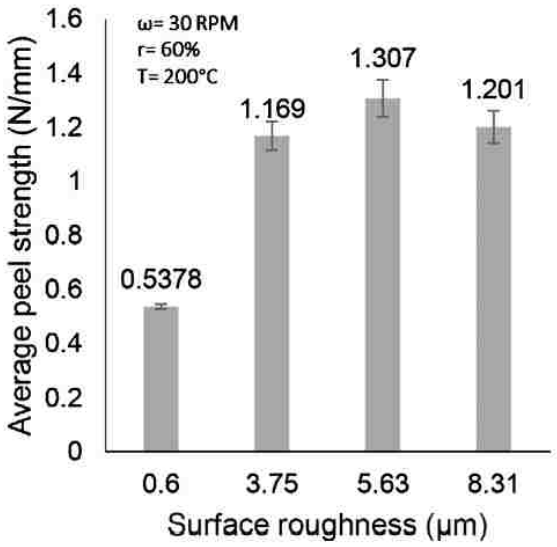

Figure 2-16: Peel strength of AL1100/PU/AL1100 fabricated with different surface roughness values ($\omega = 30\ RPM$, $t_r = 60\%$, $T = 200℃$). Data: mean (n=3) [20].

2.4 Noise and Vibration Harshness Performance for Sound-Deadening Sandwich Composites

Comfort is one of the main requirements for customers in modern vehicles. To reach a good perception of comfort, noise and vibrations, which are transmitted by the road or produced by wind, transmission or engine, have to be reduced.

Vibro-acoustic phenomena can be divided into three categories depending on the frequency range [5]:

- Ride (0-5 Hz), that is related to the accelerations provided by vehicle maneuvers and rigid body oscillations on the suspensions.
- Shake (5-25 Hz), which takes into account the resonances of the vehicle as a flexible structure.

- Noise (>100 Hz), that are the frequencies perceived by the human ear as noise.

Then, noise can be divided into two main categories, depending on the propagation mechanism: structure borne and air borne noise. The first mechanism is related to the transmission of noise through the different subsystems in the vehicle. The structural vibrations are then transmitted to the air in the cabin, producing the perceived noise. Instead, air borne noise is transmitted through external (with respect to the vehicle cabin) pressure waves that make the body panels vibrate, with consequent production of pressure waves in the cabin, perceived as noise. In both mechanisms, air inside the vehicle is induced to vibrate at high frequencies producing noise; the two categories explain the transmission between the source and the panels surrounding the vehicle. Manufacturers are focusing on these issues to give better feeling while driving to the customer.

NVH properties for sandwich composites depend obviously on both materials used (metal skin and polymer core) and their respective thicknesses. Sargianis and Suhr [38] stated that flexural bending stiffness is the mechanism which drives the low frequency damping properties, whereas the properties of the core drive the high frequency field. The authors found that a thickness reduction of the polymer core of 42% (from $18.4\ mm$ to $10.7\ mm$) improved the high frequency damping properties of 33%, whereas a thickness reduction of 45% (from $10.7\ mm$ to 5.9 mm) improved the acoustic performances of 125%. Anyway, reducing the thickness and so the flexural rigidity, the acoustic performance on the low frequency is drastically reduced.

Hara and Özgen [39] tested the performance of a sound-deadening sandwich composite ($0.1\ mm$ thick 3M-467 viscoelastic adhesive bonded between two steel sheets with 0.5 mm thickness each) with respect to a simple seat floor panel with a free layer surface damping treatment on the surface. The same viscoelastic polymer of the sandwich is used as damping material on the top of a floor panel. The authors increased the thickness of the polymer till reaching the same damping performance of the sandwich composite to assess the amount of weight the laminate can reduce.

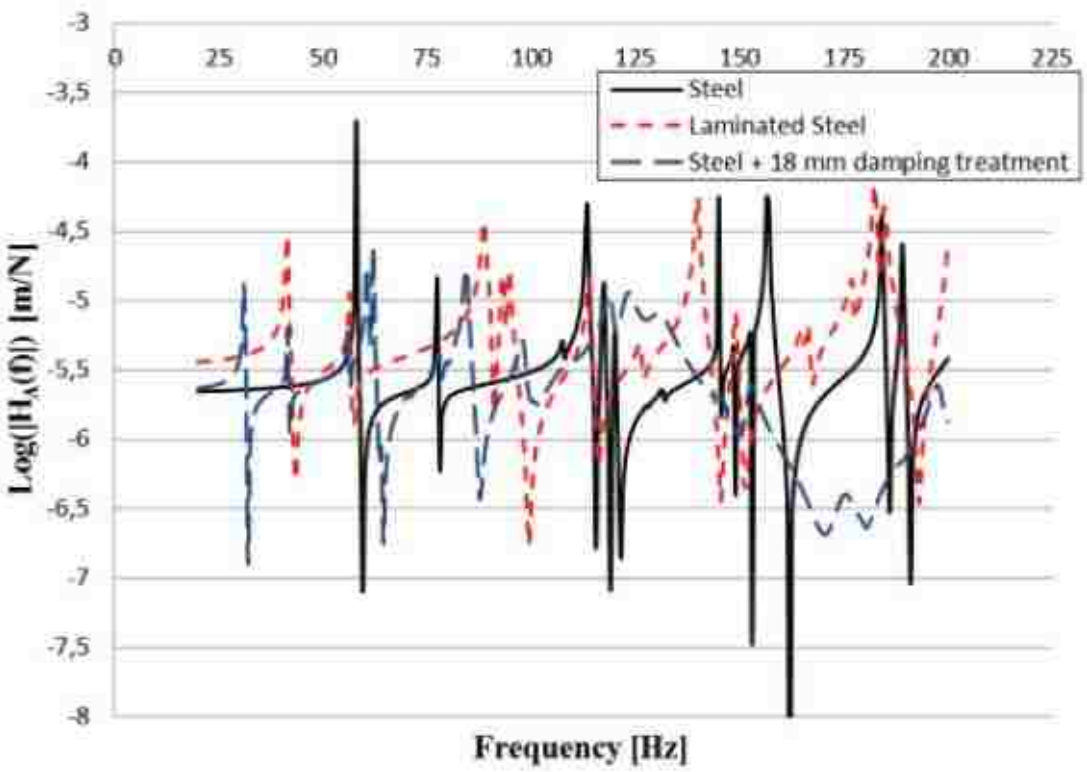

Figure 2-17: Comparison of FRF plots of floor panel [39].

The sandwich composite had the same average loss of the floor panel with $18\ mm$ damping treatment (Figure 2-17). This means 68% weight reduction using the laminated steel instead of the steel panel and the free layer surface treatment on top of it, without decreasing NVH performance.

2.5 Joining Hybrid Materials

In the automotive industry, spot welding is one of the most common techniques through which the components are joined with the rest of body. Nevertheless, the heat involved in the process and the difficulty of welding aluminum alloys (or magnesium ones) makes spot welding not advisable for joining hybrid materials. Adhesive bonding is a good alternative to spot welding because it allows the materials not to be heated nor deformed with consequent NVH improvements together with the low cost of the new high quality glues [24]. The combination of spot-welding and adhesive bonding (hybrid joints) can also be used to obtain stronger and more

versatile joints. Many other techniques as laser welding, remote laser welding or clinching are available with obviously different pros and cons.

2.5.1 Self -Piercing Riveting

Among the techniques for joining hybrid materials and especially thin and different metals sheets, Self-Piercing Riveting (SPR) is raising a lot of interests. Indeed, the technique has short cycle time (from $1.0\ to\ 4.0\ s$) and ease of automation, important factors especially in the automotive sector. SPR consists in a high speed mechanical spot joining (cold forming process) with no preparatory hole, since the rivet itself is penetrating the sheets and flaring into the bottom sheet, following the shape of the die (Figure 2-18) [40]. No thermal damage is involved on the two materials joined, so that it can be easily used for joining alternative materials such as aluminum and magnesium. SPR can be also paired with adhesives to form leak-proof and high fatigue resistant joints. Moreover, it can be used for joining two or more sheets of different materials [41].

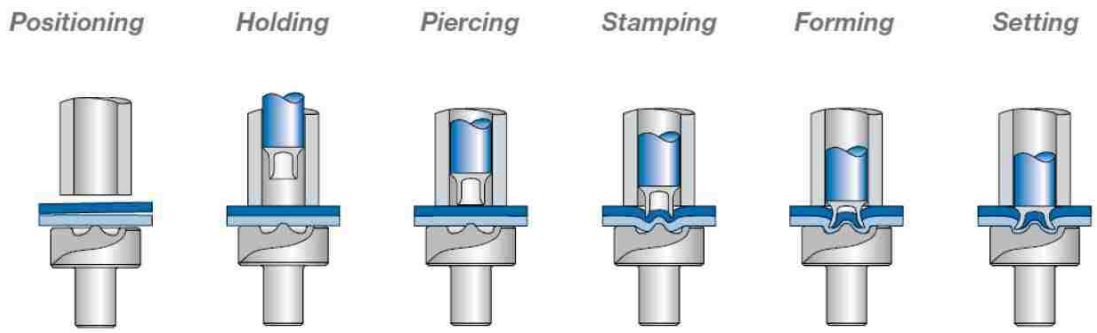

Figure 2-18: Schematization of the SPR joining technique [16].

SPR process can be dived into four main phases: Clamping, Penetration, Flaring and Compression [41].

During clamping, the rivet is pushed against a flat punch to clamp the sheets firmly, whereas in the second phase the rivet penetrates the top layer. In the expansion phase, the rivet deforms the bottom layer and expands itself following the shape of the die. This phase ensures the mechanical resistance of the joint due to a proper overlapping. Finally, in the last phase, the

punch pushes the rivet towards the two layers until the predetermined stroke or force is reached.

Atzeni, Ippolito and Settineri [41] found that the main independent variables affecting the mechanical characteristics of the joint are: the upper layer thickness and the rivet shape, then, less relevant, the die and the combination die-upper sheet. The upper layer thickness leads the type of joint failure. Indeed, a thinner material reaches the failure stress before the rivet pull-out, whereas a low yield stress of the top layer eases the pull-out of the rivet at lower loads. Moreover, the authors found that a good joint is obtained with proper expansion of the rivet and overlapping between the sheets. The above conditions are driven by the deformation characteristics of the bottom layer as well as the die and the rivet design.

An important tool to control the riveting quality during the process is the load-displacement diagram (Figure 2-19). By setting tolerances on the curve (usually based on experimental results) and using a pressure transducer and a linear displacement transducer, the end user is able to check each joining process. The graph, together with visual inspection and measurement of the rivet head position with respect to the upper sheet ("sunk", "even" or "jutting") gives a preliminarily quality control.

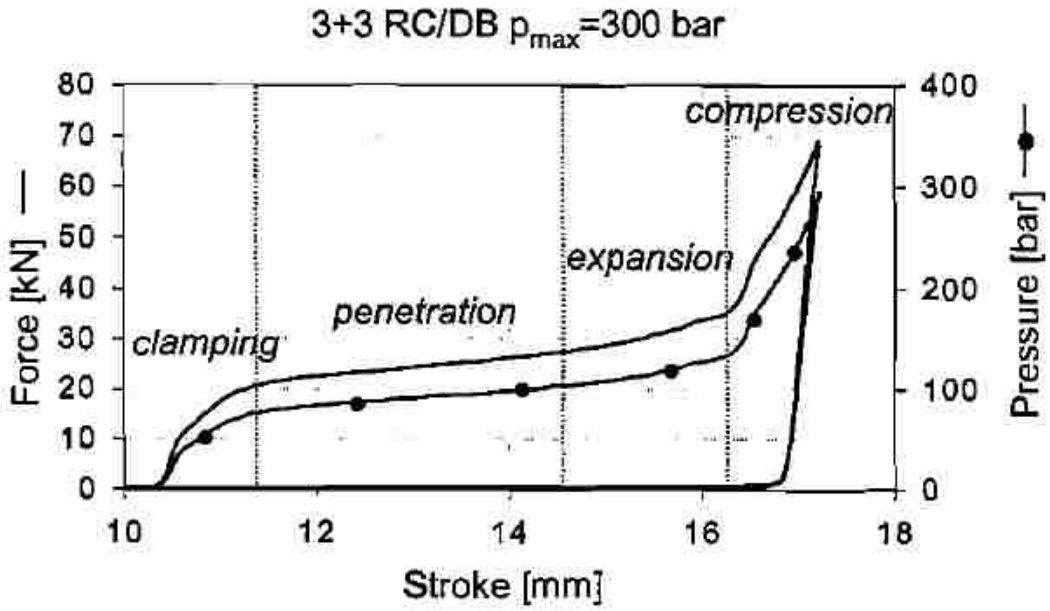

Figure 2-19: Self-Piercing Riveting joining sequence [40].

Figure 2-19 outlines a linear behavior with a steep slope in the clamping phase, whereas the penetration of the rivet into the sheets and the deformation of the lower sheet into the die are characterized by a gentler slope. In the expansion (or flaring), the rivet flairs with consequent higher gradient, that is even higher in the compression phase, where the rivet head compresses the top sheet until the curve reaches the stiffness of the tool-sheet-press system [42].

3. MATERIALS AND EXPERIMENTAL PROCEDURES

The current study is focused on determining the mechanical properties of the sandwich composite produced by MSC for automotive applications, in particular for sound-deadening panels with non-structural loads. Anyway, it must be highlighted that the sound-deadening performance of the material were already evaluated and tested by the manufacturer (Figure 3-2). For this reason, the tests performed in the current study focus on the mechanical properties necessary to replace the monolithic panels in the vehicle without considering sound attenuation. In this section, the procedures used to perform the tests are presented.

3.1 Materials: Quiet Aluminum® Sandwich Composite

The structure of the sandwich is represented in Figure 3-1, which displays the thin viscoelastic core in between of two aluminum layers. Two different sandwich composites were received from the MSC, differing from each other by the aluminum alloy used as skin:

- Two AA5754-O sheets and engineered polymer core (MSC Proprietary trademark). The designation "O" indicates that the aluminum alloys was subjected to annealing treatment.
- Two AA6061-T4 sheets and engineered polymer core. The designation "T4" indicates that the aluminum alloy was subjected to solid solution heat treatment and then natural aging.

Several panels with $300x300mm$ dimensions were received as samples to be tested. The panels were then prepared for the different tests.

Figure 3-1: Schematization of the sandwich structure. The thickness t_l is approximately $0.5\ mm$, whereas t_p is approximately $0.03\ mm$. [8]

As previously mentioned, Quiet Aluminum®, when replacing a steel component, is able to lead to weight reduction thanks to the aluminum skin. Furthermore, the sandwich composite avoid

the comprehensive use of damping patches and other components to reduce noise, vibration, and harshness. Indeed, the material itself is able to damp noise even more than the actual technology (Figure 3-2).

The manufacturer tested the same panel geometry with the following configurations: $1\ mm$ bare aluminum 5754-O, $1\ mm$ AA5754-O with damping patch, $1\ mm$ Quiet Aluminum® with Al 5754-O skin (examined in this study), $1.2\ mm$ Quiet Aluminum with Al 5754-O skin.

From the graph in Figure 3-2, it can be noticed that Quiet Aluminum® is more performant than both bare aluminum and the Al 5754-O with damping mastic patch. The NVH performance is evaluated based on the Sound Transmission Loss (STL), a logarithmic ratio that indicates the number of sound decibels that are stopped by a wall or other structure (in this case the different panels) at different frequencies. A difference of about 4 dB is found between Quiet Aluminum® and the actual solution at high frequencies and, slightly increasing the thickness of the skin alloy, the product gains an even higher STL in the low frequency range with respect to the $1\ mm$ composite. It is interesting to notice that, in accordance with Sargianis and Suhr's study [38], the material has a better NVH performance at higher frequencies with respect to the lower ones due to its low bending stiffness. Indeed, the very thin viscoelastic layer is not contributing in increasing bending flexural stiffness.

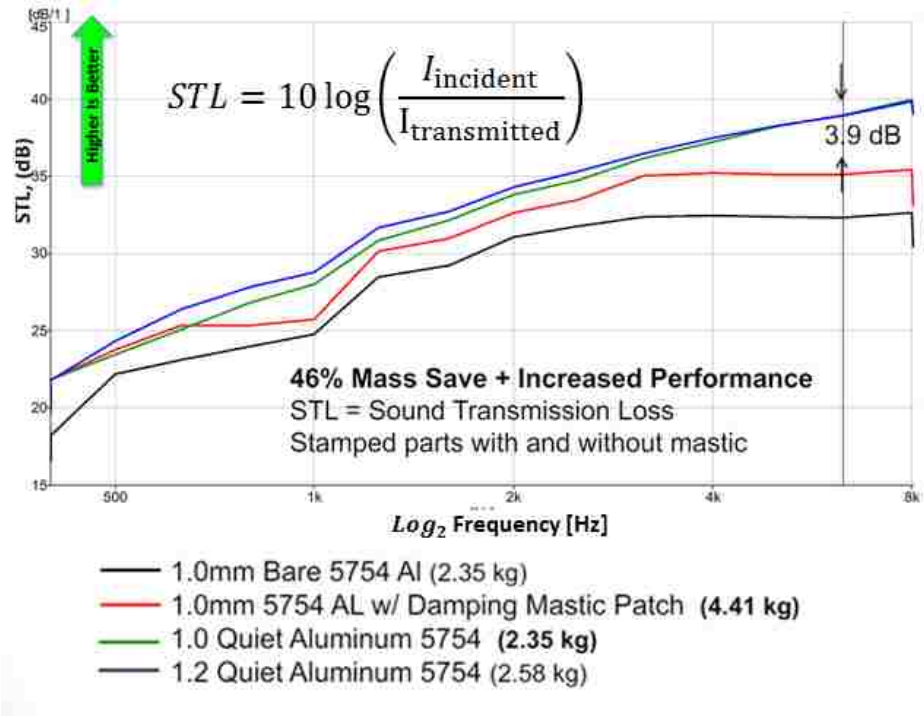

Figure 3-2: Sound Transmission Loss plot versus frequency for different materials [8].

Moreover, it is important to highlight the tremendous mass percentage save of the sandwich composite with respect to aluminum panel and damping mastic patch (46%). The sandwich structure leads to both NVH improvements and substantial weight reduction. Indeed, Quiet Aluminum® is able to save the whole weight of the damping components, since, with the same alloy thickness of the bare aluminum panel, the weight of the very thin viscoelastic layer is negligible ($2.35\ kg$ both for $1\ mm$ Bare 5754-O Al and $1\ mm$ Quiet Aluminum® 5754-O).

3.2 List of Experiments

The objective of this study is to determine the essential mechanical properties for non-structural application of Quiet Aluminum® for its implementation in the automotive sector in compliance with FCA requirements. In order to do so, several tests, described in Table 3-1, were performed. An overview on the different tests is given, whereas each testing procedure is deeply discussed in the relative section.

Table 3-1: Test matrix with the tests performed and the correspondent treatments on the examined materials.

Material	Treatment	Cross sectional analysis	Hardness	Roughness	Tensile	T-Peel	SPR
Quiet Aluminum® 5754-O skin	As Received	X	X	X	X	X	X
	$2\%\ strain$				X		
	$20min$@185°C				X	X	
	$2\% + 20min$@185°C				X		
Quiet Aluminum® 6061-T4 skin	As Received	X	X	X	X	X	X
	2% strain				X		
	1h@200°C		X		X	X	X
	$20min$@185°C				X		
	$2\% + 1h\ at\ 200$°C $+ 20min$@185°C				X		

First of all, metallography preparation on the samples in the as-received condition was carried out, then optical microscopy images and measurements were taken on the sandwich layers. Moreover, different treatments were applied to the sandwiches, especially for the tensile testing evaluation. The treatments were performed to simulate the stamping process, as well as to simulate the paint-bake cycle of the body in white. In fact, according to standard FCA procedures, the materials have to be tested in the as-received conditions to evaluate the properties of the material after production. Then in order to simulate the stamping process, tensile specimens are pulled up to a 2% strain and, after removing the load, they are pulled again until fracture occurs. In this way, it is possible to anticipate the tensile properties of a stamped component.

Another important process that has to be taken into account in designing is the paint-bake cycle. Indeed, all the panels, being part of the body in white, will undergo painting, that, according to standard FCA procedures, can be simulated with 185°C heat treatment on the material for 20 minutes by means of a furnace. In this study, both materials were tensioned after the simulated paint bake cycle. Moreover, AA6061-T4 (naturally aged designation) is often used due to high formability and good corrosion resistance together with strong mechanical properties. To further improve the strength and hardness of the material, automakers usually harden the alloy after the stamping process, so that the formability of the T4 designation can be exploited during

stamping while obtaining superior mechanical properties at the final stage. According to FCA procedure for the 6061-T4 aluminum alloy, heat treatment at $200℃$ for $1\ h$ was applied to the 6061-T4 sandwich prior to testing. Finally, a combination of the simulated stamping process and the paint bake cycle is tested for the 5754-O sandwich, whereas the Quiet Aluminum® samples with 6061-T4 skin were tested with combination of the simulated stamping process, hardening of the alloy and the paint-bake cycle simulation.

The tensile properties determined from the stress-strain curves are: Young's modulus, yield stress, tensile strength and elongation at fracture. Furthermore, strain hardening exponent and anisotropy values were computed. The latter were evaluated in the as-received condition for three specimen orientations to the rolling direction: $0°, 45°$ and $90°$.

In order to have reference information on the aluminum alloys used as skin, a hardness test was performed on the core section of the two sandwich composites in the as-received condition. Additionally, hardness on the core section of the 6061-T4 alloy after hardening treatment for $1\ h$ at $200℃$ was measured to preliminarily assess its effectiveness.

It is clear that the sandwich and the polymer in particular must be able to resist the relatively high temperatures mentioned without being affected. Consequently, a T-peel test was performed on the two sandwich composites in the as-received condition as well as after the simulated heat treatments. Another important evaluation is made by means of surface roughness measurements on the aluminum skins. It was decided to accomplish the test on both inner and outer metal surfaces of the as-received samples to deduce information on the manufacturing process. Indeed, from the literature ("*Adhesion in Metal/Polymer/Metal* " section), it is well known that roughness is one of the main parameters affecting adhesion.

Finally, since joining has tremendous importance in automotive industry, an evaluation on SPR joints between the sandwich composites (Quiet Aluminum® with 5754-O skin as-received and Quiet Aluminum® with 6061-T4 skin as received as well as after the hardening treatment) and High Strength Low Alloy steel (HSLA hot rolled with minimum $340\ MPa$ yield strength) was examined through Lap joints shear test and macro-graphic analysis, which is deeply discussed in "*SPR Joints Evaluation*".

3.3 Metallographic Sample Preparation for Cross-Sectional View

As seen in the literature, sandwich composites are often categorized by the volume fraction of their core. For this reason, as well as to obtain good images of the cross section, the samples were properly prepared and analyzed with optical microscope. It was chosen to use three specimens from three different sheets for both sandwich composites in the as-received condition. The samples, after being cut into squares $25x25mm$, were mounted (two parts of Epoxy Resin and one part of Epoxy Hardener) to obtain a maneuverable specimen and a parallel cross section to the grinding surface (Figure 3-3). Moreover, proper grinding and polishing of the sample was needed to obtain good microscopy images.

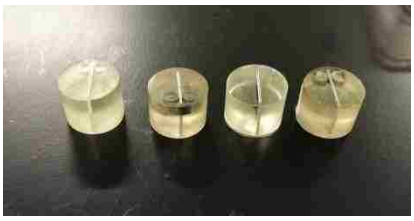

Figure 3-3: Samples were mounted in epoxy for cross-sectional view.

Grinding and polishing procedures need time and expertise, especially if the specimen is made of aluminum, which oxidizes very quickly. Nevertheless, also the polymer had to be carefully taken into account. Indeed, it was noticed that acetone affected the polymer, dissolving it. For this reason, acetone was avoided in the rinsing step between the different SiC grit papers, using ethanol instead. The different grinding steps included:

- SiC 320 grit and water as a lubricant
- SiC 400 grit and water as a lubricant
- SiC 600 grit and water as a lubricant
- SiC 800 grit and water as a lubricant

As previously mentioned, before changing the sand papers, the specimens were rinsed with ethanol to prevent oxidation and to remove all SiC particles of the previous grind papers.

It was important to push the specimen against the sand paper, especially during the first steps, maintaining it in a fixed position for few minutes and then turning it around $90°$ till completing

two rounds. After that, the specimens were polished with diamond suspension according to the following procedure:

- $3\mu m$ diamond suspension with polishing cloth
- $1\mu m$ diamond suspension with polishing cloth

Again, the specimens were rinsed with ethanol to remove all the particles and prevent oxidation. All this process was performed using the lapping/polishing machine available at the University of Windsor, shown in Figure 3-4.

Figure 3-4: UN I POL – 820 Metallographic Lapping /Polishing Machine available at the University of Windsor.

The measurements of the sandwich layers were taken with optical/laser microscope, which has $1\ \mu m$ resolution, taking three equally-spaced measurements on each one of the two aluminum skins as well as on the polymer core.

3.4 Hardness Measurement

Hardness, which is the resistance of the material to an indentation, is a characteristic of the material and it is evaluated measuring the depth or the area of a permanent indentation. In this study, hardness on the core section of the sandwich was evaluated to have a reference of the aluminum alloy skin characteristics. For this reason hardness was measured on the core section of the alloys used in the sandwich in the as-received condition, as well as on 6061-T4 alloy after hardening treatment of $1\ h$ at $200°C$. Three specimens from different batches were chosen for each material.

In this study, due to the presence of a very thin sample (about $1{,}06\ mm$ total thickness) micro-Vickers hardness test method was used. The machine used is the Buehler Micromet II Model

MHT-1B Micro Hardness Tester with a square based pyramid diamond indenter available at the University of Windsor.

In order to acquire reliable results, proper samples had to be prepared. Consequently, three squared specimens ($25x25mm$) were cut from the panels received for each of the three materials to be tested. The specimens were mounted and grinded to remove the biggest scratches which could affect the results. After this, the diagonals of the square indentation were measured to the nearest $0.5\ \mu m$ with the optical microscope of the tester and then, hardness was computed following the guidelines of ASTM E384 [43], using $25\ gf$ load and $12\ s$ dwell time.

The results computed after the tests were also compared with the reference values available in the materials database [16]. Finally, an optical/laser microscope image was taken on each of the three sandwich composites to show the indentation geometry on the core section of the aluminum skins.

3.5 Tensile test

Tensile is one of the most important tests when characterizing a material. In this study, the tensile properties of the sandwich composite are determined not only in the as-received condition, but even after stamping and paint-bake cycle simulations, respectively 2% pre-applied strain and $20\ min$ at 185℃, as well as after the hardening procedure applied to the 6061-T4 sandwich ($1\ h$ at 200℃). The mechanical properties determined in this study are:

- Young's modulus, yield strength, Ultimate Tensile Strength (UTS), Uniform Elongation (UE) and elongation at fracture retrieved from the stress-strain curves.
- r-values for the different specimen orientations, average vertical anisotropy r_m, and planar anisotropy Δr.
- Strain hardening exponent (n-value) and strength hardening coefficient K.

Table 3-2 lists the properties examined together with the different treatments applied on the sandwich composites. MTS Universal Machine for Tensile Test Model 43 (shown in Figure 3-5, $150\ kN$ load capacity and pneumatic interchangeable serrated wedges grips for testing either flat specimen with $0-25\ mm$ range) and $50\ mm$ Axial Mechanical Extensometer were used for

the experiments, then “MTS TW Elite” software connected to the machine recorded the load, displacement and strain data. The test was divided into two speed regions according to FCA internal procedures. Lower strain rate is required in the elastic region ($\dot{e_e} = 0.0025\frac{1}{s}$ is used in Equation 3), whereas higher speed is admitted in the plastic field ($\dot{e_p} = 0.003125\frac{1}{s}$ is used in Equation 4). It was decided to extend the lower speed region till reaching $2\ \%$ strain to obtain more data in the elastic region as well as close to yield and to have common procedure for both materials. The cross-head speeds relative to each strain rate were calculated through Equation 3 and Equation 4.

Equation 3: Cross-head speed equation up to 2% strain [16].

$$V_c = \dot{e_e} * 60 * l_0 = 0.75\ \frac{mm}{min}$$

Equation 4: Cross-head speed equation from 2% strain till fracture [16].

$$V_c = \dot{e_p} * 60 * l_0 = 9.375\ \frac{mm}{min}$$

Where the initial gauge length is $l_0 = 50mm$ and $\dot{e}$ is the strain rate. The results obtained from the tests were compared with the literature values available in Table 2-2, which shows the values of the monolithic aluminum alloys. Quiet Aluminum® was expected to behave as the monolithic of the same alloy since volume fraction of the viscoelastic layer can be considered negligible. Nevertheless, differences in the results could occur due to the fact that the monolithic alloys used as reference are not coming from the same supplier.

Figure 3-5: MTS Model 43 Universal Tensile Testing Machine and MTS Axial Extensometer $50\ mm$ gauge length [44].

Table 3-2: Tensile Test Matrix.

Material	Treatment	Stress-strain parameters	Anisotropy value $0°\ to\ RD$	$45°\ to\ RD$	$90°\ to\ RD$	Strain Hardening Exponent
Quiet Aluminum® 5754-O skin	As Received	X	X	X	X	X
	2% pre-applied strain	X				X
	$20min$@185°C	X				X
	2% strain+ $20min$ at 185°C	X				X
Quiet Aluminum® 6061-T4 skin	As Received	X	X	X	X	X
	2% pre-applied strain	X				X
	1h at 200°C	X				X
	$20min$ at 185°C	X				X
	2% strain + $1h\ at$ 200°C + $20min$ at 185°C	X				X

3.5.1 Specimens Preparation

In order to obtain reliable results, proper specimens were needed. After a comparison between the ASTM International (American Society for Testing and Materials) standards for tensile testing (ASTM E8/E8M [45]), strain hardening exponent (ASTM E646 [46]) and anisotropy values (ASTM E517 [47]) the specimen geometry shown in Figure 3-6 was selected. Moreover, taking into account the plastic strain ratio evaluation, three specimens with $0°, 45°$ and $90°$ orientation to the Rolling Direction (RD) were needed.

Computer-Aided Design (CAD) drawings from SolidWorks software were used to provide the cutting machine with the correct file format. The software permitted to draw different layouts (Figure 3-7 and Figure 3-8) based on the received panels dimensions (approximately $300x300mm$ each). Obviously sufficient tolerance space, $6\,mm$, was left in between of the specimens not to be damaged during cutting. After that, high precision cutting method had to be chosen to obtain the specimens. Computer Numerical Control (CNC) milling machine available at the university was used to prepare the tensile specimens, but unfortunately, the results were not satisfying. For this reason, water jet cutting method was adopted, with the big advantage of avoiding heat affected zone in the material, due to the small heat generation, which is absorbed by the water. Finally, high precision specimens were grinded (400 SiC grit sand paper) to remove any notch at the edges. Figure 3-9 shows a set of the specimens after cutting.

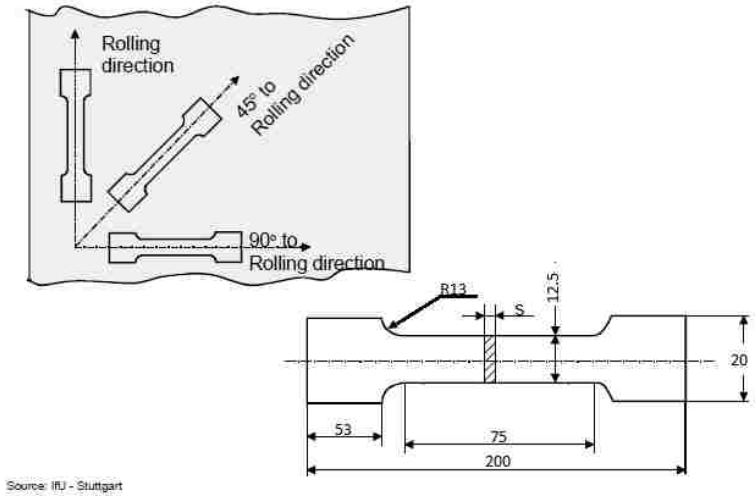

Figure 3-6: Tensile specimens geometry, dimensions and orientations [13].

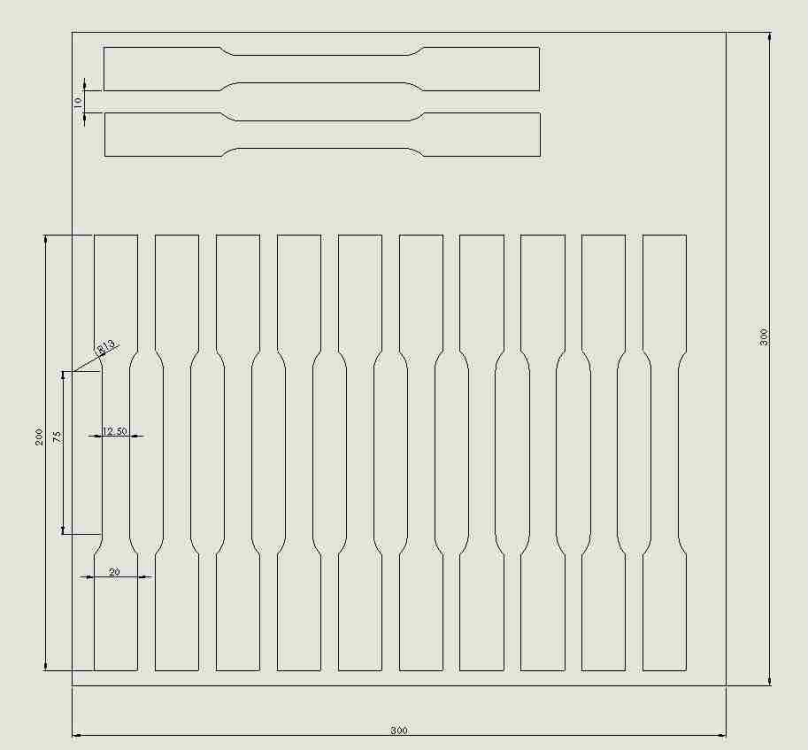

Figure 3-7: Specimens layout 1 prepared with SolidWorks software.

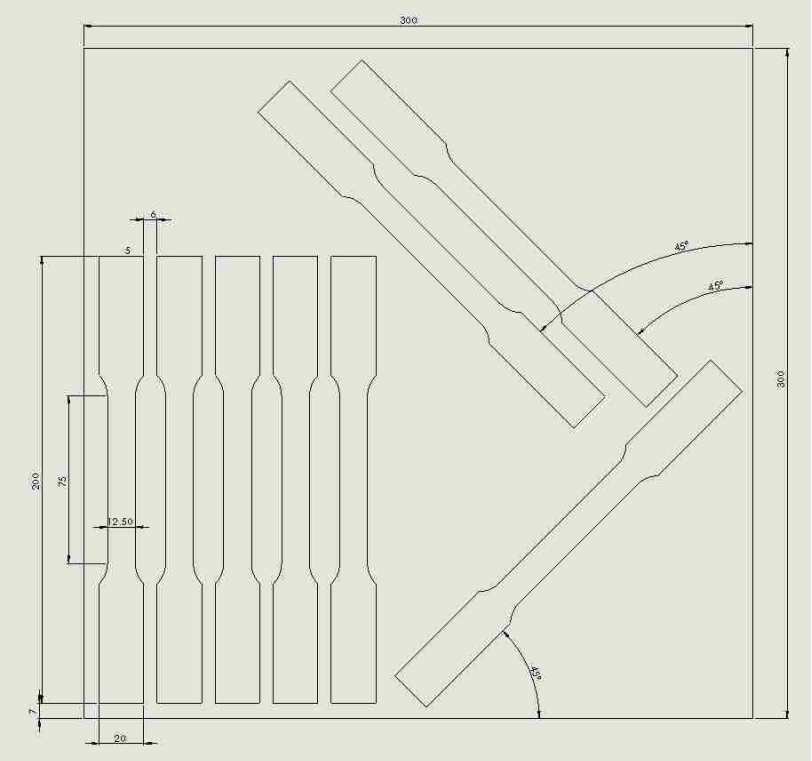

Figure 3-8: Specimens layout 2 prepared with SolidWorks software.

Figure 3-9: Specimens cut with water jet technology.

3.5.2 Mechanical Properties

As previously mentioned, in order to simulate the stamping process, some specimens were pulled up to 2% strain, whereas the paint-bake cycle and the hardening treatment on the 6061-T4 alloy, respectively $20\ min$ at $185℃$ and $1\ h$ at $200℃$, were performed with the ovens available at the University of Windsor. The guidelines of ASTM E8/E8M standard [45] were followed so that Young's modulus, yield strength, elongation at fracture, Ultimate Tensile Strength (UTS) and Uniform Elongation (UE) were extrapolated from the stress-strain curves of the specimens with $0°$ to the rolling direction. The abovementioned parameters were evaluated for each of the following:

- Quiet Aluminum® with 5754-O skin, as-received
- Quiet Aluminum® with 5754-O skin, with pre-applied 2% strain
- Quiet Aluminum® with 5754-O skin, after paint-bake cycle simulation ($20\ min\ at\ 185℃$)
- Quiet Aluminum® with 5754-O skin, with pre-applied 2% strain and, then, treated for $20\ min\ at\ 185℃$ to simulate paint-bake cycle
- Quiet Aluminum® with 6061-T4 skin, as-received

- Quiet Aluminum® with 6061-T4 skin, with pre-applied 2% strain
- Quiet Aluminum® with 6061-T4 skin treated for $20\ min\ at\ 185℃$ to simulate paint-bake cycle
- Quiet Aluminum® with 6061-T4 skin, with pre-applied 2% strain, then hardened at $200℃$ for $1\ h$ and, finally, treated for $20\ min\ at\ 185℃$ to simulate paint-bake cycle

The results were retrieved averaging the data obtained from five different specimens. Before starting the test, a micrometer was used to record width and thickness of each specimen to compute the cross sectional area. The Universal Tensile Machine and the axial extensometer provided the load and the engineering strain, *e*, in Excel format file, then MatLab software was used to elaborate the graphs and the related parameters with high computation performance.

The MatLab script written for the current study calculates the elastic modulus retrieving the slope of a linear approximation of the data in the elastic region. Instead, according to the standard [45] the yield strength was evaluated in two different ways, depending on the characteristic stress-strain curve of the two materials examined. In fact, as seen in the literature section "*5xxx and 6xxx Aluminum Alloys*", yield point elongation was expected from the sandwich with 5754-O aluminum alloy skin, whereas uniform strain hardening was expected on the sandwich with 6061-T4 skin. In case of a uniform stress-stress curve, offset yield, $R_{p0.2}$, calculated with an offset of $0.2\ \%$ strain was used. This means that a parallel line to the elastic region of the real curve was drawn starting from $0.2\ \%$ strain, then, the intersection between the test curve and the drawn line was recorded as $R_{p0.2}$. In case of discontinuous yielding, Upper Yield Point (UYP) and Lower Yield Point (LYP), if present, have to be recorded in the following way: UYP is the stress corresponding to the maximum force at the onset of discontinuous yielding, whereas LYP is the minimum stress occurring during discontinuous yielding. Yield point elongation was recorded as the length in which the stress-strain curve appears flat. As far as tensile strength is concerned, the stress corresponding to the maximum force sustained during the test divided by the original cross section area of the specimen was recorded as Ultimate Tensile Strength (UTS), whereas the strain corresponding to the maximum force collected was registered as Uniform Elongation. Instead, elongation at fracture comprehends both elastic and plastic engineering strain recorded till specimen fracture. The stresses and the strains were approximated to the nearest unity $1\ MPa$ for stresses, and to the nearest $1\ \%$ for strains.

3.5.3 Strain Hardening Exponent "n"

The stress-strain curve region in which plastic deformation occurs is called flow curve. In this region, the material is subjected to work hardening, but there is also a reduction in area due to the elongation (constant volume). The flow stress, k_f, is considered uniform when the positive effect of the work hardening is compensating the reduction of area (uniaxial state of stress) and can be described by Ludwik-Hollomon's equation (Equation 5):

Equation 5: Ludwik-Hollomon's flow stress equation [13].

$$k_f = K\varepsilon^n$$

Where the constant K is the strength hardening coefficient, ε is the true strain and n is the strain hardening exponent. The coefficient K and the n-value were calculated following ASTM E646 standard guidelines [46].

Based on FCA internal procedures, it was decided to compute the hardening parameters in two strain ranges, which are 4-6 % and 10%-20/UE (Uniform Elongation is used if it is lower than 20% strain).The two parameters were computed for every condition mentioned in "*Mechanical Properties*" section.

3.5.4 Anisotropy "r" Value

It is well known that anisotropy properties are significantly important for metal sheets used in the automotive industry, but more in general, wherever stamping process occurs. Indeed, the mechanical properties of the material vary in relation to the orientation with respect to the rolling direction. Hence it is useful to determine the anisotropy property of the material. The guidelines of ASTM E517 standard [47] were followed to compute: average vertical r-value and the earing tendency (planar anisotropy Δr) for the two sandwich composite in the as-received condition (Quiet Aluminum® with 5754-O skin and with 6061-T4 skin).

The testing procedure consisted in:

- Measuring the specimen cross sectional area.
- Starting the test, using the same speed fields of the tensile test.
- Forcing the test to stop at 10% strain, in this way, it was possible to measure the change in thickness and compute the plastic strain ratio, r, according to the standard [47].

As previously mentioned, three specimens per each orientation were needed ($0°, 45°, 90°$ to the Rolling Direction) to compute the average vertical anisotropy, r_m, and the earing tendency, Δr.

A high resistance of the material to thinning will produce a vertical anisotropy value close to unity or higher, which is optimal in deep-drawing process due to a consequently large limiting draw ratio [13]. Instead, the planar anisotropy is useful to predict where earing will occur. In fact, for positive planar anisotropy Δr value, earing is expected in $0°$ and $90°$ direction, whereas for negative values earing is expected at $45°$ to RD.

3.6 T-peel Test

The most common test used to assess adhesion strength in laminates, and in general adhesive bonds between flexible adherends, is the T-peel test. Sufficient flexibility is required to the aluminum alloys skins since they have to bend through $90°$ without cracking or breaking. The test consists in simple traction of two adherends strips without special fixture and without external devices such as extensometers. The load recorded by the tensile machine and its cross-head position is sufficient to determine the peel resistance. Figure 2-15 illustrates how the laminate is gripped onto the tensile machine and its concept.

The material samples examined in this study are:

- Quiet Aluminum® with AA5754-O skin, as-received
- Quiet Aluminum® with AA5754-O skin, after paint-bake simulation ($20\ min$ at $185℃$)
- Quiet Aluminum® with AA6061-T4 skin, as-received
- Quiet Aluminum® with AA6061-T4skin, after hardening treatment ($1\ h$ at $200℃$)

In this way, it was possible to evaluate the peel resistance of the sandwich in the as-received conditions as well as after the paint-bake cycle. Moreover, the adhesive properties of the viscoelastic core were evaluated after the hardening procedure with its considerably high temperature and long exposure time. Five samples were tested for each condition, following ASTM D1876 guidelines [48], which required $254\ mm/min$ speed and $25x305\ mm$ strips specimens. Note that the specimens were cut from the received panels with a shear cutting machine available at the University of Windsor. It was necessary to manually separate the first $76\ mm$ to properly grip the specimen, since the panels received were fully bonded.

The outcome of the test, apart from the load-displacement graphs, is the average peel strength, a_s , described in Equation 6:

Equation 6: average peel strength according to ASTM D1876 [48].

$$\alpha_s = \frac{P}{w}$$

where P $[N]$ is the average load and w $[cm]$ is the bond width. The average load was calculated according to the ASTM D1876 standard by picking ten load values after the initial peak every $25\ mm$ of cross-head position, which correspond to $12.5\ mm$ of bond separation. Then, the values were averaged and divided by the bond width, was previously measured using a caliper (three equally spaced measurements along the specimen). The width measurements were averaged and approximated to the nearest $0.01\ mm$. Furthermore, the failure mode was reported, distinguishing between apparent adhesive failure, cohesive failure and mixed mode failure, previously described in "*Adhesion in Metal/Polymer/Metal* " section.

Finally, the results got from the experiments were compared with the specific FCA requirement for laminates with non-structural loads, which presents a minimum range of $10 - 15\,\frac{N}{cm}$.

3.7 Roughness Measurements

Surface roughness is another valuable parameter measured in this study. Referring to the "*Adhesion in Metal/Polymer/Metal* " section, it was possible to understand the main role roughness plays in adhesion joints. For this reason, the metal surfaces of the sandwich composites in the as-received condition were accurately prepared to be examined. Three specimens of approximately $25x25\ mm$ dimensions from different batches were cut for each of the two sandwich composites, then the whole set was submerged overnight in acetone to dissolve the polymer (Figure 3-10).

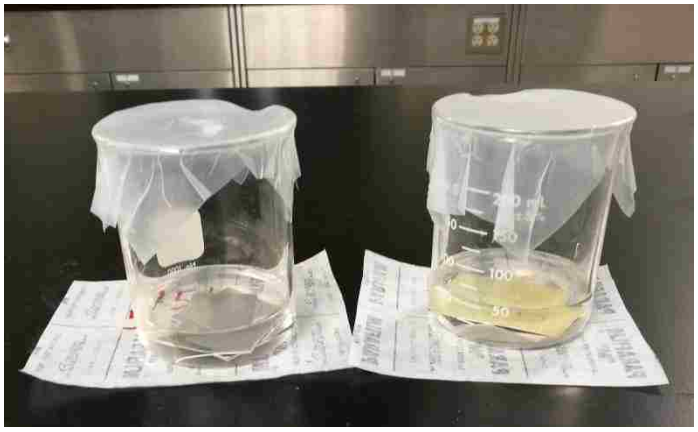

Figure 3-10: Roughness specimens submerged into acetone to dissolve the polymer core.

Once separated, roughness was examined in both inner (surface that faces the viscoelastic core) and outer (visible surface) side. Then, three measurements on each surface were taken with the optical microscope available at the University of Windsor (examined area $0.270\ mm^2$). In this study, the arithmetical mean height, R_a, and maximum profile height, S_z, were retrieved together with their standard deviation ($n = 9$). Moreover, 3-D images of the surface were taken on the inner and outer surface of the two Quiet Aluminum® sandwich composites. Equation 7 describes the maximum profile height parameter:

Equation 7: Maximum profile height [48].

$$S_z = S_p + S_v$$

where S_p and S_v are respectively the maximum height and the absolute value of the largest pit within the defined area.

In order to characterize the Quiet Aluminum® surface topography and measure the surface roughness, WYKO NT 1100 optical surface profilometer was used. The profilometer exploits the vertical scanning interferometry (VSI) mode to obtain the results. Unfiltered white light reflected from a reference mirror combines with the light reflected from the sample to produce interference fringes where the fringe with best contrast occurs at best focus. The device then measures the degree of fringe (produced by the reflection of light from the sample and the unfiltered white light from a reference mirror) modulation to acquire the surface profile.

3.8 SPR Joints Evaluation

As already said, SPR can be used to join two or more sheets of different materials. In the current study, Quiet Aluminum® samples were joined with a structural steel alloy, hot rolled High Strength Low Alloy steel with minimum $340\ Mpa$ yield strength ($1.8\ mm$ thickness). This alloy is popular because is produced by almost all steel mills and is available at reasonable price. Moreover, it is very lean in alloying elements, and therefore easy to weld into vehicle body.

3.8.1 SPR Joints Setup and Macro-Graphic Requirements

The SPR joints, as well as a preliminarily development study, were performed at Stanley Engineered Fastening facility, which has over 40 years of experience in fastening and assembly technologies.

Usually, the softer material in SPR joints is chosen to be the bottom layer, but in this study the HSLA steel, which is harder, is used on the die side, to have a thicker portion of material undergoing severe plastic deformation. A 33% thickness ratio between the bottom layer and the total thickness of the joint is the minimum value according to standard internal procedures [49]. It can be noticed that, if the sandwich is used on the bottom (joint 2 in Table 3-3), from the rivet perspective the lower layer is just half of the sandwich thickness. It must be highlighted that $t_{bottom} = 0.53\ mm$, referred to joint 2 in Table 3-3, is an approximate average of half the thickness for both sandwich composites. This configuration has insufficient material portion (23%) to undergo severe deformation. Instead, by using Quiet Aluminum® samples on the top (joint 1 in Table 3-3), the bottom layer portion is above the minimum value, with 63% thicknesses ratio.

Table 3-3: SPR joint matrix for layout evaluation.

Joint	Thickness t_{top}	Material	Thickness t_{bottom}	Material	Total thickness t_{tot}	Thicknesses ratio t_{bottom}/t_{tot}
1	1.06	Quiet Aluminum®	1.80	HSLA340	2.88	63%
2	1.80	HSLA340	0.53	Quiet Aluminum®	2.33	23%

The rivets used for the joints (Ø $5.3\ mm$ x $5.0\ mm$ lenght and Ø $5.3\ mm$ x $5.5\ mm$ lenght) have hardness equal to $480 \pm 25\ HV$ and a $Tin/Zinc$ alloy mechanical plating, which can resist the paint-bake cycle. Then, the component is e-coated after assembly. In this way, atmosphere cannot reach the Steel/Aluminum connection, avoiding electrochemical compatibility issues. The technical parameters used by the SPR gun such as riveting speed, clamp force, adhesive clamp cannot be mentioned for confidentiality reasons.

At the company's facility it was possible to measure the head flushness of the rivet head with respect to the upper sheet. Moreover, a macro-graphic examination on the joint cross section was carried out for each joint configuration by taking optical microscope measurements. Then, the results were compared with the main FCA requirements for SPR joints, shown in Figure 3-11. The joint should fulfill:

- Residual thickness $r_t > 0.2\ mm$ to avoid piercing of the bottom layer.
- Interlocking $i_{dx} = i_{sx} \geq 0.2\ mm$ to ensure proper mechanical interlocking and symmetry of the rivet.

The head flushness was measured with a digital dial gauge approximating the values to the nearest $0.01\ mm$. The values were taken from the undeformed surface of the top layer to the rivet head as shown in Figure 3-12. Moreover, no plate piercing is permitted due to corrosion, mechanical interlocking and appearance problems.

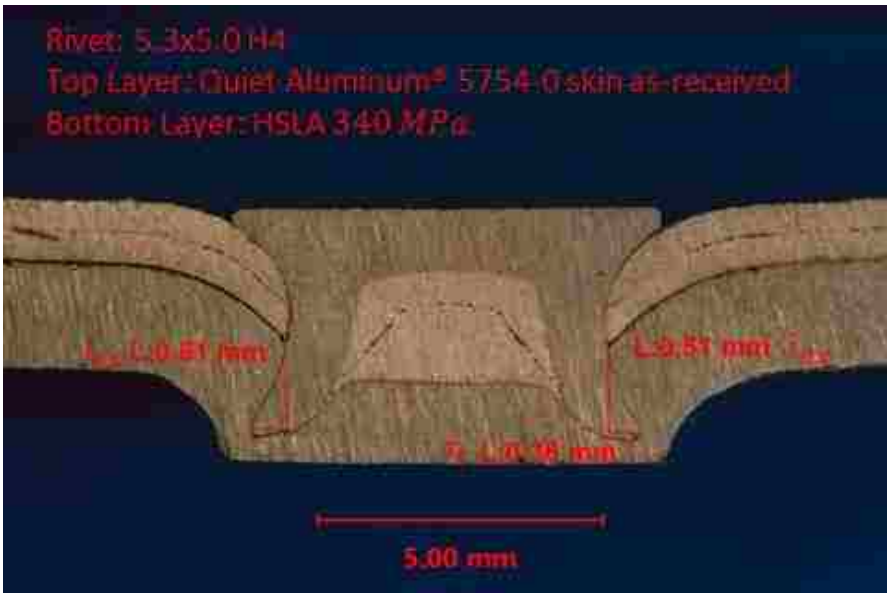

Figure 3-11: Macro-graphic appearance: parameters examination.

Figure 3-12: Example of the rivet head measurement using connected dial gauge.

3.8.2 Lap Shear Test on SPR Joints

In order to evaluate the strength of the SPR joint between the HSLA $340\ MPa$ steel alloy and the sandwich composites, lap shear tests were performed with the layout described in Figure 3-13. As previously discussed, the sandwich was positioned on top of the structural steel. The specimen strip dimensions were chosen according to FCA internal standards for lap shear tests ($100x40\ mm$ strips with $25\ mm$ overlap) [16]; consequently, the strips were cut with shear machine before joining. The test consists in pulling the two ends of the specimen with constant crosshead speed $V_c = 10\ mm/min$ till reaching failure of the joint. The universal tensile machine available at FCA's facility was used for testing (Instron 3382 Floor Model Universal Testing System with $100\ kN$ load capacity). Then, the force-displacement curve was retrieved from the output of the machine software. Average and relative standard deviation were computed for each joint configuration (ten specimens each). Quiet Aluminum® with 5754-O skin as received, Quiet Aluminum® with 6061-T4 skin as received, as well as after the hardening procedure ($1\ h\ at\ 200$℃) were joined with the HSLA steel. The experiment is considered acceptable if the base material fails and no failure due to deformation of the rivet head or button is allowed.

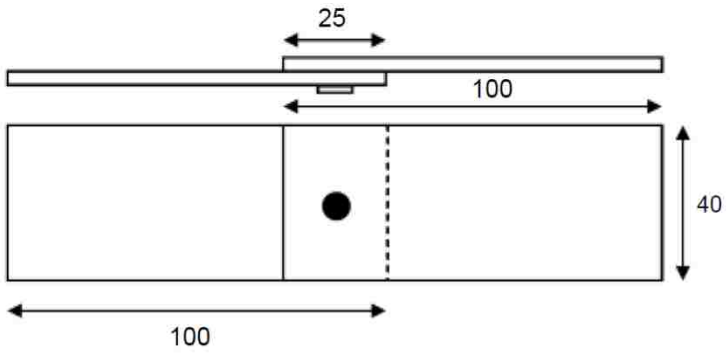

Figure 3-13: Lap shear specimen layout and dimensions for SPR joints [16].

4. RESULTS AND DISCUSSIONS

In this section, the Quiet Aluminum® properties obtained from the current study are presented and discussed following the methodology procedures described in the previous chapter.

4.1 Cross Sectional Microstructure

Thanks to the cross section images taken on the sandwich samples, it was possible to measure the volume fraction of the polymer core and the dimensions of the layers. (Figure 3-1 gives a schematization of the sandwich structure). Figure 4-1 and Figure 4-2 show the optical microscope images with measurements, whereas Table 4-1 summarizes the results retrieved from the whole set of samples.

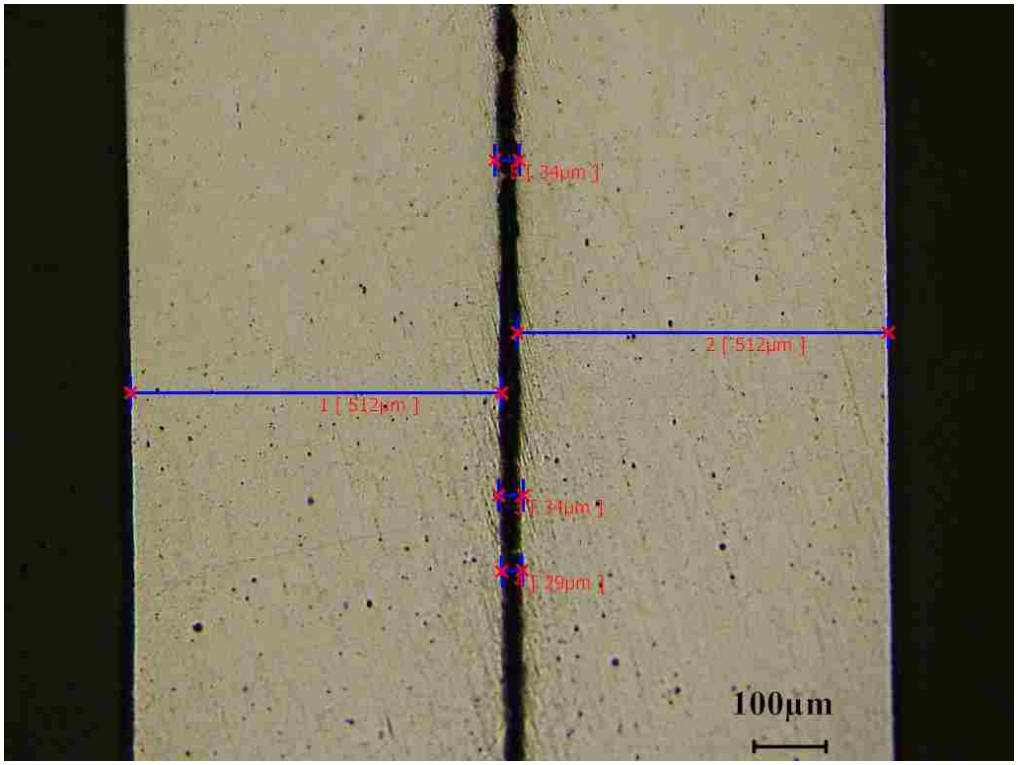

Figure 4-1: Optical microscope image on the cross section of Quiet Aluminum® with AA5754-O skin. The cross section comprehensive of measurements on the aluminum and polymer layers highlights a very thin and homogeneous polymer core all over the aluminum surface.

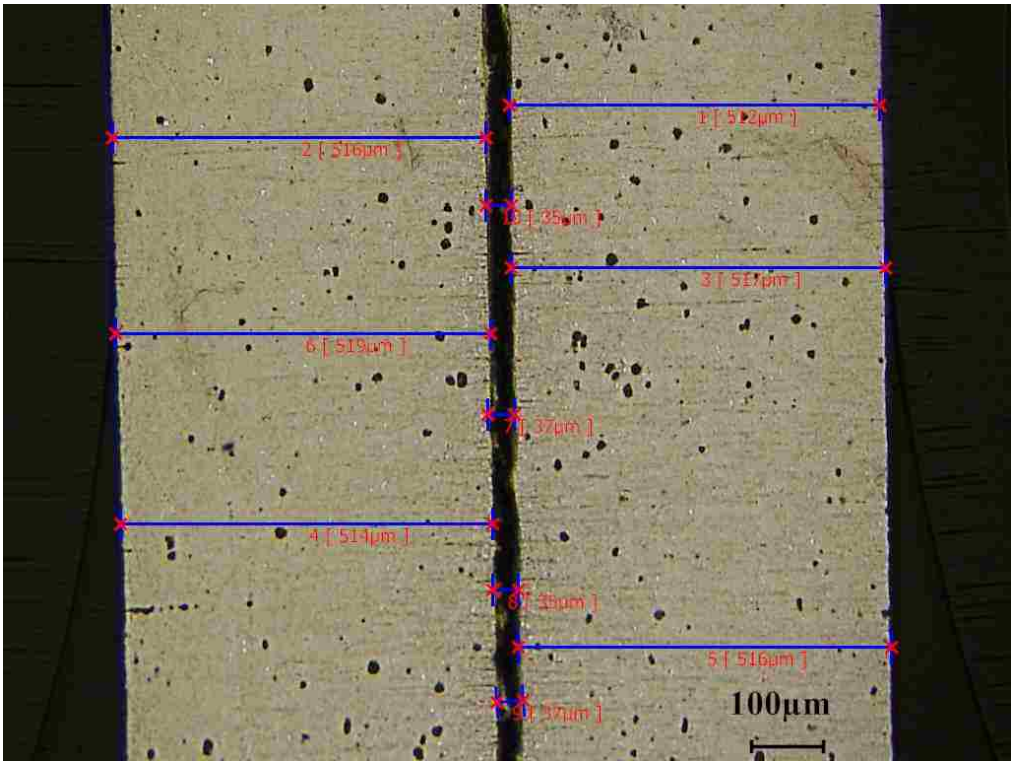

Figure 4-2: Optical microscope image on the cross section of Quiet Aluminum® with AA6061-T4 skin. The cross section comprehensive of measurements on the aluminum and polymer layers highlights a very thin and homogeneous polymer core all over the aluminum surface.

Table 4-1: Measurements of the different layers on Quiet Aluminum® with AA5754-O and AA6061-T4 skin. Note the very thin viscoelastic layer t_p in both materials.

$\boldsymbol{Layer/Sample}$	Quiet Aluminum® with 5754-O skin $[\boldsymbol{\mu m}]$	Quiet Aluminum® with 6061-T4 skin $[\boldsymbol{\mu m}]$
t_1	511 ± 4	514 ± 3
t_2	510 ± 4	512 ± 3
t_p	28 ± 6	31 ± 4
t_{tot}	1051 ± 7	1059 ± 10

It can be noticed that the two materials have very similar thickness, even though the sandwich with 6061-T4 skin can be considered slightly thicker $t_{tot} = 1.06\ mm$ against $t_{tot} = 1.05\ mm$ for the sandwich with AA5754-O. The polymer volume fraction is $t_p = 2.7\ \%$ of the total thickness for Quiet Aluminum® with 5754-O skin and $t_p = 2.9\ \%$ for Quiet Aluminum® with

6061-T4 skin. The results gave consistent evidence on the nature of the sandwich composites examined. Indeed, as previously mentioned in "*Metal/Polymer*/Metal Sandwich Composites" section, laminates with polymer volume fraction lower than 20% are classified as sound-deadening laminates. Moreover, the cross section images highlighted a homogeneous and uniform polymer layer, spread all over the aluminum skin surfaces. Furthermore, the differences between the two aluminum layers are negligible in both sandwich composites.

4.2 Hardness Measurements

In the current study, the experimental hardness measurements got from the Quiet Aluminum® samples were compared with the monolithic values available in FCA material database (Table 2-3). The measurements, taken on the core section of the aluminum alloy skin, are presented in a clustered column chart in Figure 4-3.

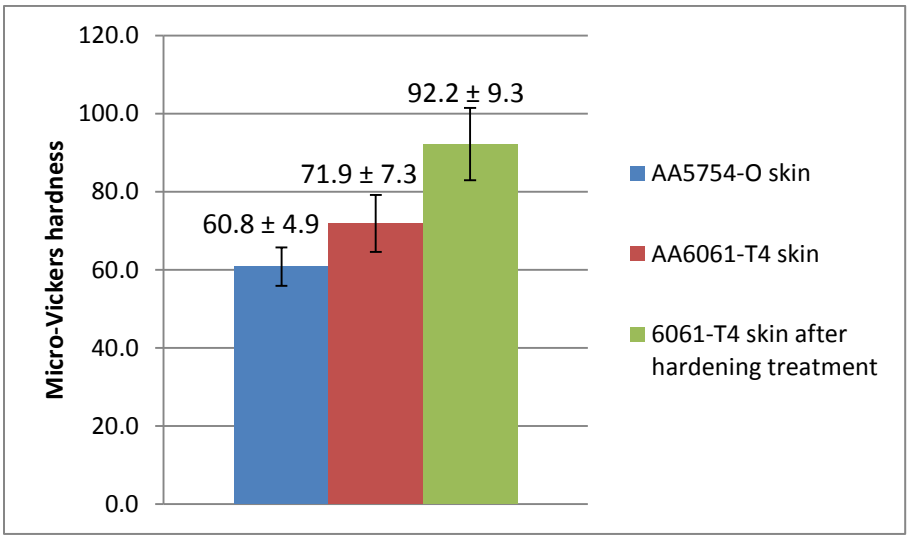

Figure 4-3: Clustered chart with Micro-Vickers hardness measurements and the relative standard deviation bars for the different materials tested.

The AA5754-O skin of the sandwich, with $HV = 60.8$, appeared to be the softest material, whereas the AA6061-T4 skin after the hardening treatment, with $HV = 92.2$, was the hardest. Obviously the intermediate hardness value belonged to the as-received sandwich with 6061-T4 skin ($HV = 71.9$).

The values of the as-received samples are also very similar to the literature ones, $HV = 62$ for monolithic AA5754-O and $HV = 75$ for AA6061-T4. Instead, the hardness difference for the

treated sandwich with 6061-T4 skin concerning the monolithic AA6061-T6 was relevant, respectively $HV = 92.2$ and $HV = 107$. The outcome was predictable since the skin of the sandwich was not solution heat treated and then artificially aged as prescribed by the T6 designation (the polymer would not be able to withstand such temperatures).

The alloys used in the Quiet Aluminum® showed similar values to the monolithic ones. Furthermore, the hardening treatment on the sandwich with 6061-T4 skin was able to enhance precipitation hardening, increasing the hardness of 28% with respect to the as-received condition. Nevertheless, the obtained value was not sufficient to reach the hardness of a proper T6 temper.

Figure 4-4, Figure 4-5 and Figure 4-6, display the indentation on each of the three materials tested.

Figure 4-4: Micro-Vickers indentation on the AA5754-O skin with typical square indentation and diagonals.

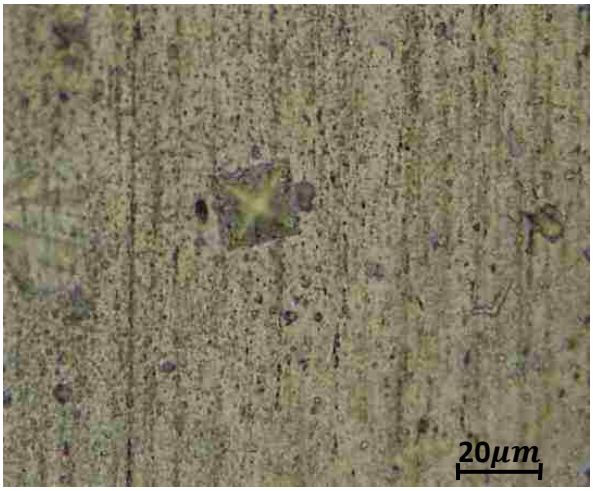

Figure 4-5: Micro-Vickers indentation on the AA6061-T4 skin with typical square indentation and diagonals.

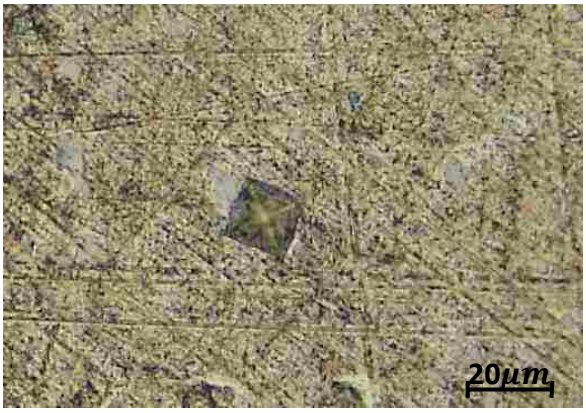

Figure 4-6: Micro-Vickers indentation on the AA5754-O skin with typical square indentation and diagonals.

In all images, the square of the diamond pyramid and its diagonals could be distinguished, showing a homogeneous shape and a well formed indentation. By comparing Figure 4-5 and Figure 4-6, the indentation on the hardened 6061-T4 aluminum alloy is significantly smaller than the as-received one, with consequent higher hardness. This gives an evidence of precipitation hardening phenomena on the material. Instead, it was not possible to make a visual comparison between the indentation on the 5754-O skin and 6061-T4 skin, both in the as-received condition (respectively Figure 4-4 and Figure 4-5), due to very similar diagonal dimensions. Indeed, the average diagonal of the two samples differed just from few microns (about $3\ \mu m$ measured with the optical microscope tool of the hardness tester).

4.3 Tensile Test

4.3.1 Mechanical Properties

In this section, all the tensile testing results are presented following the procedure illustrated in the "*Tensile test*" methodology section. It is important to mention that the sandwich composites were considered to behave as the respective monolith due to negligible volume fraction of the viscoelastic core. Indeed the rule of mixtures was found to be valid even for sandwich composites [22], [23].

First of all, the stress-strain curves and the relative mechanical properties for Quiet Aluminum® with 5754-O skin in the different conditions tested are presented (values shown in Table 4-2). The as-received samples showed the same stress-strain curve shape depicted in the "*5xxx and 6xxx Aluminum Alloys*" section, with discontinuous yielding ("top of knee" UYP) and serrated stress-strain curve (Figure 4-7 and Figure 4-8). The values are reasonably similar to the monolithic reference, taking into account that the sandwich and the reference materials were manufactured by different suppliers. For example, by comparing the as-received data in Table 4-2 with the monolithic values available in Table 2-2, the sandwich with 5754-O skin in the as-received condition presented higher yield strength and UTS, as well as slight lower elongation ($R_{p0.2} = 125, UTS = 237\ MPa\ and\ 18\%$ strain at fracture). It must be taken into account that the materials were rolled and so could have been stretched during the sandwich manufacturing process. After the stamping simulation (stress-strain curves in Figure 4-9 and Figure 4-10), the material did not exhibit discontinuous yielding due to the pre-applied plastic deformation, with consequent higher yield stress, evaluated with the offset method ($R_{p0.2} = 152\ MPa$). Note that the pre-applied strain of 2% is not counted in the graph and the original undeformed cross section area was considered for the results computation.

Instead, the samples treated in the oven for $20\ min\ at\ 185°C$ to simulate the paint bake-cycle (Figure 4-11 and Figure 4-12), again presented a discontinuous yielding phenomenon, with a $10\ MPa$ lower UYP value than the as-received one. In this case, the difference could be attributed to a slight stress relief. The experimental results obtained with the combination of stamping and painting simulation on the 5754-O sandwich composite exhibited no significant difference with respect to the as-received condition for UTS and elongation at fracture. By

looking at the stress-strain graphs (Figure 4-13 and Figure 4-14), a hint of discontinuous yielding could be noticed, probably due to the resting period and stress relief. Anyway, its delineation was not sufficiently clear, so it was decided to use the offset method to compute the yield stress ($R_{p0.2} = 125\ MPa$).

The values retrieved from the different conditions tested with the Quiet Aluminum® and AA6061-T4 used as skin are shown in Table 4-3. The as-received condition presented similar results concerning its monolithic reference (data available in Table 2-2), as well as the typical uniform stress-strain curve (Figure 4-15 and Figure 4-16). Then, the material preserved uniform plastic deformation after the stamping simulation (Figure 4-17 and Figure 4-18), with approximately 20% higher $R_{p0.2}$ concerning the as-received samples (respectively $169\ MPa$ and $145\ MPa$).

The samples treated to simulate the paint-bake cycle ($20\ min$ at $185°C$) showed no relevant alteration in $R_{p0.2}$ and UTS from the as-received ones (stress-strain curves shown in Figure 4-19 and Figure 4-20), meaning that the heat treatment was not sufficient to enhance precipitation hardening in the 6061-T4 aluminum alloy. Indeed, the graph in Figure 2-1 revealed that, for temperatures such as the paint-bake one, longer time is needed to age harden the aluminum alloy. Instead, the samples treated for $1h$ at $200°C$ were clearly affected by the hardening procedure. Indeed, even from a visual comparison between the graphs in Figure 4-17 (as-received sample) and Figure 4-21 (heat treated samples), it is clear that Quiet Aluminum®, after the hardening procedure, presented higher $R_{p0.2}$ and UTS, but lower ductility. The results in Table 4-3 confirmed the visual inspection, highlighting 68% higher $R_{p0.2}$ and 13% higher UTS for the treated material, which broke with just 9% strain (not even comparable with the 20% elongation at fracture of the as-received condition).

Finally, the tensile properties of the Quiet Aluminum® samples with 6061-T4 skin after the combination of stamping simulation, then hardening procedure and eventually the paint-bake cycle simulation are shown in Figure 4-23 and Figure 4-24. The sandwich presented $R_{p0.2} = 253\ MPa$ and $UTS = 276\ MPa$. Nevertheless, the consequence of significant hardening is a very low elongation at fracture, which had an average of 8% strain.

Overall, the two sandwich composites showed good mechanical properties, comparable to the monolithic values, confirming the hypothesis of negligible contribution of the polymer core

during tension. The samples with 5754-O skin presented almost constant tensile parameters (or predictable values in case of stamping) and the expected stress-strain curve in every condition tested. The Quiet Aluminum® with AA6061-T4 skin showed good mechanical properties and expected stress-strain curves in the as-received condition as well as after the stamping simulation. Apparently, the material did not exhibit significant property differences after the paint-bake simulation. Nevertheless, the suggested hardening procedure presented relevant changes in tensile parameters such as yield stress, UTS and elongation at fracture. Indeed, high yield stress/UTS ratio ($\frac{R_{p0.2}}{UTS} = 0.89$) together with low elongation at fracture were detected. Further experiments, varying temperature and exposure time of the hardening treatment should be carried out to find an optimal tradeoff between hardening and ductility. It is worth noting that the Young's modulus appeared lower for both sample materials compared to their respective monolithic ones. Again, the difference was attributed to the wide range of reasonable values for the aluminum alloys used, as well as to the relatively high standard deviations found. The 6061-T4 sandwich was found to be more performant for its higher mechanical properties such as tensile and adhesion strength, but also for its uniform yielding, which is preferable to the discontinuous yielding of the 5754-O sandwich for aesthetic reasons.

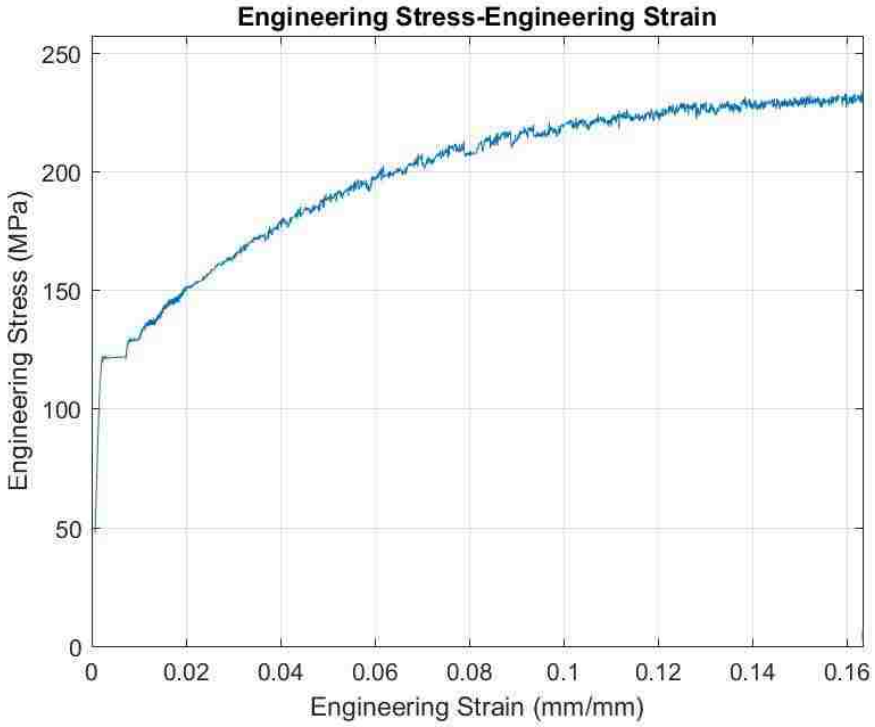

Figure 4-7: Engineering Stress-Engineering Strain curve for Quiet Aluminum® with 5754-O skin in the as-received condition. Serrated curve and yield point elongation were detected after the elastic region.

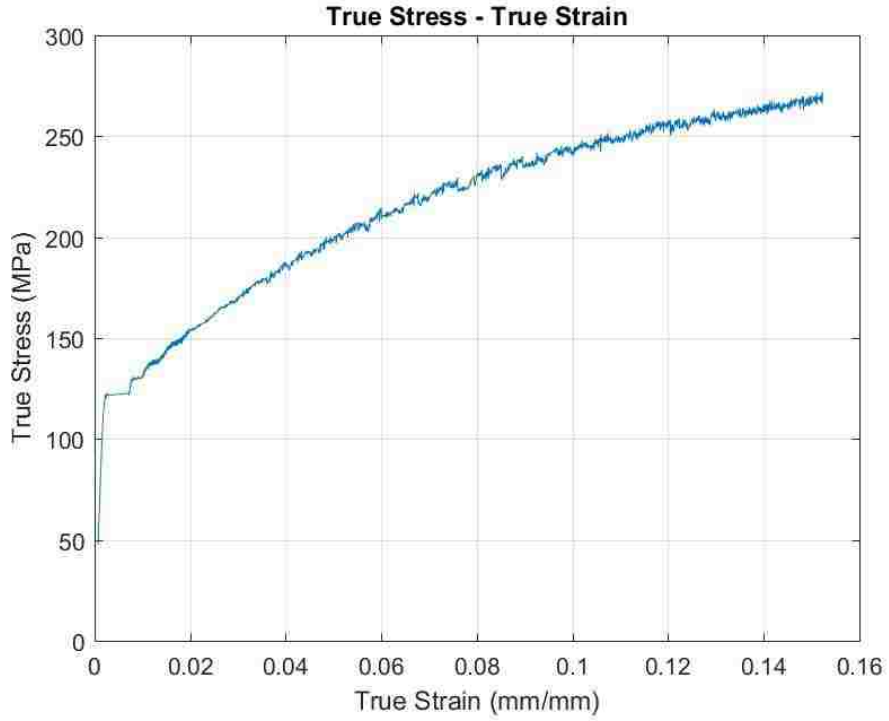

Figure 4-8: True Stress-True Strain curve for Quiet Aluminum® with 5754-O skin in the as-received condition. Serrated curve and yield point elongation were detected after the elastic region.

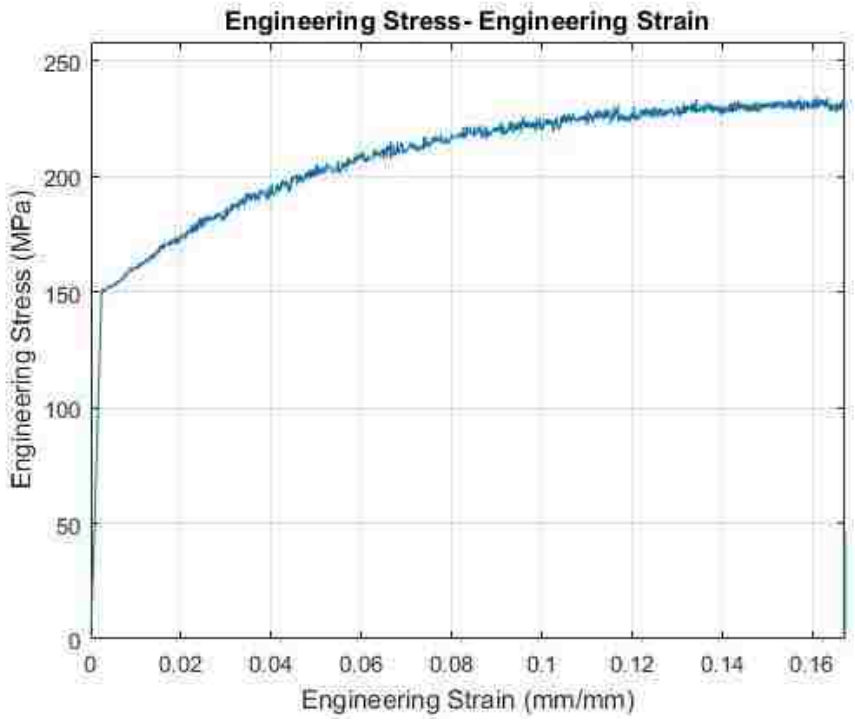

Figure 4-9: Engineering Stress-Engineering Strain curve for Quiet Aluminum® with 5754-O skin after stamping simulation (2% pre-applied strain). Cross section area of the undeformed specimen was used to compute the stress. Serrated curve, but no yield point elongation were detected after the elastic region.

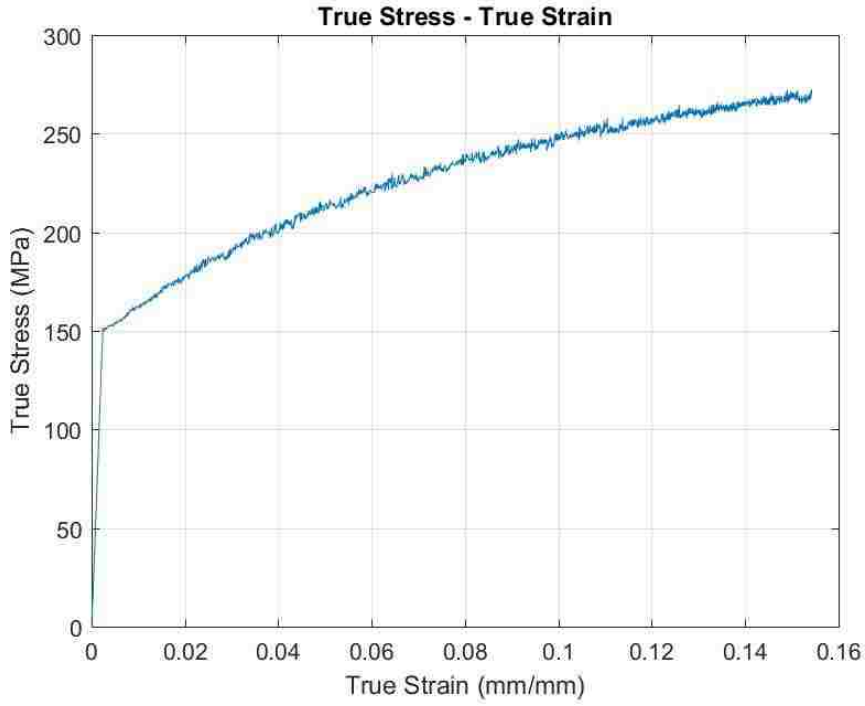

Figure 4-10: True Stress-True Strain curve for Quiet Aluminum® with 5754-O after the stamping simulation (2% pre-applied strain). Cross section area of the undeformed specimen was used to compute the stress. Serrated curve, but no yield point elongation were detected after the elastic region.

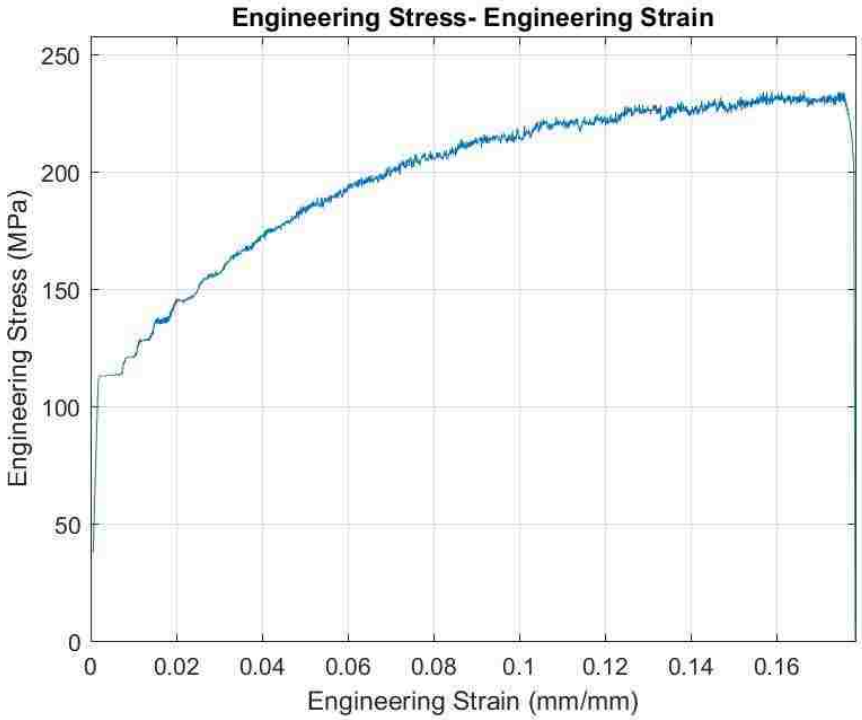

Figure 4-11: Engineering Stress-Engineering Strain curve for Quiet Aluminum® with 5754-O skin after the paint-bake simulation condition ($20\ min\ at\ 185℃$). Serrated curve and well-defined yield point elongation were detected after the elastic region.

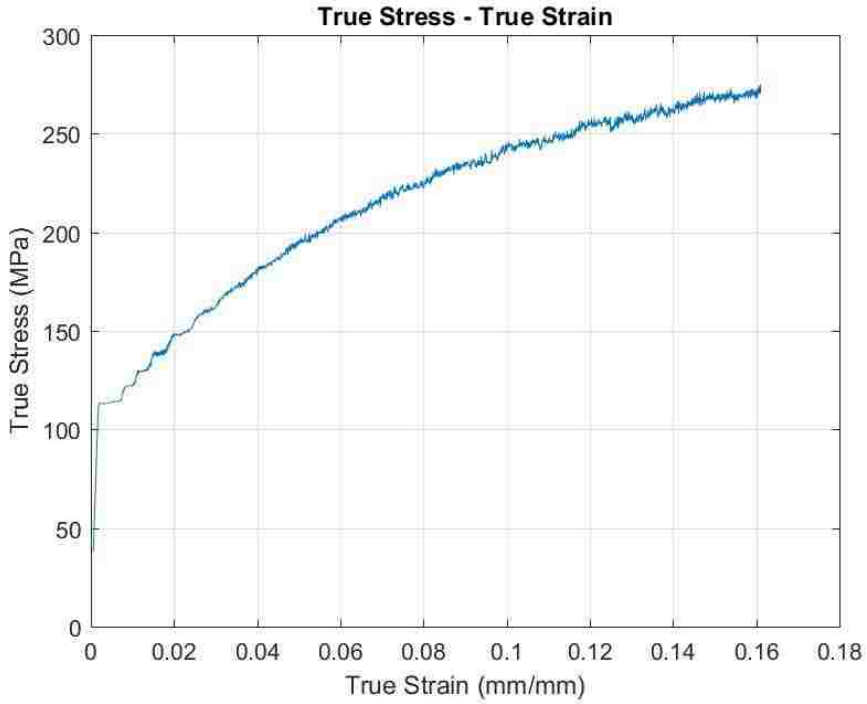

Figure 4-12: True Stress-True Strain curve for Quiet Aluminum® with 5754-O skin after the paint-bake simulation ($20\ min\ at\ 185℃$). Serrated curve and well-defined yield point elongation were detected after the elastic region.

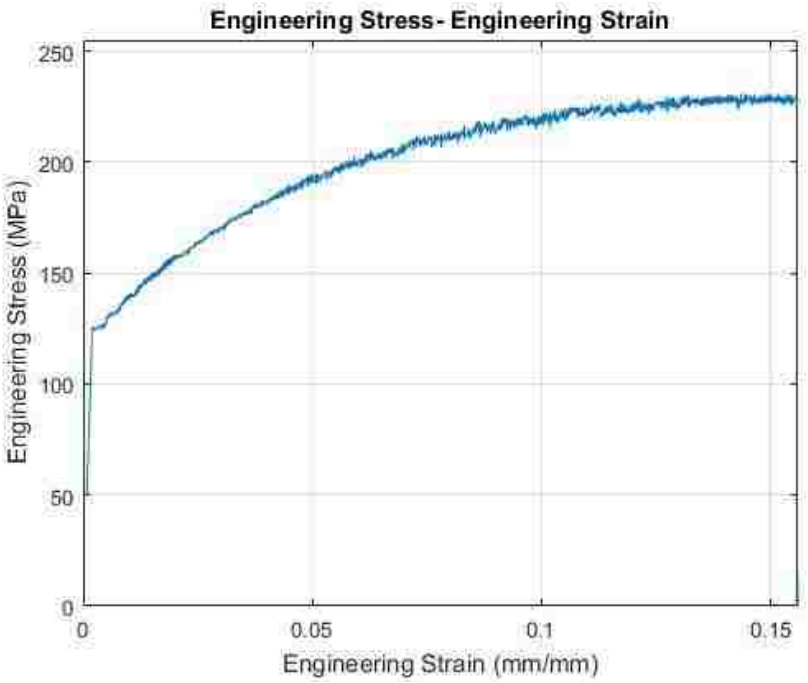

Figure 4-13: Engineering Stress-Engineering Strain curve for Quiet Aluminum® with 5754-O skin after stamping and paint-bake simulation (2% pre-applied strain and $20\ min\ at\ 185℃$). Cross section area of undeformed specimen was used to compute the stress. Serrated curve and slight discontinuous yielding were detected after the elastic region.

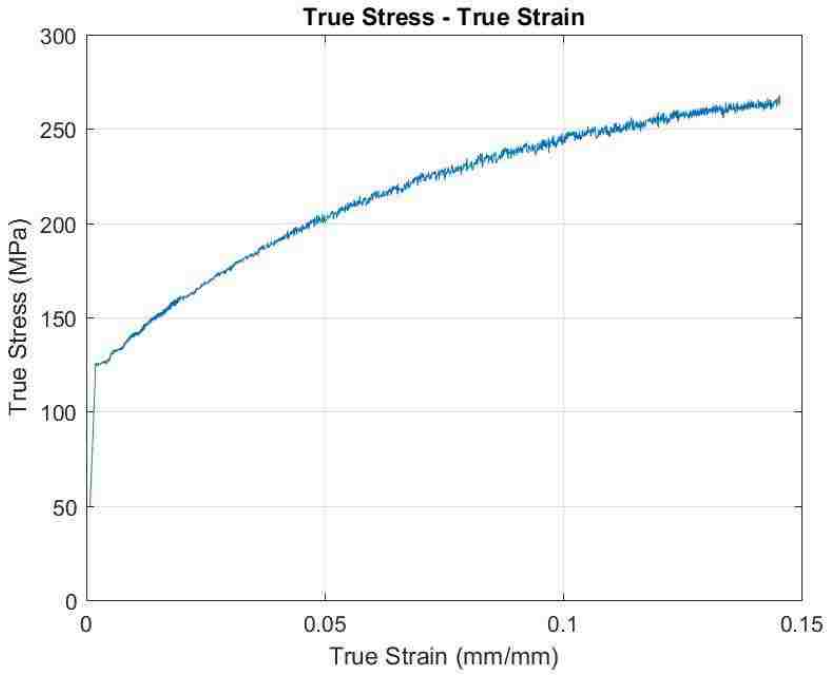

Figure 4-14 True Stress-True Strain curve for Quiet Aluminum® with 5754-O skin after stamping and paint-bake simulation (2% pre-applied strain and $20\ min\ at\ 185℃$). Cross section area of undeformed specimen was used to compute the stress. Serrated curve and slight discontinuous yielding were detected after the elastic region.

Table 4-2: Mechanical properties of Quiet Aluminum® with AA5754-O skin in different conditions.

Quiet Aluminum® with AA5754-O skin		*Young Modulus [Mpa]*	*UYP [Mpa]*	*Yield Point Elong.*	$R_{p0.2}$ *[MPa]*	*UTS [Mpa]*	*UE*	*Elong. at fracture*
As received	AVG	65510	123	0.5 %	-	237	16 %	18 %
	SD	3968	2	0.1 %	-	4	1 %	1 %
With 2% pre-applied strain	AVG	62273	-	-	152	235	17%	18%
	SD	2841	-	-	2	2	1%	2%
After 20 *min at* 185℃	AVG	64533	112	0.6%	-	232	17%	19%
	SD	2980	1	0.1%	-	2	1%	1%
After 2% strain and 20 *min at* 185℃	AVG	63978	-	-	125	233	16%	17%
	SD	3102	-	-	1	1	1%	1%

Table 4-3: Mechanical properties of Quiet Aluminum® with AA6061-T4 skin in different conditions.

Quiet Aluminum® with AA6061-T4 skin		*Young Modulus [Mpa]*	*UYP [Mpa]*	*Yield Point Elong.*	$R_{p0.2}$ *[MPa]*	*UTS [Mpa]*	*UE*	*Elong. at fracture*
As received	AVG	63140	-	--	145	241	17%	20%
	SD	3110	-	-	1	2	3%	3%
With 2% pre-applied strain	AVG	60540	-	-	169	243	16%	19%
	SD	3190	-	-	1	3	2%	3%
After 20 *min at* 185℃	AVG	64256	-	-	148	242	16%	17%
	SD	2633	-	-	2	3	2%	2%
After 1 *h at* 200℃	AVG	66927	-	-	242	273	8%	9%
	SD	1692	-	-	3	4	1%	1%
With 2% strain, after 1 *h at* 200℃ and 20 *min at* 185℃	AVG	62991	-	-	253	276	7%	8%
	SD	2472	-	-	2	3	1%	1%

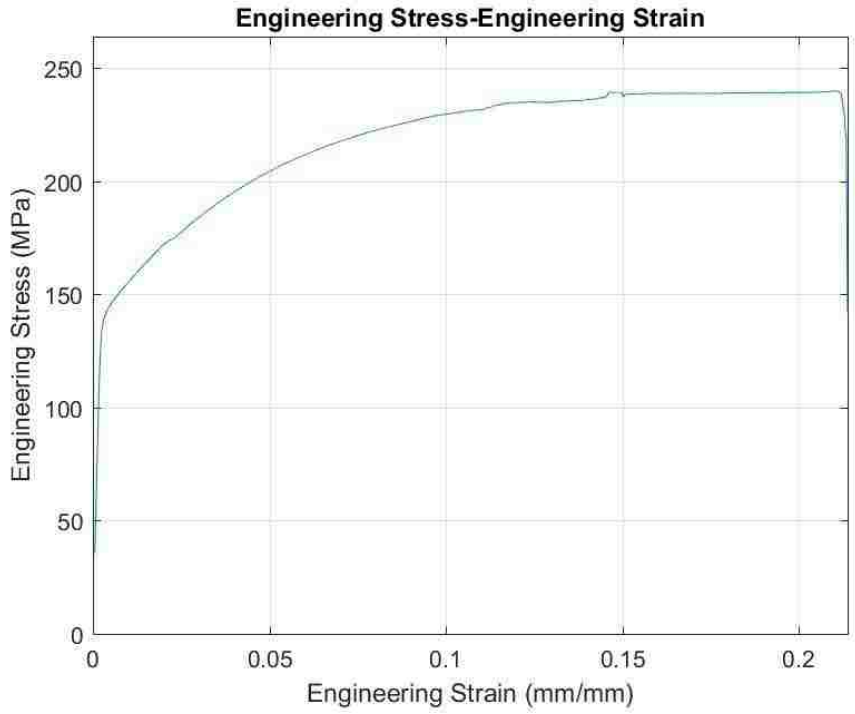

Figure 4-15: Engineering Stress-Engineering Strain curve for Quiet Aluminum® with 6061-T4 skin in the as-received condition. Uniform deformation after the elastic region.

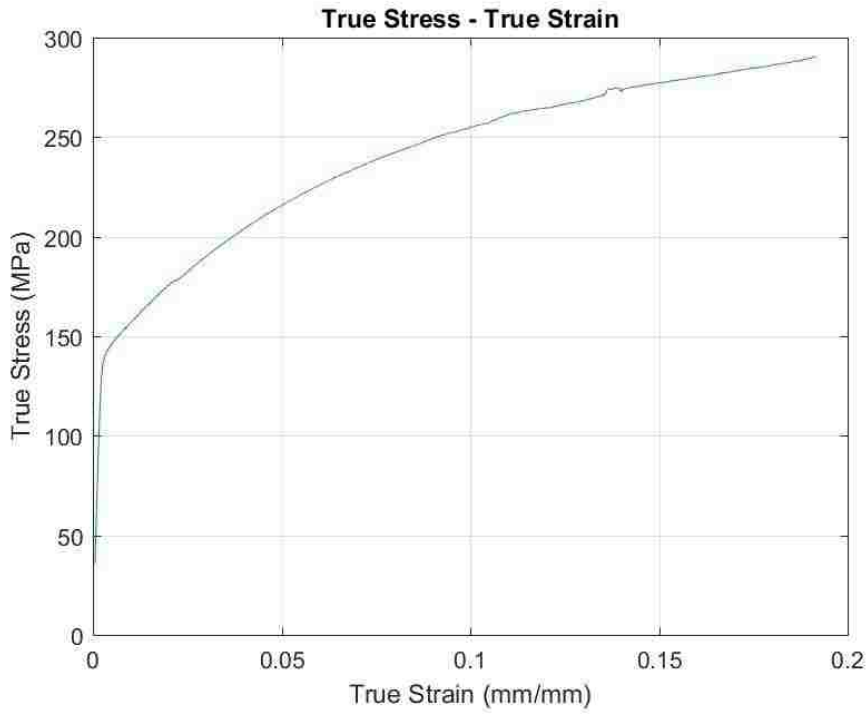

Figure 4-16: True Stress-True Strain curve for Quiet Aluminum® with 6061-T4 skin in the as-received condition. Uniform deformation after the elastic region.

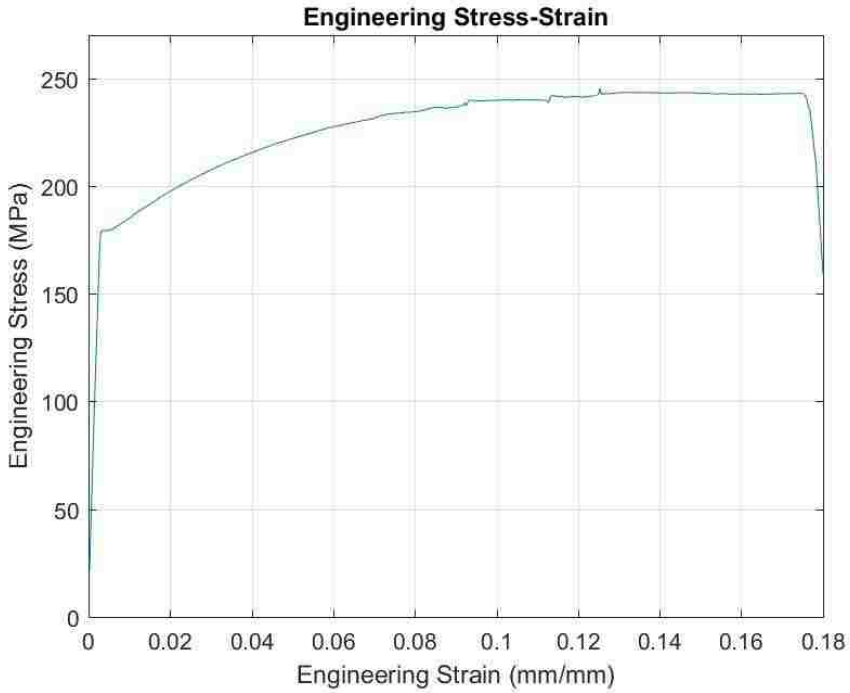

Figure 4-17: Engineering Stress-Engineering Strain curve for Quiet Aluminum® with 6061-T4 skin after the stamping simulation (2% pre-applied strain). Cross section area of undeformed specimen was used to compute the stress. Uniform deformation after the elastic region.

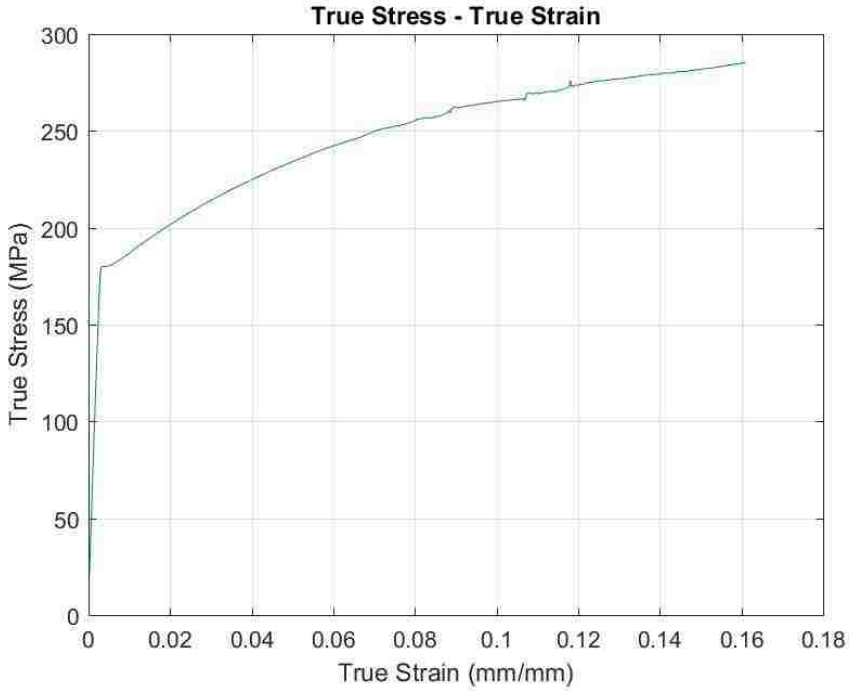

Figure 4-18: True Stress-True Strain curve for Quiet Aluminum® with 6061-T4 skin after the stamping simulation (2% pre-applied strain). Cross section area of undeformed specimen was used to compute the stress. Uniform deformation after the elastic region.

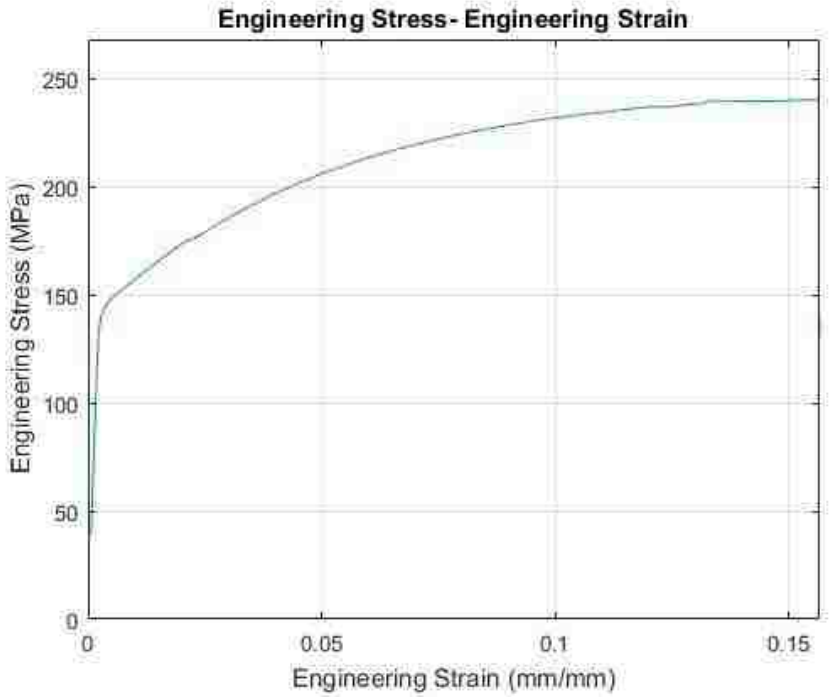

Figure 4-19: Engineering Stress-Engineering Strain curve for Quiet Aluminum® with 6061-T4 skin after the paint-bake cycle simulation ($20\ min\ at\ 185℃$). Uniform deformation after the elastic region. No evident precipitation hardening was detected after the treatment.

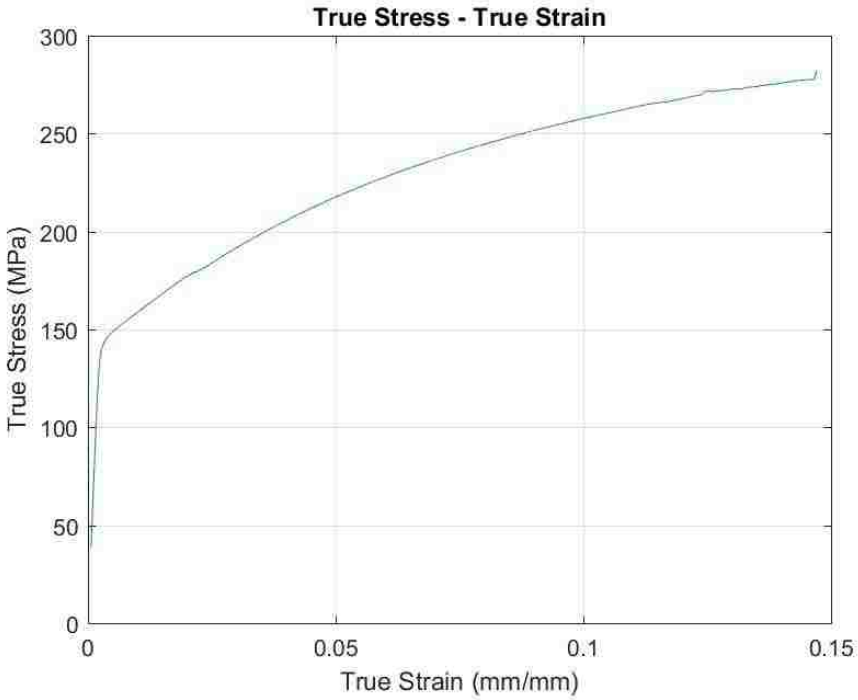

Figure 4-20: True Stress-True Strain curve for Quiet Aluminum® with 6061-T4 skin after the paint-bake cycle simulation ($20\ min\ at\ 185℃$). Uniform deformation after the elastic region. No evident precipitation hardening was detected after the treatment.

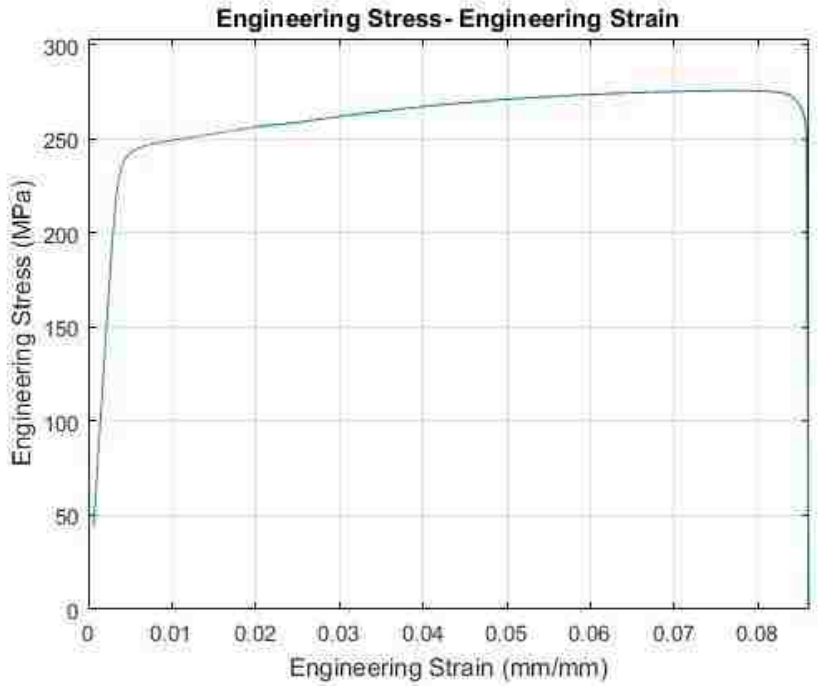

Figure 4-21: Engineering Stress - Engineering Strain curve for Quiet Aluminum® with 6061-T4 skin after hardening procedure ($1\ h\ at\ 200$).Significantly higher $R_{p0.2}$ and UTS concerning the as-received samples due to precipitation hardening. Uniform deformation after the elastic region.

Figure 4-22: True Stress-True Strain curve for Quiet Aluminum® with 6061-T4 skin after the hardening procedure ($1\ h\ at\ 200℃$). Significantly higher $R_{p0.2}$ and UTS concerning the as-received samples due to precipitation hardening. Uniform deformation after the elastic region.

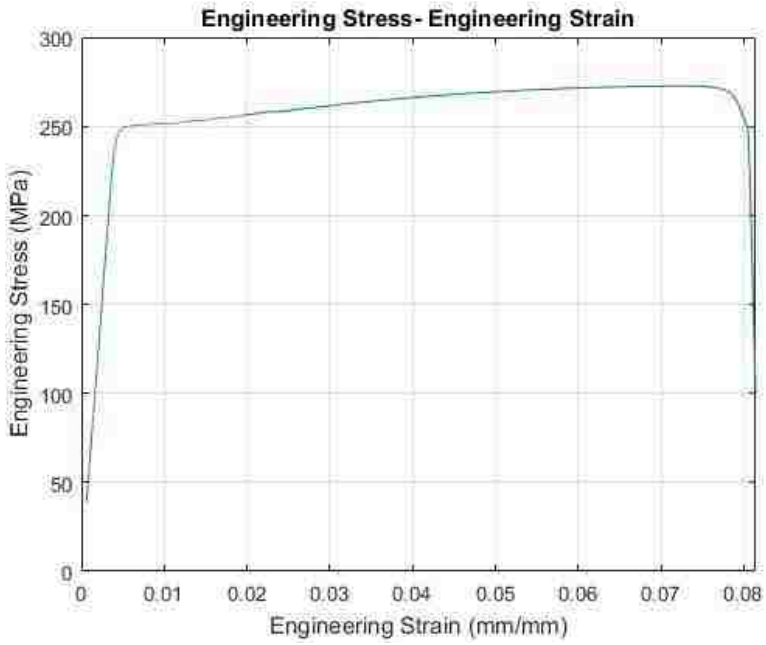

Figure 4-23: Engineering Stress - Engineering Strain curve for Quiet Aluminum® with 6061-T4 skin after combination of stamping (2% pre-applied strain) and painting simulation ($20\ min\ at\ 185℃$), as well as the hardening procedure ($1\ h\ at\ 200℃$). Cross section area of undeformed specimen was used to compute the stress Significantly higher $R_{p0.2}$ and UTS concerning the as-received samples were observed due to precipitation hardening. Uniform deformation encountered after the elastic region.

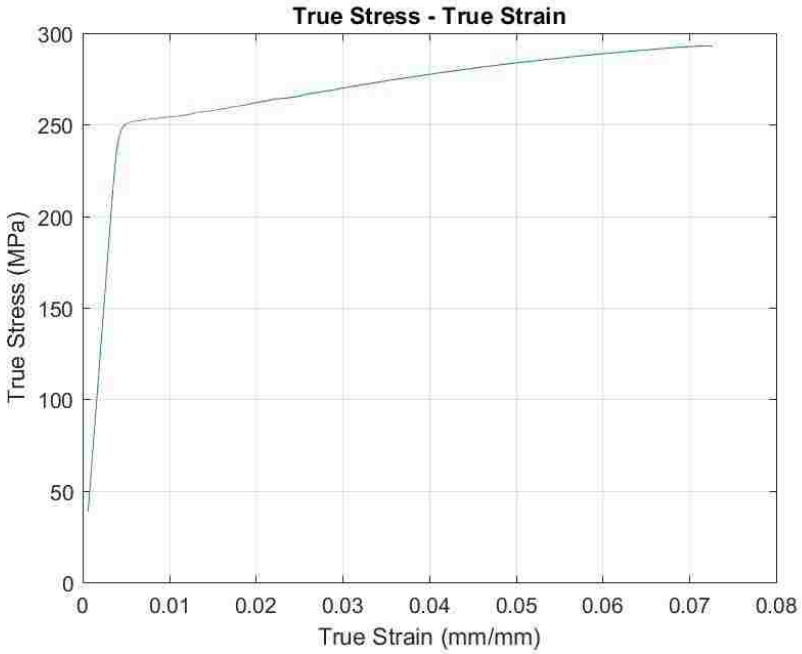

Figure 4-24: True Stress - True Strain curve for Quiet Aluminum® with 6061-T4 skin after combination of stamping (2% pre-applied strain) and painting simulation ($20\ min\ at\ 185℃$), as well as the hardening procedure ($1\ h\ at\ 200℃$). Cross section area of undeformed specimen was used to compute the stress. Significantly higher $R_{p0.2}$ and UTS concerning the as-received samples were observed due to precipitation hardening. Uniform deformation encountered after the elastic region.

4.3.2 Strain Hardening Exponent

In this section, the strain hardening exponent and the strength coefficient are presented following the methodology section "*Strain Hardening Exponent "*n*""*. From Table 4-4 and

Table 4-5, it is possible to compare the parameters cited above in the strain ranges 4-6% and 10-20%/UE between the samples as-received, after the stamping simulation, the paint-bake cycle, the hardening treatment (only for the 6061-T4 sandwich composite) and their combinations. The two composites showed comparable values to the respective monolithic alloys (Table 2-2). Indeed, the samples with AA5754-O skin presented $n_{10-20\%/UE} = 0.26$ against the reference $n_{10-20\%/UE} = 0.24$, whereas the samples with AA6061-T4 skin exhibited $n_{10-20\%/UE} = 0.22$ (monolithic value $n_{10-20\%/UE} = 0.24$). It is interesting to notice that the 5754-O sandwich unveiled higher strain hardening exponent and strength coefficient value in all conditions. For instance, the as-received samples revealed $n_{4-6\%,} = 0.31$ and $K_{4-6\%} = 515$, whereas the sandwich with AA6061-T4 skin reported $n_{4-6\%} = 0.25$ and $K_{4-6\%} = 461$.

The samples with the 2 % pre-applied strain showed a decrement of the strain hardening exponent and the strength hardening coefficient in both strain ranges. This trend was predictable considering that the material was subjected to previous plastic deformation. After the paint-bake cycle, the sandwich with 5754-O skin showed a slight increment, especially in the lower strain range ($n_{4-6\%} = 0.33$) with respect to the as-received condition. Instead, the sandwich with AA6061-T4 skin, in accordance with the tensile results previously described, did not present precipitation hardening after the heat treatment involved in the paint-bake simulation. Nevertheless, the sandwich composite after the hardening treatment presented significant differences with respect to the undeformed and untreated samples. In fact, the samples after the hardening treatment recorded $n_{4-6\%} = 0.11$, less than half of the same parameter for the as-received samples($n_{4-6\%} = 0.25$). It was not even possible to report the strain hardening exponent and the strength coefficient for the strain range 10%-20%/UE, since the material could not reach the minimum elongation to be included in the rage. This behavior was even more accentuated with the combination of stamping, hardening and paint-bake simulation, leading to the lowest values found, $n_{4-6\%} = 0.10$ and $K = 378$. Instead, the combination of the stamping process and the paint-bake simulation gave another hint of a

possible stress relief due to the paint-bake for sample with 5754-O skin, with an increment of the strain hardening exponent concerning the samples with 2% pre-applied strain, respectively $n_{4-6\%} = 0.28$ and $n_{4-6\%} = 0.22$ in the lower strain range and $n_{10-20\%} = 0.25$ with respect to $n_{10-20\%} = 0.23$ in the higher strain region. Overall, that the samples with AA5754-O skin showed good formability properties even after the stamping and painting simulation. The same consideration can be inferred for the samples with AA6061-T4 skin in the as-received conditions, as well as after the paint-bake simulation. Nevertheless, after the hardening procedure the formability properties of the sandwich dropped consistently.

Table 4-4: Strain hardening exponent n and strength hardening coefficient K for Quiet Aluminum with AA5754-O skin in different conditions.

Quiet Aluminum® with AA5754-O skin	$n_{4-6\%}$	$K_{4-6\%}$	$n_{10-20\%/UE}$	$K_{10-20\%/UE}$
As-received	0.31 ± 0.02	515 ± 40	0.26 ± 0.02	450 ± 30
With 2% pre-applied strain	0.22 ± 0.04	415 ± 48	0.23 ± 0.02	425 ± 19
After 20 min at 185℃	0.33 ± 0.01	516 ± 26	0.27 ± 0.02	451 ± 23
With 2% strain and after 20 min at 185℃	0.28 ± 0.02	474 ± 25	0.25 ± 0.02	440 ± 8

Table 4-5: Strain hardening exponent n strength hardening coefficient K for Quiet Aluminum with AA6061-T4 skin in different conditions.

Quiet Aluminum® with AA6061-T4 skin	$n_{4-6\%}$	$K_{4-6\%}$	$n_{10-20\%/UE}$	$K_{10-20\%/UE}$
As received	0.25 ± 0.01	461 ± 4	0.22 ± 0.02	428 ± 21
With 2% pre-applied strain	0.18 ± 0.01	397 ± 4	0.19 ± 0.01	405 ± 8
After 20 min at 185℃	0.25 ± 0.01	461 ± 8	0.22 ± 0.02	426 ± 17
After 1 h at 200℃	0.11 ± 0.01	390 ± 8	n/a	n/a
With 2% strain, after 1 h at 200℃ and 20 min at 185℃	0.10 ± 0.01	378 ± 4	n/a	n/a

4.3.3 Anisotropy Parameters

The anisotropy parameters recorded following the "*Anisotropy "r" Value"* section are presented in Table 4-6 and plotted in Figure 4-25. Note that the parameters were measured at 10% strain for each specimen. Both sandwich composite showed higher anisotropy properties than the reference materials, with $r_m = 0.78$ for the sandwich with AA5754-O skin and $r_m = 0.73$ for the sandwich with 6061-T4 skin. Table 2-2 refers to their monolithic alloys, respectively $r_m = 0.72$ for AA5754-O and $r_m = 0.58$ for AA6061-T4). The difference can be attributed to the fact that the materials were produced by different suppliers. Indeed, the polymer volume core cannot contribute in increasing the anisotropy of the composite due its negligible volume fraction. The outcome of the test is considered positive since it is preferable to have higher anisotropy properties in order to avoid stamping defects as earing or small limiting draw ratios in deep drawing. The computed planar anisotropy of the samples with AA6061-T4 skin exhibited an almost negligible value, whereas earing is expected at $0°$ and $90°$ orientation to the Rolling Direction in the samples with AA5754-O skin due to the positive $\Delta r = 0.17$.

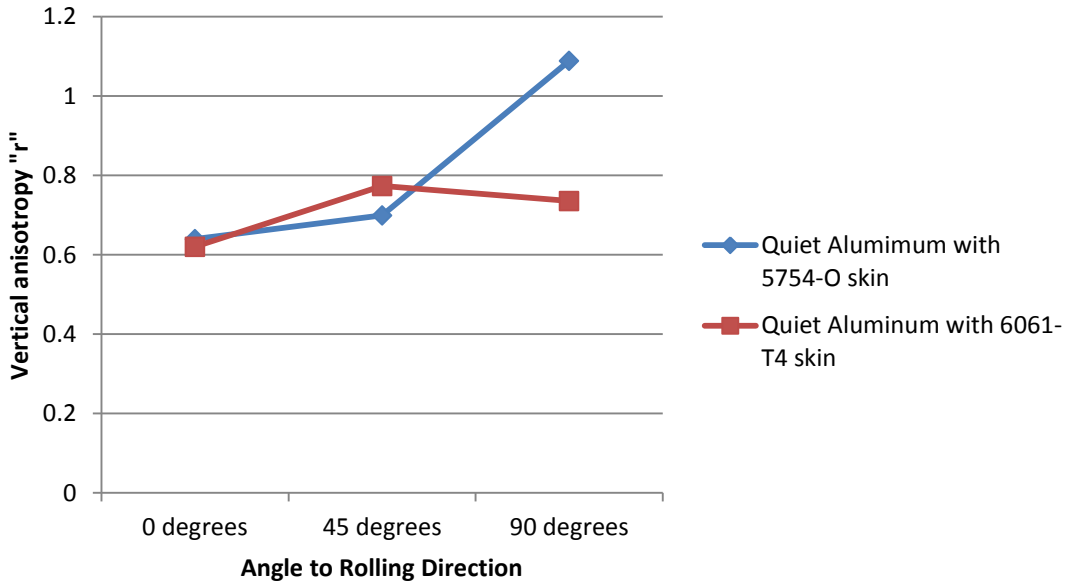

Figure 4-25: Graphic representation of the vertical anisotropy "r" (measured at 10% strain) as a function of the angle to the rolling direction. The Quiet Aluminum samples with 6061-T4 skin (red line) showed almost constant parameters. The Quiet Aluminum samples with AA5754-O skin (blue line) presented higher r-value for the samples with $90°$ to the Rolling Direction.

Table 4-6: Anisotropy r-values measured for Quiet Aluminum® samples with AA5754-O and AA6061 skin at 10% strain for different specimen orientation to the Rolling Direction ($0°$, $45°$ and $90°$). Three specimens tested in each orientation.

r-value at 10% strain	Quiet Aluminum® with AA5754-O skin	Quiet Aluminum® with AA6061-T4 skin
$r_0°$: $(AVG \pm SD)$	0.64 ± 0.01	0.62 ± 0.01
$r_{45}°$: $(AVG \pm SD)$	0.70 ± 0.02	0.77 ± 0.03
$r_{90}°$: $(AVG \pm SD)$	1.01 ± 0.08	0.73 ± 0.01
r_m	0.78	0.73
Δr	0.17	-0.10

4.4 T-Peel Test

T-Peel test is crucial for laminates since sufficient adhesion strength under the applied loads is the most important requirement. Indeed, if the sandwich is not able to maintain proper adhesion, it will consequently lose all the other mechanical properties. Figure 4-26 and Figure 4-27 show the force-displacement curve of the sandwich with AA5754-O skin and with AA6061-T4 skin for the five specimens tested in the as-received conditions. The former exhibited a more pronounced initial peak and a plateau region until the end of the strip length, with $59 - 72\ N$ load range. Test 1 in Figure 4-27, which represents the Quiet Aluminum samples with 6061-T4 skin, presented a significant drop after the initial peak due to weaker adhesion in the corresponding strip area. Nevertheless, higher peeling resistance could be observed in the sandwich with 6061-T4 skin; indeed, the force range applied by the crosshead oscillated around $67 - 95\ N$.

Higher peel resistance was expected for the samples with 6061-T4 alloy since the sandwich revealed higher tensile yield strength concerning the 5754-O sandwich, as shown in the "*Mechanical Properties*" section. Indeed, yield in tension and bending is known to be strictly correlated.

Thanks to the samples treated for $20\ min$ at $185℃$, it was possible to evaluate the adhesive performance of the viscoelastic layer after the paint-bake cycle (Figure 4-28). No relevant differences from the samples as-received could be detected. This means that the polymer core

was able to sustain the temperature of the treatment without being affected. Figure 4-29 instead, describes the adhesion strength of the sandwich after the hardening procedure (treated at $200℃$ for $1\ h$). The force-displacement curve was significantly more fluctuant with respect to the samples in the as-received condition. Moreover, the load range sustained by the laminate was tremendously lower ($14 - 52\ N$ instead of $67 - 95\ N$). The peel strength results for the different samples are shown in Figure 4-30. From the clustered chart, it is even clearer that the 5754-O sandwich presented the same resistance as-received and after the paint-bake cycle, whereas the 6061-T4 sandwich samples, which showed the highest peel strength, $\alpha_s = 33.4 \frac{N}{cm}$, lost part of its adhesion performance due to the hardening treatment. The experimental values were then compared with FCA requirements in Table 4-7. Even though all Quite Aluminum® samples met the FCA requirements, the hardening procedure applied on the 6061-T4 affected significantly the polymer. In fact, apart from the differences in peel strength regarding the as-received condition, a comparison between the inner surfaces of the specimen strip after the test (Figure 4-31 and Figure 4-32) revealed a visibly degenerated polymer. The polymer in the as-received samples was light yellow in color, whereas after the hardening treatment changed to muddy yellow and even brownish at the edges of the strip.

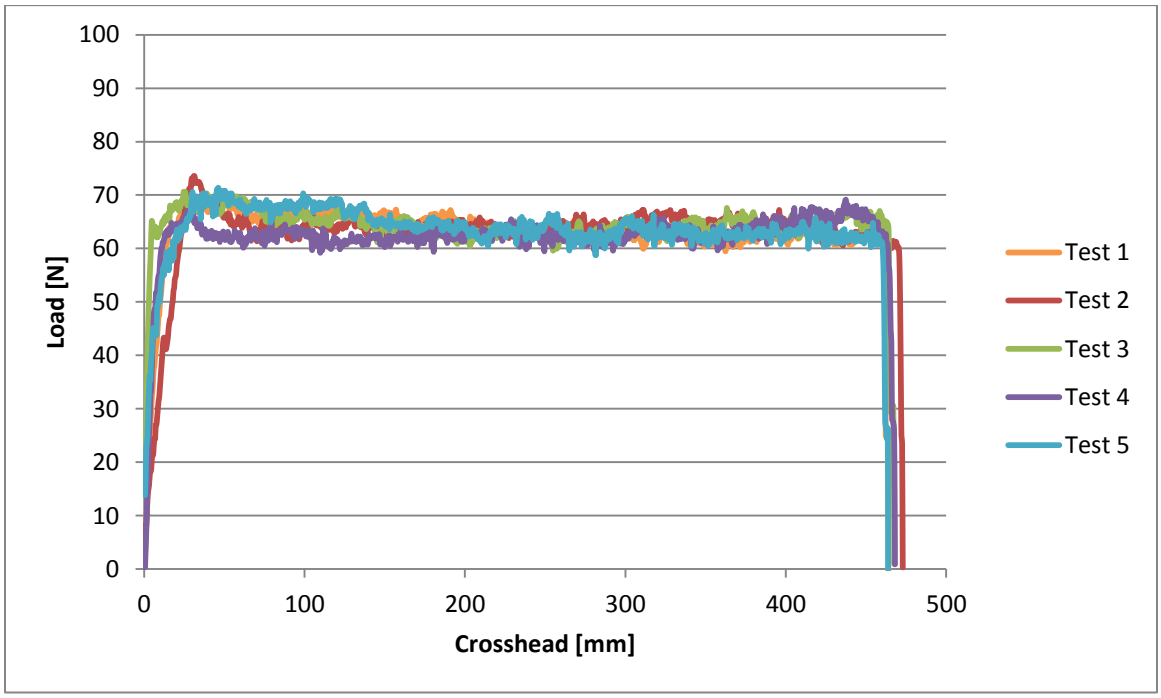

Figure 4-26: T-Peel test load displacement curves for the five samples, Quiet Aluminum® with 5754-O skin, in the as received condition. The curves slightly fluctuated between $59 - 72\ N$ till fracture.

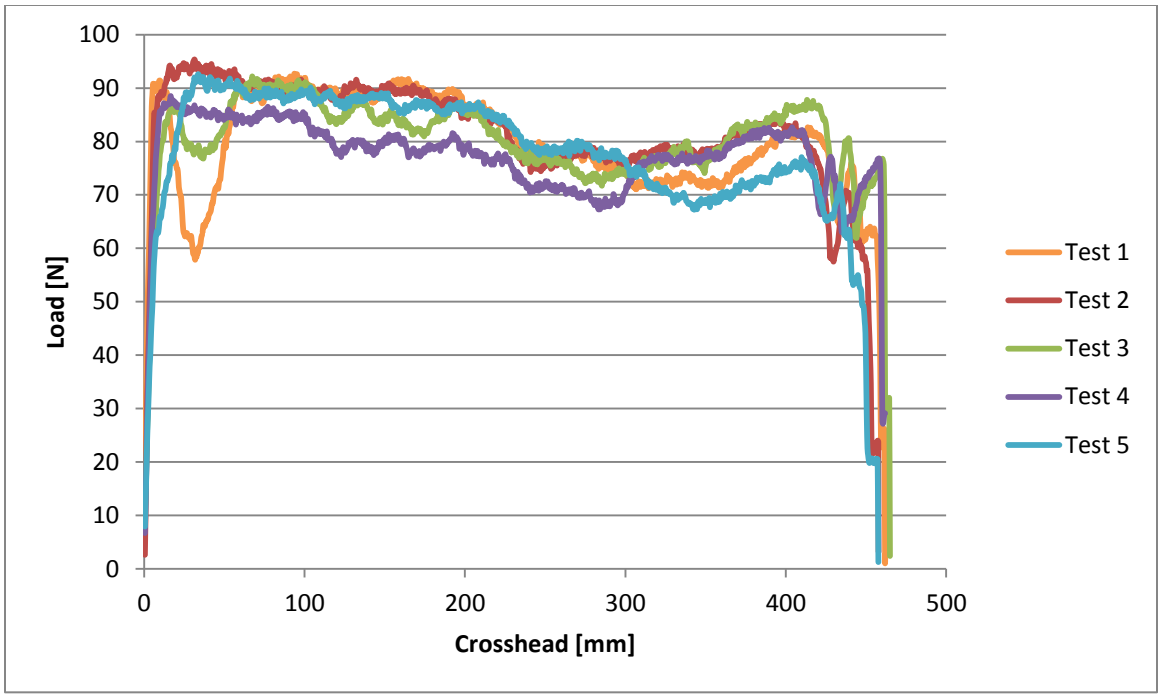

Figure 4-27: T-Peel test load displacement curves for the five samples, Quiet Aluminum® with 6061-T4 skin, in the as received condition. The curves fluctuated between $67 - 95\ N$ along the strip length. Test 1 curve (orange line) dropped after the initial peak, reaching 58 N.

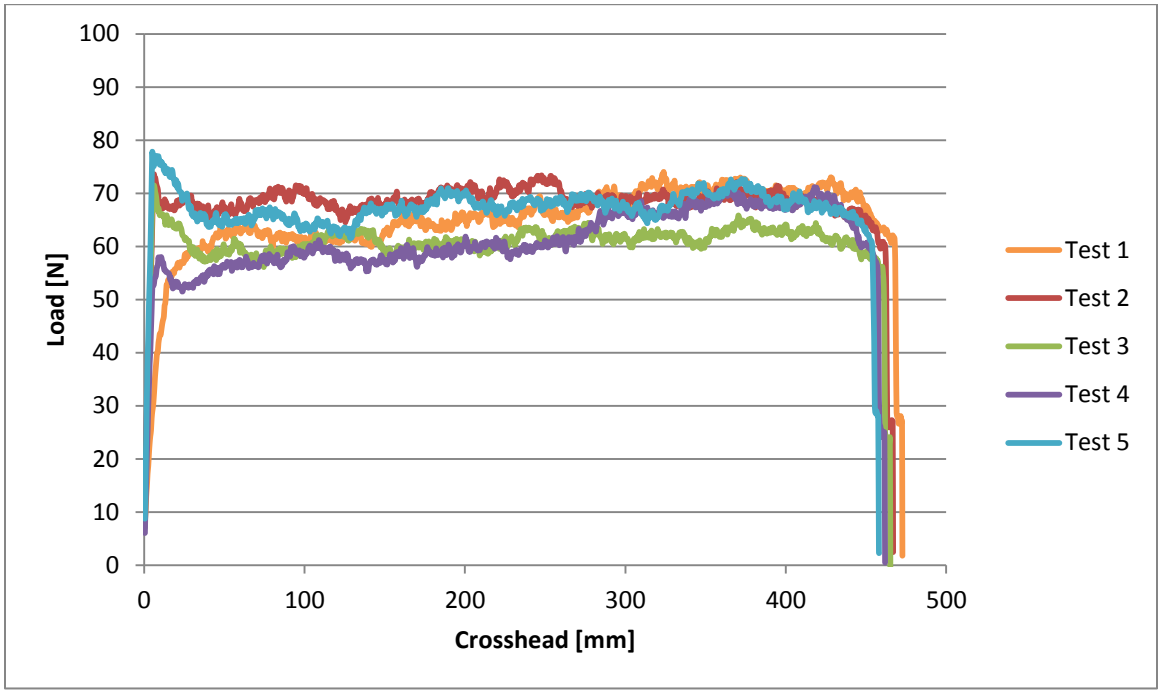

Figure 4-28: T-Peel test load displacement curves for the five samples, Quiet Aluminum® with 5754-O skin, after the paint-bake simulation ($20\ min\ at\ 185℃$). The curves fluctuated between $51 - 78\ N$ along the strip length.

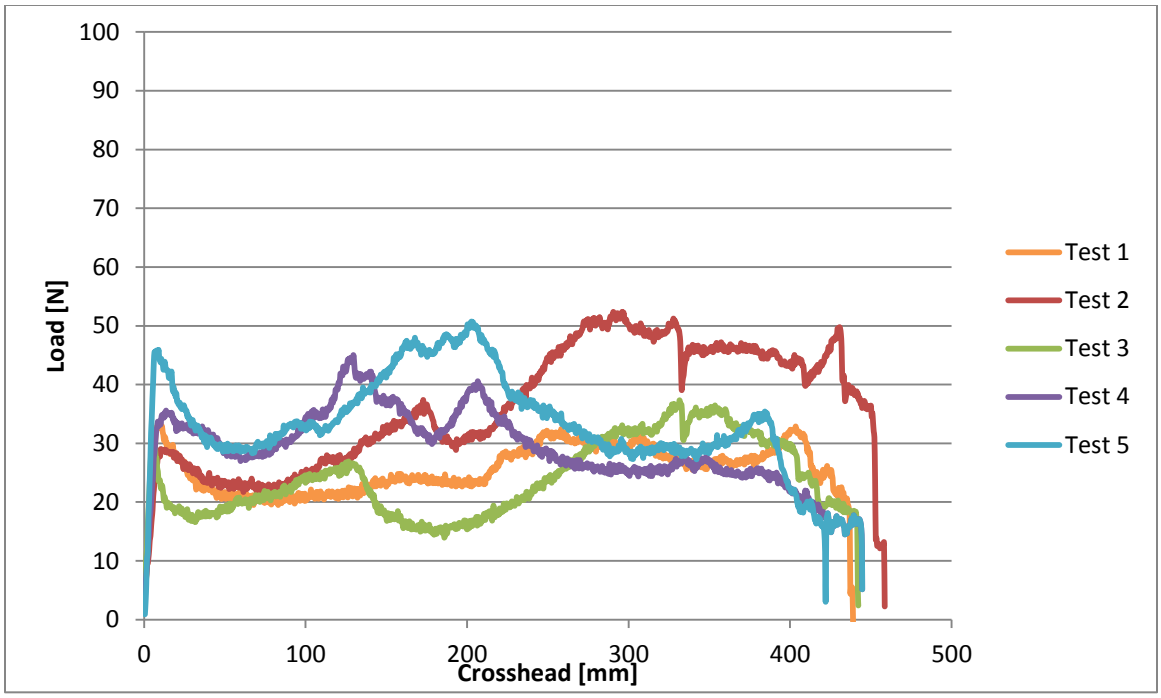

Figure 4-29: T-Peel test load displacement curves for the five samples, Quiet Aluminum® with 6061-T4 skin, after hardening treatment ($1\ h\ at\ 200℃$). The curves fluctuated significantly between $14 - 52\ N$ (in particular Test 2 had a minimum of 21 N, then reached a peak of 52 N.

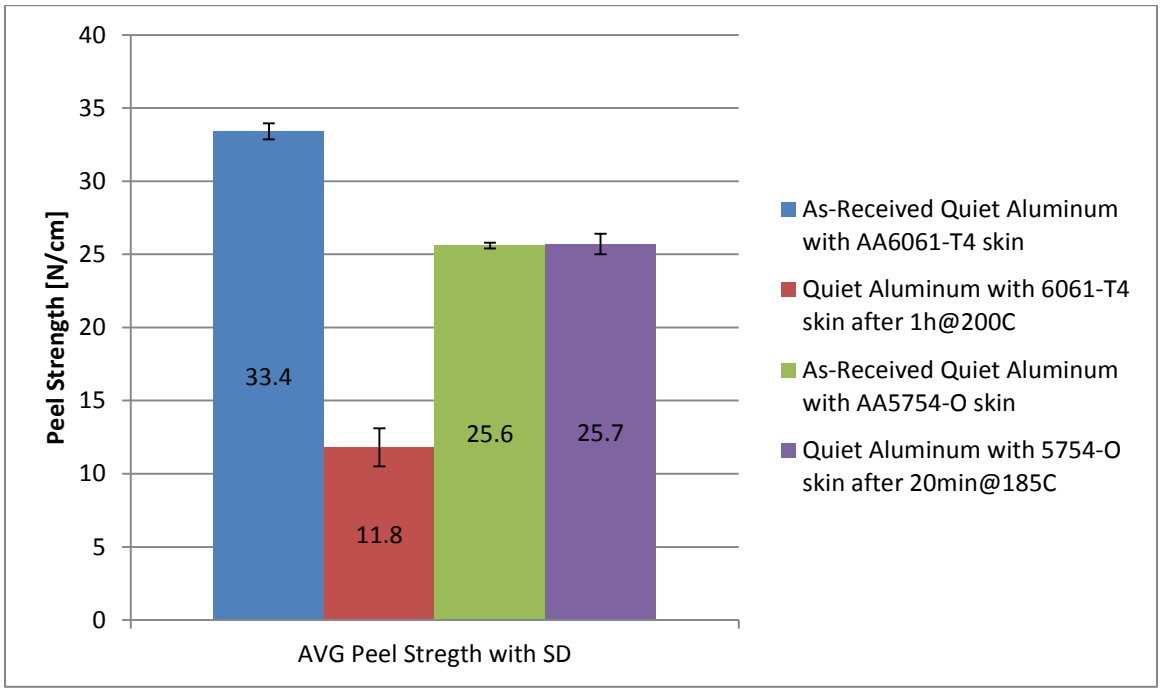

Figure 4-30: Peel strength clustered column chart for the different Quiet Aluminum® samples.The samples with 5754-O skin as-received and treated to simulate the paint-bake cycle showed equal peel strength. Highest peel strength measured in samples with 6061-T4 skin, but significant drop after hardening procedure was encountered.

Table 4-7: T-peel test results for the Quiet Aluminum® samples in all conditions with FCA requirements. All samples met FCA adhesion strength requirement for panels with non-structural loads.

Material	Treatment	Peel strength $\left[\frac{N}{cm}\right]$	Minimum FCA Requirement $\left[\frac{N}{cm}\right]$
Quiet Aluminum® with 5754-O skin	As-Received	25.6	1015
	After paint-bake simulation ($20min$ at 185℃)	25.7	$10-15$
Quiet Aluminum® with 6061-T4 skin	As-Received	33.4	$10-15$
	After hardening procedure ($1\ h$ at 200℃)	11.8	$10-15$

The failure mode of the samples were addressed in the "*Adhesion in Metal/Polymer/Metal* " section. From the inspection of the inner surfaces of the specimen strips after the T-peel test, the following considerations could be made:

- All specimens showed adhesive failure mode.
- The polymer in the sandwich composite with AA6061-T4 skin attached entirely to one side (Figure 4-31 and Figure 4-32).
- The polymer in the sandwich composite with AA5754-O skin remained on one adherend surface and the other in a complementary way. In fact, by superposing the two surfaces of the strip, the areas with the polymer and the areas with absence of the viscoelastic layer were perfectly matching (Figure 4-33 and Figure 4-34).

The adhesive failure (or apparent adhesive failure) could be caused by a weak boundary layer at the interface polymer/aluminum [34], whereas the fact that the polymer remained attached just to one side (6061-T4 sandwich) or to both sides in a complementary way (5754-O sandwich), was generated by the different treatments applied on the two aluminum alloys during the sandwich manufacturing process.

Figure 4-31: Quiet Aluminum® strips with 6061-T4 skin in the as-received condition. The image shows the two inner surfaces of the sandwich strip after T-peel test. The specimen presented adhesive failure mode, with the polymer completely attached to one surface.

Figure 4-32: Quiet Aluminum® strips with 6061-T4 skin after the hardening procedure ($1\ h$ at $200℃$). The image shows the inner surfaces of the sandwich strip after T-peel test. The specimen presented adhesive failure mode, with the polymer completely attached to one surface. Degradation of the polymer could be observed due to burning.

Figure 4-33: Quiet Aluminum® strips with AA5754-O skin in the as-received condition. The image shows the inner surfaces of the sandwich after T-peel test. The specimen presented adhesive failure mode. The black circles are examples of the polymer attached to one surface and the other in a complementary way.

Figure 4-34: Quiet Aluminum® strips with AA5754-O skin after the paint-bake simulation ($20\ min$ at $185℃$). The image shows the inner surfaces of the sandwich after T-peel test. The specimen presented adhesive failure mode. The black circles are examples of the polymer attached to one surface and the other in a complementary way.

4.5 Roughness Measurements

In this section, the surface roughness measurements with the relative optical profilometry images taken on the aluminum surfaces of the sandwich composites received are presented referring to the "Roughness Measurements" methodology section. Figure 4-35 and Figure 4-36 refer to the inner and outer surface topographies of the AA5754-O sandwich skin, whereas Figure 4-37 and Figure 4-38 show the AA6061-T4 ones. The rolling direction can be clearly distinguished in every image. Indeed, during the sandwich manufacturing process, the rollers give the typical surface pattern displayed, which is exploited by the viscoelastic layer to form proper mechanical inter-locking.

The profilometer results in Table 2-1 (averaged values with standard deviation, $n = 9$) showed a surface roughness range $R_a = 0.49 - 0.56\ \mu m$, common value for commercial rolling mill-finish on aluminum surfaces [16] [50]. Even the surface maximum peak presented similar results, with all values around $S_z \cong 20\ \mu m$. Both alloys showed similar roughness, as well as between the inner and outer surface, meaning that no different treatment was applied on the inner side of the sandwich with respect to the outer one. Taking into consideration the profilometer results together with the peel strength found in "*T-peel Test*" section, the surface roughness of Quiet Aluminum® provided by the rolling mill guaranteed more than acceptable adhesion strength. MSC's manufacturing process does not exploit extremely rough surfaces as in Mousa and Kim's study [20]. In fact, rough surfaces would lead to unacceptable aesthetic quality for exposed sheets in vehicles.

Table 4-8: Surface roughness results for Quiet Aluminum® samples obtained from WYKO NT 1100 optical surface profilometer.

Material	Surface side	Surface roughness S_a, $AVG \pm SD$ $[\mu m]$	Surface maximum peak S_z, $AVG \pm SD$ $[\mu m]$
Quiet Aluminum® with 5754-O skin	Inner	0.56 ± 0.09	19.75 ± 9.62
	Outer	0.56 ± 0.06	24.02 ± 13.85
Quiet Aluminum® with 6061-T4 skin	Inner	0.49 ± 0.04	20.68 ± 10.90
	Outer	0.54 ± 0.05	19.11 ± 13.96

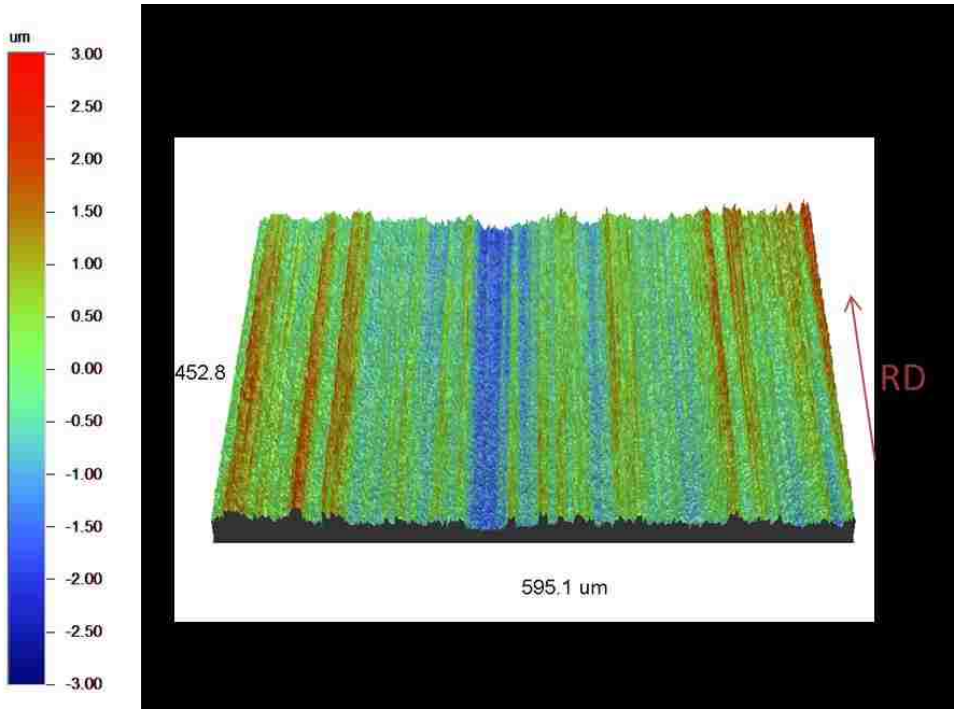

Figure 4-35: Surface profilometry image of Quiet Aluminum® with AA5754-O skin as-received. The image shows the inner surface of the sandwich, which faces the polymer layer. Rolling mill-finish pattern with clear distinction of the Rolling Direction (RD), showed with red arrow on the right side of the image.

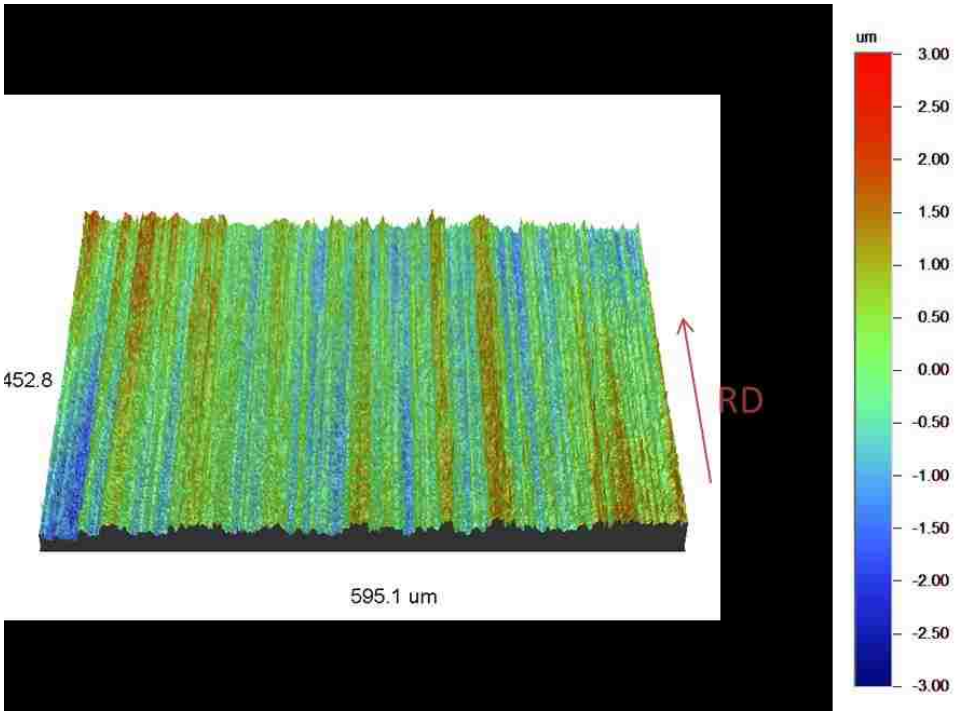

Figure 4-36: Surface profilometry image of Quiet Aluminum® with AA5754-O skin as-received. The image shows the outer surface of the sandwich. Rolling mill-finish pattern with clear distinction of the Rolling Direction (RD), showed with red arrow on the right side of the image.

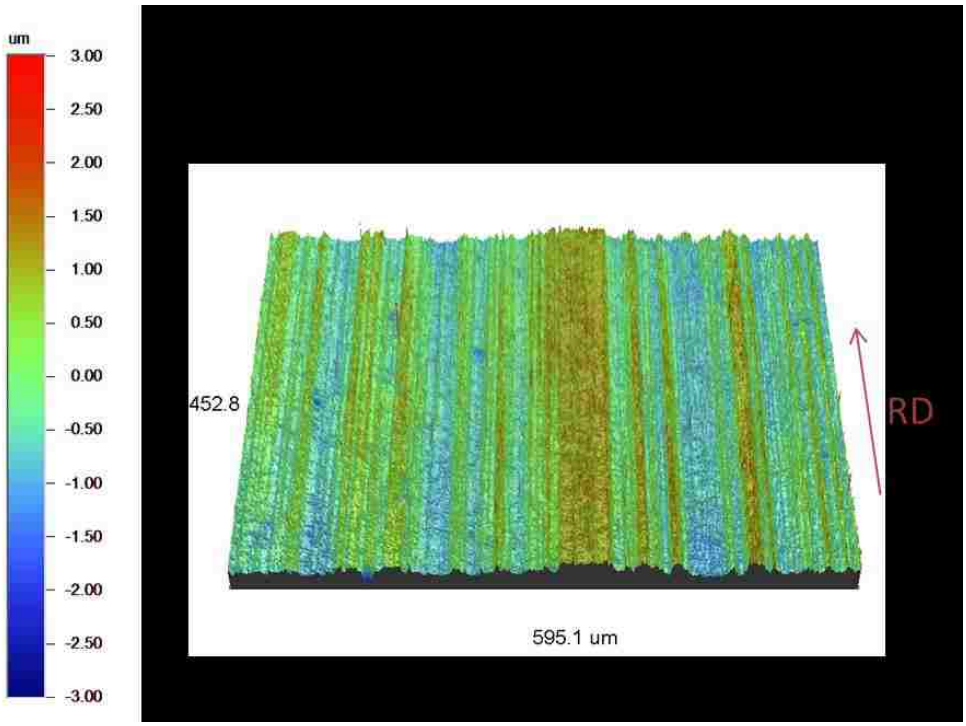

Figure 4-37: Surface profilometry image of Quiet Aluminum® with AA6061-T4 skin as-received. The image shows the inner surface of the sandwich, which faces the polymer layer. Rolling mill-finish pattern with clear distinction of the Rolling Direction (RD), showed with red arrow on the right side of the image.

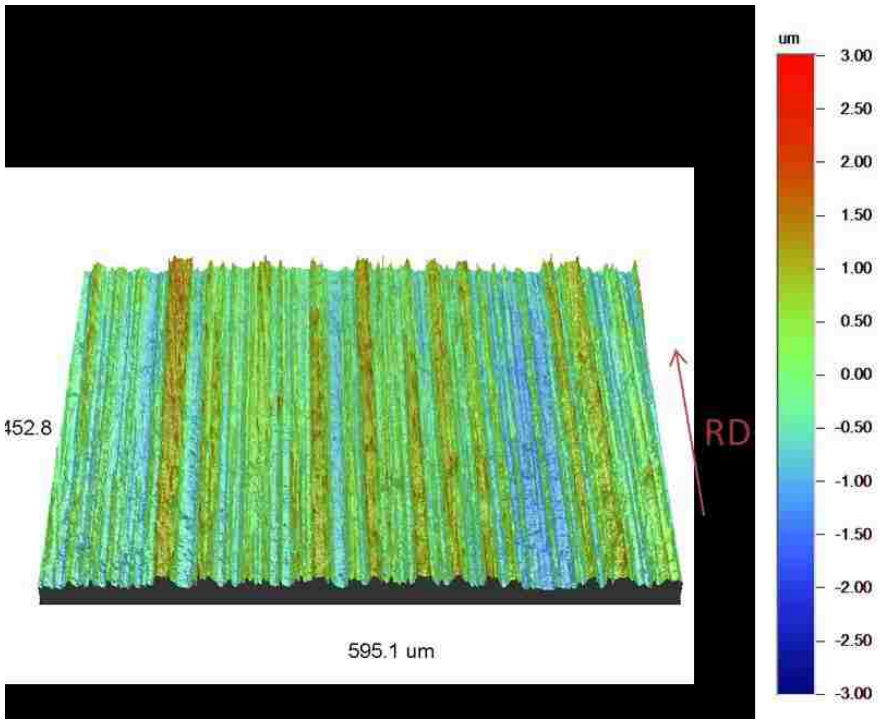

Figure 4-38: Surface profilometry image of Quiet Aluminum® with AA6061-T4 skin as-received. The image shows the outer surface of the sandwich. Rolling mill-finish pattern with clear distinction of the Rolling Direction (RD), showed with red arrow on the right side of the image.

4.6 SPR Joints Evaluation

In this section, the results obtained from lap-shear test and macro-graphic analysis on the SPR joints formed by the Quiet Aluminum® samples and the HSLA steel are presented following the "*SPR Joints Evaluation"* methodology section.

4.6.1 Macro-graphic Results on SPR joints

In order to obtain an optimal joint, multiple combinations of rivet dimensions and die shape were examined. First of all, a rivet with Ø $5.3\ mm$ and $5.5\ mm$ length was used to join the sandwich with 6061-T4 skin and the HSLA steel with a flat die. From the cross section image in Figure 4-39, it can be seen that the rivet kept its symmetry ($i_{sx} \cong i_{dx}$) and had more than enough interlocking with respect to the minimum requirement ($i_{dx} = 0.70\ mm$ whereas $i_{min} = 0.20\ mm$). Nevertheless, the joint could not be considered acceptable due low residual thickness of the bottom layer ($r_t = 0.19\ mm$ against the minimum requirement $r_t = 0.20\ mm$). This could lead to piercing of the HSLA steel, reason why the combination was considered unacceptable.

In order to increase the residual thickness, a shorter rivet was used to join the sandwich composite and the HSLA steel, but a die with a tip was used instead of a flat one. Figure 4-40 presents the joint cross section, highlighting that, with this configuration, the residual thickness of the bottom layer ($r_t = 0.36\ mm$) was above the minimum requirement. Nevertheless, the rivet partially lost its symmetry, with $i_{sx} = 0.83$ with respect to $i_{dx} = 0.72\ mm$. Moreover, on the right side of the button, the start of a crack was detected in the HSLA steel. Obviously, no cracks are admitted in any part of the joints, reason why also this configuration was considered unacceptable.

After the previous experiments, it was then decided to use a flat die and the shorter rivet diameter (Ø $5.3\ mm$ with $5.0\ mm$ length and $480\ HV$ (H4 code in the legend). With this rivet/die configuration, the joints showed acceptable macro-graphic parameters.

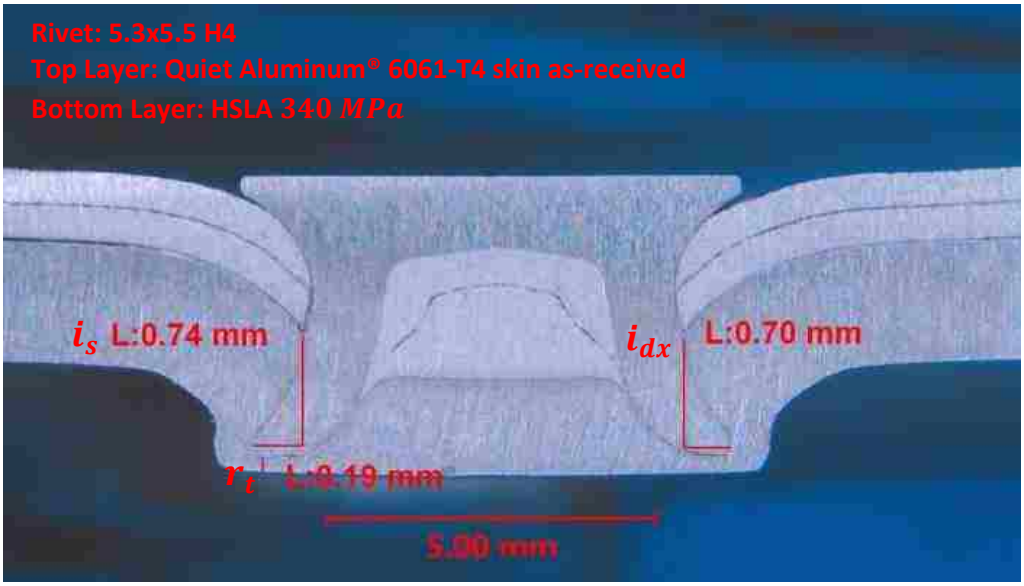

Figure 4-39: Microscope image on the cross section of the SPR joint with Quiet Aluminum® (6061-T4 skin as-received) and HSLA steel $340\ MPa$ using flat die and 5.3x5.5 H4 rivet. The measurements in red indicate the inspected parameters of the joint. Low residual thickness was detected ($r_t = 0.19\ mm$).

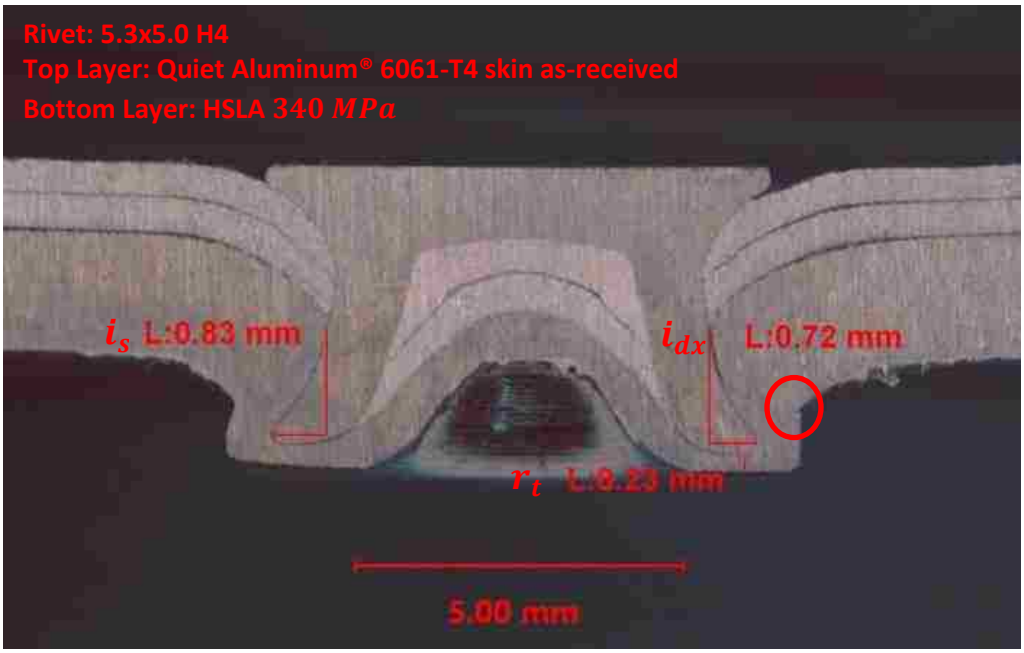

Figure 4-40 Microscope image on the cross section of the SPR joint with Quiet Aluminum® (6061-T4 skin as-received) and HSLA steel $340\ MPa$ using die with tip and 5.3x5.0 H4 rivet. The measurements in red indicate the inspected parameters of the joint. Starting of a crack detected on the right side of the button (red circle).

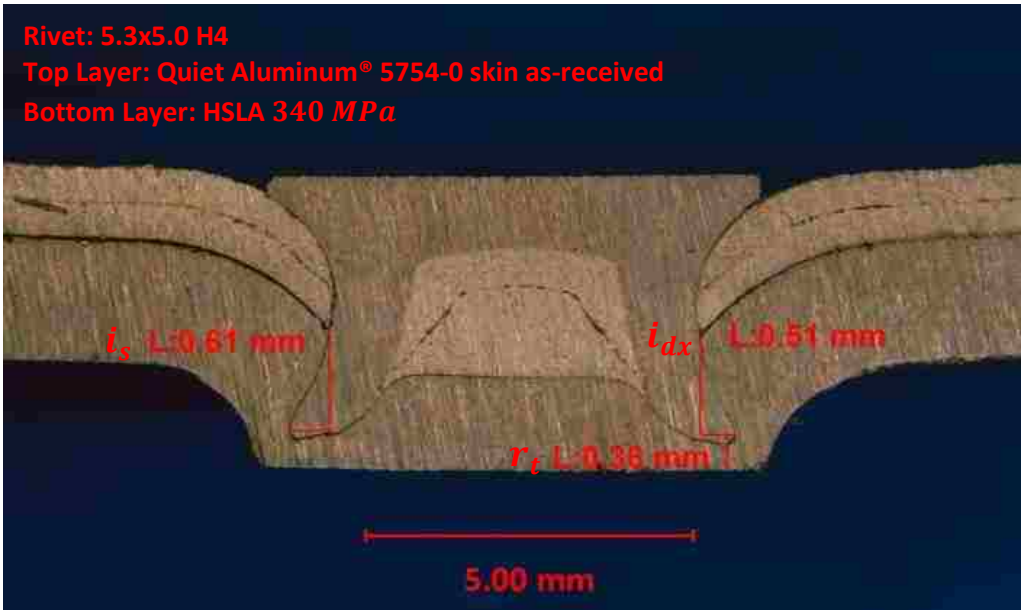

Figure 4-41: Microscope image on the cross section of the SPR joint with Quiet Aluminum® (5754-O skin as-received) and HSLA steel 340 MPa using flat die and 5.3x5.0 H4 rivet The measurements in red indicate the inspected parameters of the joint, which showed proper interlocking and sufficient symmetry.

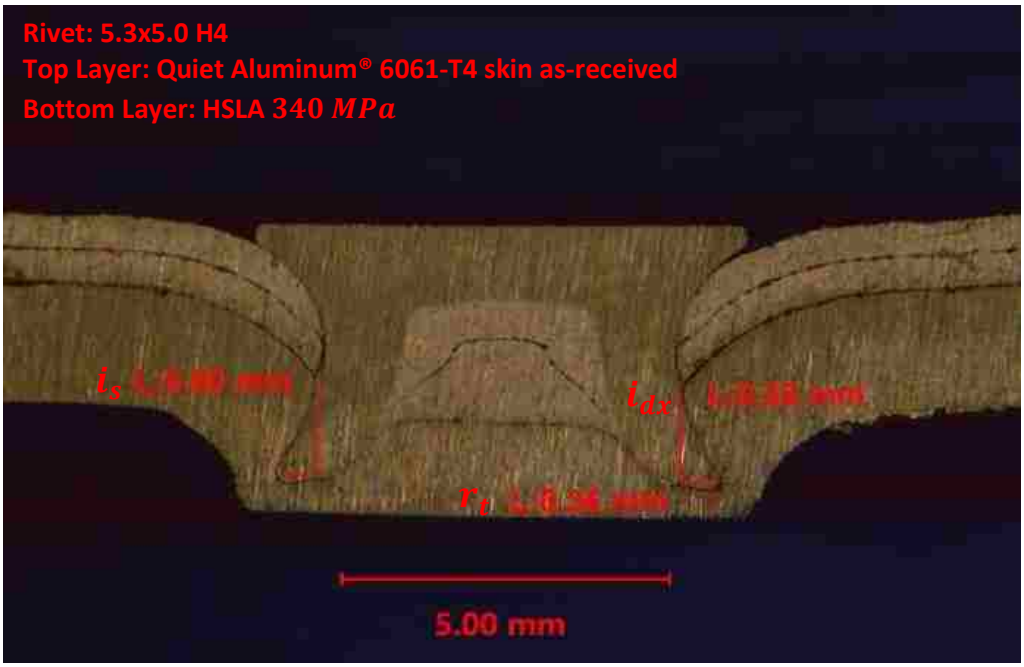

Figure 4-42: Microscope image on the cross section of the SPR joint with Quiet Aluminum® (6061-T4 skin as-received) and HSLA steel 340 MPa using flat die and 5.3x5.0 H4 rivet. The measurements in red indicate the inspected parameters of the joint, which showed proper interlocking and symmetry.

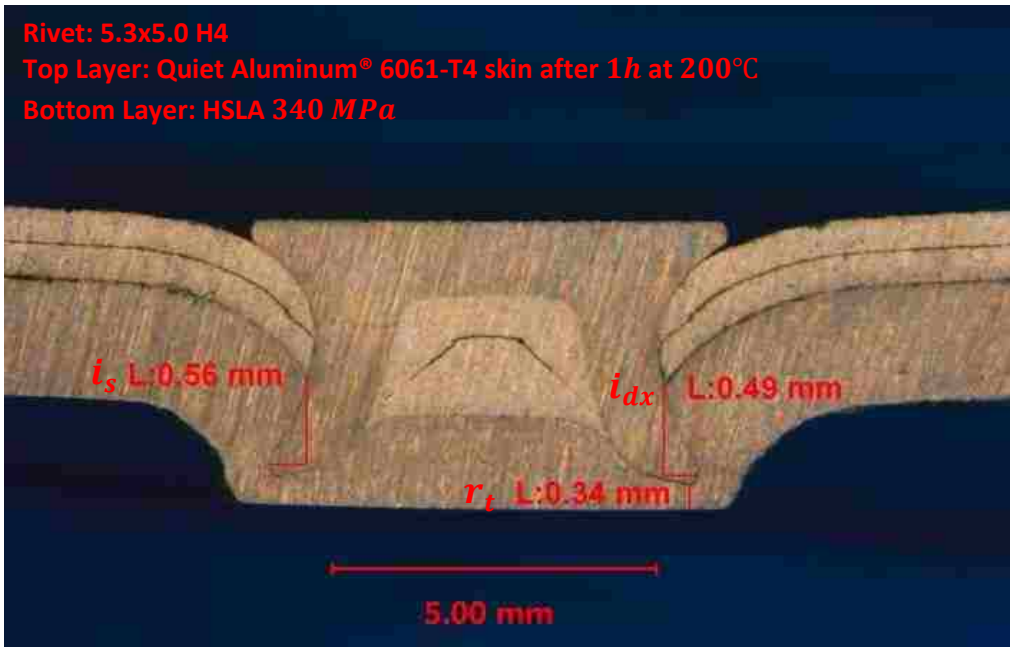

Figure 4-43: Microscope image on the cross section of the SPR joint with Quiet Aluminum® (6061-T4 skin after $1h\ at\ 200℃$) and HSLA steel $340\ MPa$ using flat die and 5.3x5.0 H4 rivet. The measurements in red indicate the inspected parameters of the joint, which showed proper interlocking and symmetry.

In fact, Figure 4-41, which represents the joint with the AA5754-O sandwich and the HSLA steel, shows enough residual thickness $r_t = 0.36\ mm$ and proper mechanical interlocking, even though the rivet exhibited not perfect symmetry ($i_{sx} = 0.61\ mm$ and $i_{dx} = 0.51\ mm$). Anyway, the shape of the deformed rivet could still be considered acceptable. Instead, Figure 4-42 and Figure 4-43 illustrate the cross sections of, respectively, the joints with the sandwich composites with 6061-T4 skin in the as received condition and after the hardening procedure. All the parameters of the two joints fulfilled the requirements, with symmetric interlocking and sufficient residual thickness. For these reasons, the joints with flat die, $\emptyset\ 5.3\ mm$ and $5.0\ mm$ rivet, Quiet Aluminum® on the top of the $340\ MPa$ HSLA steel alloy were considered macro-graphically acceptable and ready to be examined with head flushness measurements and lap -shear test (Table 4-9 summarizes all parameters measured).

As mentioned in "*SPR Joints*" section, the rivet head position with respect to the upper sheet was measured with a digital dial gauge. Ten specimens for every joint combination were examined (Table 4-10). The measurements showed low standard deviations and negligible differences for the entire set of samples. Moreover, the values are consistently close to zero,

leading to "even" rivet head position [40]. This means that the head rivet positioning control method used by Stanley Engineered Fastening for SPR joints was accurate and repeatable for all specimens tested.

Table 4-9: Macro-graphic measurements on SPR joints between Quiet Aluminum® samples and HSLA steel. The residual thickness r_t of the first joint combination was considered insufficient (marked in red).

Top Layer	Bottom Layer	Rivet	Die	i_{sx} [mm]	i_{dx}[mm]	r_t[mm]
AA6061-T4 sandwich as-received	HSLA steel	Ø5.3 mm x 5.5 mm $H4$	Flat die	0.74	0.70	0.19
AA6061-T4 sandwich as-received	HSLA steel	Ø5.3 mm x 5.0 mm $H4$	Die with tip	0.83	0.72	0.23
AA5754-O sandwich as-received	HSLA steel	Ø5.3 mm x 5.0 mm $H4$	Flat die	0.61	0.51	0.36
AA6061-T4 sandwich as-received	HSLA steel	Ø5.3 mm x 5.0 mm $H4$	Flat die	0.60	0.58	0.36
AA6061-T4 sandwich After $1h$ at 200℃	HSLA steel	Ø5.3 mm x 5.0 mm $H4$	Flat die	0.56	0.49	0.34

Table 4-10: Head flushness measurements on SPR joints with Quiet Aluminum® samples and HSLA 340 MPa steel. The measurements showed good head rivet positioning control with respect to the upper sheet.

SPR joints	AA5754-O sandwich/HSLA steel	AA6061-T4 sandwich/HSLA steel	AA6061-T4 sandwich after 1 h at 200℃/HSLA steel
Specimen number #	Head height $[mm]$		
1	-0.12	-0.10	-0.15
2	-0.12	-0.09	-0.13
3	-0.12	-0.12	-0.12
4	-0.11	-0.13	-0.15
5	-0.14	-0.13	-0.13
6	-0.10	-0.12	-0.11
7	-0.11	-0.10	-0.11
8	-0.12	-0.09	-0.12
9	-0.12	-0.11	-0.123
10	-0.14	-0.12	-0.13
$AVG \pm SD$	-0.12 ± 0.01	-0.11 ± 0.01	-0.13 ± 0.01

4.6.2 Lap Shear Test with SPR Joints

Referring to the "*Lap Shear Test on SPR Joints*" section, ten specimens for each joint configuration were pulled. The force-displacement graphs retrieved from the experiments are presented in Figure 4-44, Figure 4-45 and Figure 4-46 and refer, respectively, to the joints with: the sandwich with 5754-O skin, the sandwich with 6061-T4 skin and the sandwich with 6061-T4 skin after $1\ h$ at $200℃$ as upper layers, whereas the HSLA steel was the bottom one. Hence the maximum forces sustained by the joints are reported in Table 4-11.

All the specimens presented the same trend: the force sustained by the joint increases steeply with the initial displacement of the crosshead till reaching the maximum, then the force decreases smoothly till reaching failure of the SPR joint. In Figure 4-45, specimens 5 and 8 behaved differently due to slippage from the grips. Anyway, the curves and the peak forces were considered valid since they were within the values recorded in the other specimens. In fact, the two curves are just slightly shifted to the right.

The detachment of the rivets occurred due to failure of the Quiet Aluminum® samples (Figure 4-47, Figure 4-48 and Figure 4-49) for every joint combination. Indeed, as explained in the "*Self - Piercing Riveting" section,* the low yield stress of the upper sheet eases the pull-out of the rivet at lower loads [41]. Consequently, the joints were considered valid. In accordance with the joint failure, the maximum force registered increases with the increasing yield strength of the material. In fact, the joint with AA5754-O sandwich showed the lowest peak load, $F_{peak} = 1.95\ kN$, whereas the joint formed by the sandwich with 6061-T4 skin after the hardening procedure, which exhibited the highest yield stress in tensile testing, presented the highest peak force, $F_{peak} = 2.43\ kN$.

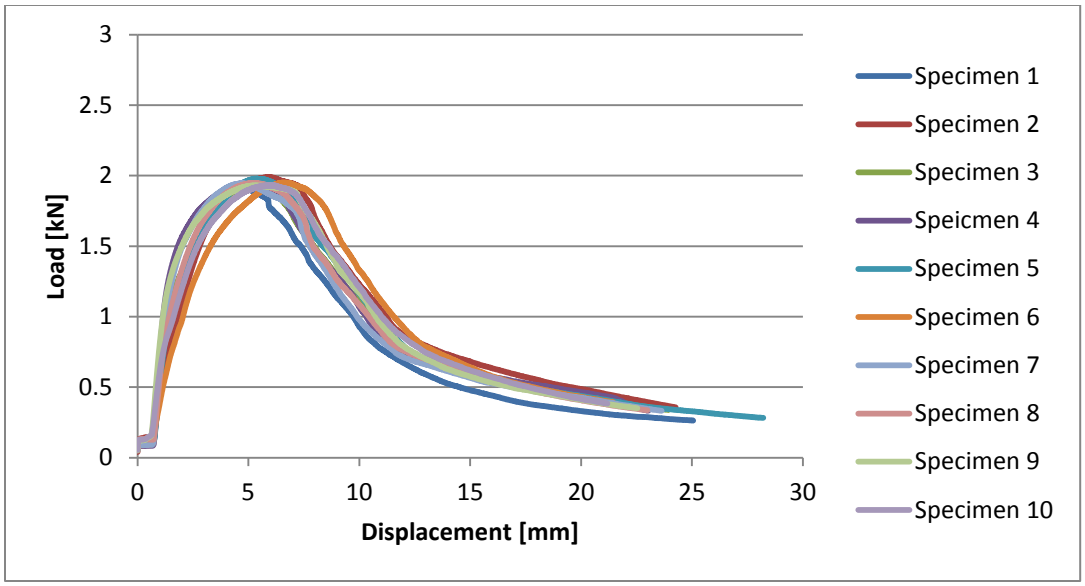

Figure 4-44: Load-displacement curve from lap-shear test with SPR joints formed by Quiet Aluminum® with 5754-O skin (as-received) and HSLA steel. Every curve presented the same trend with similar maximum sustained forces ($F_{peak} = 1.95 \pm 0.03\ kN$).

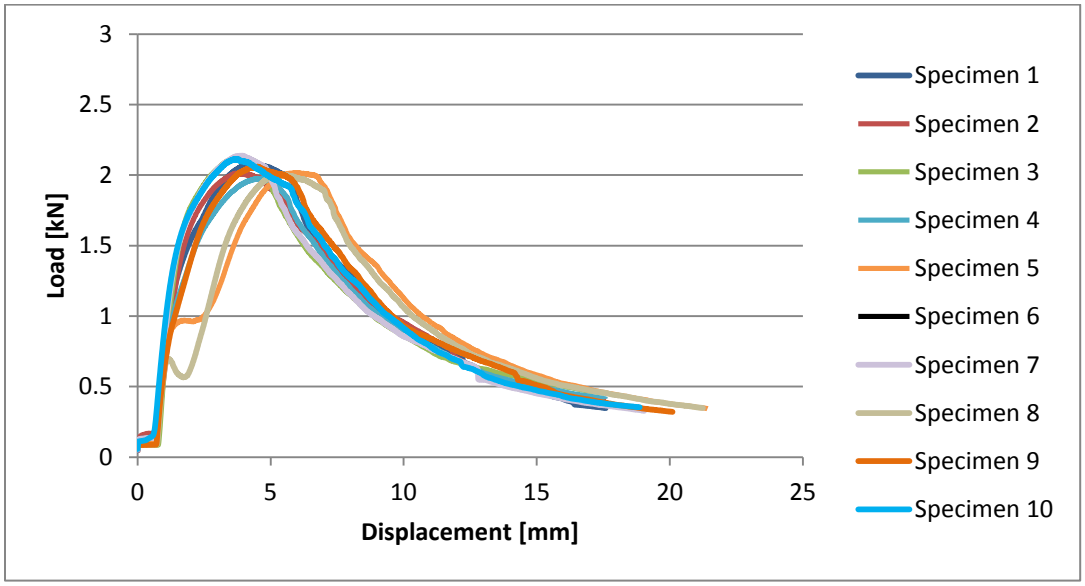

Figure 4-45: Load-displacement curve from lap-shear test with SPR joints formed by Quiet Aluminum® with 6061-T4 skin (as-received) and HSLA steel. Every curve presented the same trend with similar maximum sustained forces ($F_{peak} = 2.05 \pm 0.06\ kN$). Note that slippage occurred with specimen 5 and 8 (orange and grey lines).

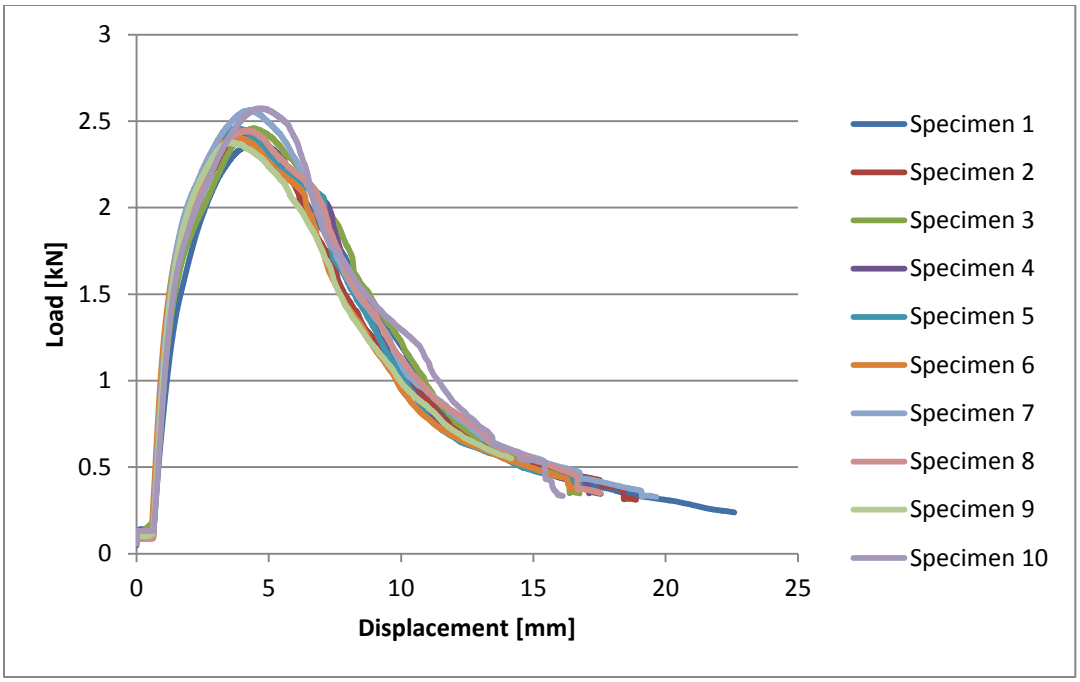

Figure 4-46: Load-displacement curve from lap-shear test with SPR joints formed by Quiet Aluminum® with 6061-T4 skin (after $1\ h$ at $200℃$) and HSLA steel. All the curves presented the same trend with similar maximum sustained forces ($F_{peak} = 2.43 \pm 0.03\ kN$).

Table 4-11: Peak values recorded from Lap Shear test on SPR joints between Quiet Aluminum® and HSLA steel. The maximum force sustained by the joint increased with the increasing yield strength of the Quiet Aluminum® samples used as top layer.

SPR joints	AA5754-O sandwich/HSLA steel	AA6061-T4 sandwich/HSLA steel	AA6061-T4 sandwich after $1\ h$ at $200℃$/HSLA steel
Specimen number #	Peak Force F_{peak} [kN]		
1	1.92	2.07	2.38
2	1.99	2.01	2.41
3	1.92	2.13	2.46
4	1.92	1.98	2.42
5	1.98	2.02	2.46
6	1.95	2.02	2.40
7	1.95	2.14	2.56
8	1.95	2.01	2.45
9	1.93	2.06	2.38
10	1.93	2.12	2.58
$AVG \pm SD$	1.95 ± 0.03	2.05 ± 0.06	2.43 ± 0.03

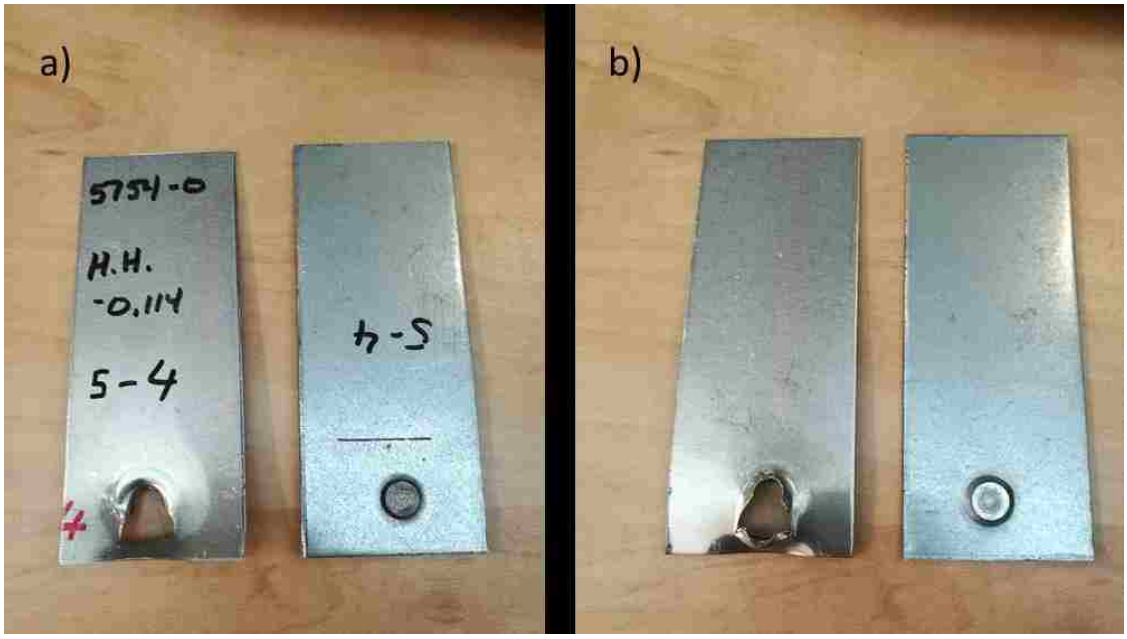

Figure 4-47: SPR joints after lap-shear test (Quiet Aluminum® with 5754-O skin in as-received condition and HSLA steel). a) Deformed upper sheet (sandwich) and detached rivet head. b) Back side of the deformed upper sheet (sandwich) and button on the HSLA steel. Severe deformation of the upper sheet was noticed in every specimen tested.

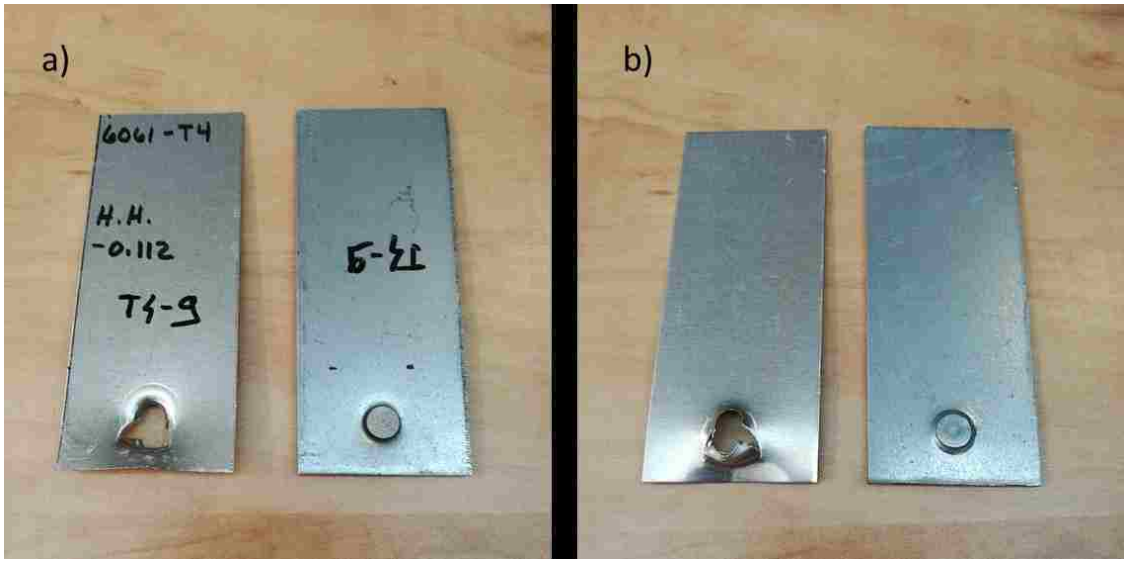

Figure 4-48: SPR joints after Lap Shear test (Quiet Aluminum® with 6061-T4-O skin in as-received condition and HSLA steel). a) Deformed upper sheet (sandwich) and detached rivet head. b) Back side of the deformed upper sheet (sandwich) and button on the HSLA steel. Severe deformation of the upper sheet was noticed in every specimen tested.

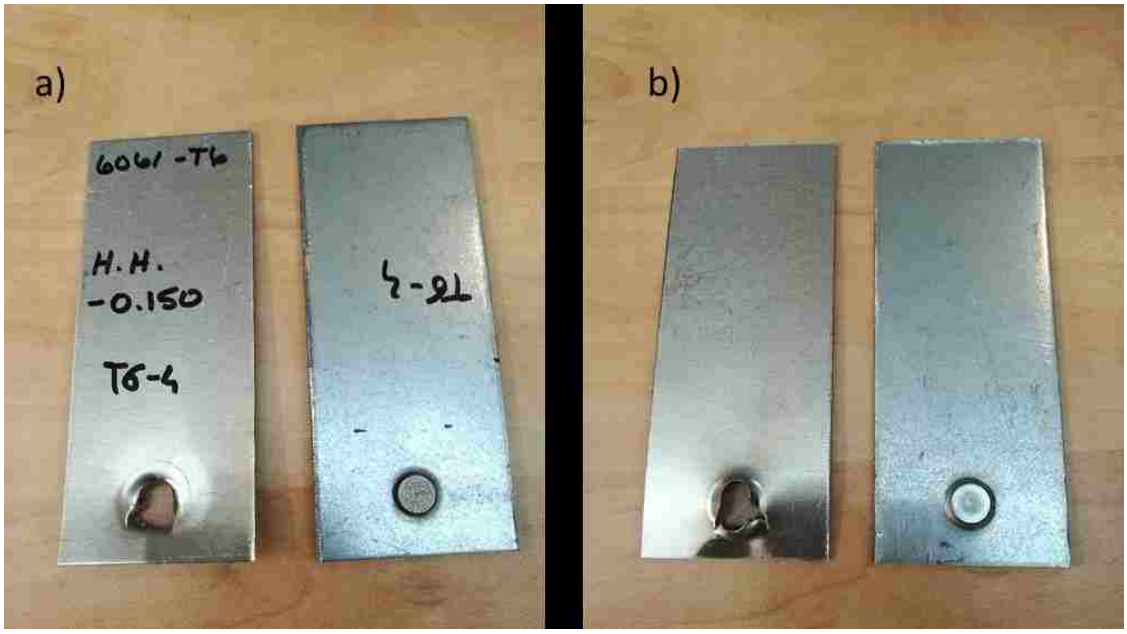

Figure 4-49: SPR joints after Lap Shear test (Quiet Aluminum® with 6061-T4 skin after $1\ h$ at $200℃$ and HSLA steel). a) Deformed upper sheet (sandwich) and detached rivet head. b) Back side of the deformed upper sheet (sandwich) and button on the HSLA steel. Severe deformation of the upper sheet was noticed in every specimen tested.

5. CONCLUSIONS AND RECOMMENDATIONS

5.1 Conclusions

Sandwich composites are raising interests in the automotive sector due to lightweight and noise attenuation. Moreover, the possible applications of these materials are really wide open; indeed they can replace every panel of the vehicle with non-structural loads. Since the sound-deadening characteristics of Quiet Aluminum® were already tested by the manufacturer, the comprehensive testing performed in the current study focused on determining the mechanical properties of Quiet Aluminum® necessary to replace the monolithic panels in the vehicle. The two sandwich composites received were examined through T-Peel test, roughness measurements, tensile test with different treatments, hardness test on the core section of the aluminum skin and, finally, an evaluation of Self-Piercing Riveting technique. The abovementioned tests contributed to finding, respectively, the following:

- The samples tested revealed superior adhesion strength concerning FCA requirements ($\alpha_s = 33.4 \frac{N}{cm}$ for the samples with 6061-T4 skin and $\alpha_s = 25.6 \frac{N}{cm}$ for samples with 5754-O skin against a minimum range required of $10 - 15 \frac{N}{cm}$) even after the paint-bake simulation, with no changes in peel resistance, as well as in its characteristic adhesive failure mode
- The heat treated samples ($1\ h$ at $200°C$) presented a steep drop in peel resistance ($\alpha_s = 11.8 \frac{N}{cm}$) due to damaged polymer. However, the adhesion strength was still within the minimum range required
- Roughness measurements confirmed typical rolling mill-finish pattern with clear distinction of the rolling direction for both aluminum alloys as well as for their inner (in contact with the polymer core) and outer (external and so visible side) surfaces. The samples exhibited surface roughness R_a range of $0.49 - 0.56\ \mu m$
- SPR joining technique was considered successful since the joints (Quiet Aluminum® samples of $1.06\ mm$ thickness, with structural HSLA steel, $1.8\ mm$ thickness and $340\ MPa$ minimum yield strength) examined with lap-shear test and macro-graphic measurements revealed good mechanical strength, increasing with the increasing yield

stress of the sandwich composites and acceptable macro-graphic results regarding FCA requirements

- Expected tensile stress-strain curves and related parameters, even after the different treatments were applied to the sandwich composite, confirmed the negligible contribution of the polymer core
- The paint-bake cycle did not affect the tensile properties of the sandwich composite with AA6061-T4 skin, whereas the hardening procedure revealed very high hardness, yield stress and UTS, but low ductility ($HV = 92.2, R_{p0.2} = 173\ MPa, UTS = 245\ MPa$ and elongation at break equal to 9%).
- The 6061-T4 sandwich was found to be more performant for its higher mechanical properties such as tensile and adhesion strength, but also for its uniform yielding, which is preferable to the discontinuous yielding of the 5754-O sandwich for aesthetic reasons.

5.2 Recommendations

Tests on the influence of temperature and exposure time on precipitation hardening of the aluminum 6061-T4 as well as the resistance of the viscoelastic core to high temperatures could be analyzed to find an optimal tradeoff. Further formability experiments are suggested, such as construction of FLD diagrams and Erichsen Cupping test. Then tests on the monolithic aluminum alloys used in the sandwich composites should be carried out to obtain more precise comparisons. Moreover, tensile experiments with different orientations with respect to the rolling direction could enlarge the data resulting from this work. Investigations on the engineered viscoelastic core on vibrations and noise could be an interesting proposal. Finally, another joining technique evaluation, such as welding or adhesive bonding could be performed to find an optimal solution to join the sandwich composites with the rest of the body.

BIBLIOGRAPHY

[1] D. Kodjak, "Policies to Reduce Fuel Consumption, Air Pollution and Carbon Emissions from Vehicles in G20 Nations," The International Council on Clean Transportation, 2015.

[2] A. Bandivadekar, K. Bodek, L. Cheah, C. Evans, T. Groode, J. Heywood, E. Kasseris, M. Kromer and M. Weiss, "On the road on 2035," Laboratory for Energy and the Environment Massachusetts Institute of Technology, 2008.

[3] A. J. G. Isenstadt, "Lightweighting Technology Developments," Interntional Council on Clean Transportation, 2017.

[4] D. Rosato, "NPE 2015 end-use regulatory impact review: Automotive lightweighting," 2015. [Online]. Available: http://exclusive.multibriefs.com/content/npe-2015-end-use-regulatory-impact-review-automotive-lightweighting/engineering. [Accessed 27 June 2017].

[5] L. Morello, L. R. Rossini, G. Pia and A. Tonoli, The Automotive Body, Volume II: System Design, Springer, 2011.

[6] "Zone Enterprises," [Online]. Available: http://www.zoneenterprisesusa.com/products-zone-butyl-and-sealant.html . [Accessed 10 05 2017].

[7] Tomasz Czarnecki, economic care technologies, "Continuous Production of Thermoplastic Honeycomb Sandwich Components for Automotive Interiors. Low weight-Low Cost Technology," in *Society of Plastic Engineers*, Novi, 2016.

[8] Material Sciences Corporation.

[9] F. Campbell, Lightweight Materials - Understanding the Basics, ASM International, 2012.

[10] M. F. Ashby and D. R. H. Jones, "Light Alloys," in *Engineering Materials 2 - An Introduction to Microstructures and Processing (4th Edition)*, Elsevier Ltd, 2013, pp. 100-111.

[11] B. Milkereit, L. Giersberg, O. Kessler and C. Schick, "Isothermal Time-Temperature-

Precipitation Diagram for an Aluminum Alloy 6005A by In Situ DSC Experiments," *Materials,* vol. 7, pp. 2631-2649, 2014.

[12] ASM International, "ASM International Handbook Committee," *ASM Handbook,* Vols. Volume 04 - Heat Treating, 1991.

[13] K. Siegert and S. Wagner, "Formability Characteristics of Aluminum Sheet," Institut für Umformtechnik, Universität Stuttgart, TALAT Lecture European Aluminium Association, Brussel, 1994.

[14] J. Davis, Corrosion of Aluminum Alloys, ASM International., 1993.

[15] "Make It From Database," [Online]. Available: http://www.makeitfrom.com/glossary/Alloy-Composition. [Accessed 5 06 2017].

[16] Fiat Chrysler Automobiles.

[17] F. Campbell, Structural Composite Materials, ASM International, 2010.

[18] D. B. M. a. S. L. Donaldson, "Introduction to composites," *ASM Handbook,* vol. 21, pp. 3-17, 2008 (6th printing).

[19] l.-K. Kim and T.-X. Yu, "Forming and failure behaviour of coated, laminated and sandwiched sheet metals: a review," *Journal of Materials Processing Technology,* vol. 63, pp. 33-42, 1997.

[20] S. Mousa and G.-Y. Kim, "Experimental Study on Warm Roll Bonding of Metal/Polymer/Metal Multilayer Composites," *Journal of Materials Processing Technology,* vol. 222, pp. 84-90, 2015.

[21] S. Mousa and G.-Y. Kim, "A Direct Adhesion Metal-Polymer-Metal Sandwich Composite by Warm Roll Bonding," *Journal of Materials Processing Technology,* vol. 239, p. 133–139, 2017.

[22] G.-J. Liu and W. Xue, "Formability of AA5052/polyethylene/AA5052 sandwich sheets,"

Trans. Nonferrous Met. Soc., vol. 23, pp. 964-969, 2013.

[23] K. S. Shin, K. J. Kim, S.-W.Choi and M. H. Rhee, "Mechanical Properties of Aluminum/Polypropylene/Aluminum Sandwich Sheets," *Metals and Materials,* vol. 5, pp. 613-618, 1999.

[24] H. Palkowski, O. Sokolova and A. Corrado, "Joining Hybrid Materials," in *Enciclopedia of Automotive Engineering*, John Wiley & Sons, Ltd., 2015.

[25] A. Carrado, J. Faerber, S. Niemeyer, G. Ziegmann and H. Palkowski, "Metal/polymer/metal hybrid systems: Towards potential formability applications," *Composite Structures,* vol. 93, p. 715–721, 2011.

[26] K. Kim, D. Kim, S. Choi, K. Chung, K. Shin, F. Barlat, K. Oh and J. Youn, "Formability of AA5182/polypropylene/AA5182 sandwich sheets," *Journal of Materials Processing Technology,* vol. 139, pp. 1-7, 2003.

[27] G. Fourche, "An overview of the basic aspects of polymer adhesion. Part I: Fundamentals," *Polym. Eng.Sci.,* vol. 35, pp. 957-967, 1995.

[28] Zisman, Autoadhesion, New York: Wiley, 1963.

[29] A. Baldan, "Adhesion phenomena in bonded joints," *International Journal of Adhesion & Adhesives,* vol. 38, pp. 95-116, 2012.

[30] F. Awaja, M. Gilbert, G. Kelly, B. Fox and P. Pigram, "Adhesion of polymers," *Progress in Polymer Science,* vol. 34, p. 948–968, 2009.

[31] S. Voyutski, Autohesion and Adhesion of High Polymers, Wiley, 1963.

[32] Y. Shuo, G. Lan and R. F. Gibson, "Nondestructive detection of weak joints in adhesively bonded composite structures," *Composite Structures,* vol. 51, pp. 63-71, 2001.

[33] J. Bikerman, "The probability of rupture in adhesion," *Polymer Mechanics,* vol. 9, no. 3, p. 457–459, 1973.

[34] J. Bikerman, The Science of Adhesive Joints, New York: Academic Press, 1961.

[35] A. Baldan, "Adhesively-bonded joints and repairs in metallic alloys, polymers and composite materials: Adhesives, adhesion theories and surface pretreatmen," *Journal of Materials Science,* vol. 391, no. 1, pp. 1-49, 2004.

[36] "Adhesive and Sealant Council," [Online]. Available: http://www.adhesives.org/adhesives-sealants/science-of-adhesion/adhesion-cohesion. [Accessed 06 20 2017].

[37] R. W. Messler, Joining of materials and structures from pragmatic process to enabling technology, Elsevier, 2004.

[38] J. Sarfgianis and J. Suhr, "Effect of core thickness on wave number and damping properties in sandwich composites," *Composites Science and Technology,* vol. 72, no. 6, pp. 724-730, 2012.

[39] D. Hara and G. O. Özgen, "Investigation of weight reduction of automotive body structures with the use of sandwich materials," *Elsevier, 6th Transport Research Arena,* pp. 18-21, 2016.

[40] E. Atzeni, R. Ippolito and L. Settineri, "Experimental and Numerical Investigation on Self-Piercing Riveting," *Transactions of NAMRI/SME, Polythechnic of Turin,* vol. 33, pp. 477-484, 2005.

[41] E. Atzeni, R. Ippolito and L.Settineri, "Self-Piercing Riveting for Metal-Polymer Joints," *International Journal of Material Forming,* vol. 3, pp. 995-998, 2010.

[42] E. Atzeni, R. Ippolito and L. Settineri, "Experimental and numerical appraisal of self-piercing riveting," *CIRP Annals - Manufacturing Technology,* vol. 58, p. 17–20, 2009.

[43] "ASTM E384-11, Standard Test Method for Microindentation Hardness of Materials," ASTM International, West Conshohocken, PA, 2011.

[44] MTS®, "MTS Criterion® Series 40 Electromechanical Universal Test Systems," [Online]. Available: https://www.mts.com/cs/groups/public/documents/library/mts_006225.pdf.

[Accessed 10 07 2017].

[45] "ASTM E8/E8M-16a, Standard Test Methods for Tension Testing of Metallic Materials," ASTM Internationa, West Conshohocken, PA, 2016.

[46] "ASTM E646-16, Standard Test Method for Tensile Strain-Hardening Exponents (n -Values) of Metallic Sheet Materials," ASTM International, West Conshohocken, 2016.

[47] "ASTM E517-00 (Reapproved 2010), Standard Test Method for Plastic Strain Ratio r for Sheet Metal," ASTM International, West Conshohocken, PA, 2010.

[48] "ASTM D1876-08 (Reapproved 2015), Standard Test Method for Peel Resistance of Adhesives (T-Peel Test)," ASTM Internationa, West Conshohocken, 2015.

[49] Stanley Engineered Fastening.

[50] J. Sun, S. Ying and M. Lu, "Optimize aluminum's surface roughness in rolling lubrication process," *Industrial Lubrication and Tribology,* vol. 65, no. 3, pp. 175-180, 2013.

[51] "Introduction to Roughness," [Online]. Available: http://www.keyence.com/ss/products/microscope/roughness/index.jsp. [Accessed 04 07 2017].

[52] "Vickers Hardness Test," [Online]. Available: https://en.wikipedia.org/wiki/Vickers hardness_test. [Accessed 10 05 2017].

[53] "BS EN ISO 20482, Metallic materials – sheets and strips – Erichsen cupping test," The British Standard Institution, 2013.

[54] Zisman, "Influence of Constitution on Adhesion," *Ind. Eng. Chem.,* vol. 55, no. 19, 1963.

[55] ASM International, "Al (Aluminum) Binary Alloy Phase Diagrams, Alloy Phase Diagrams.," *ASM Handbook,* vol. 3, p. 113–139, 2016.

[56] D. S. W. M. N. H. Halim, "The Portevin-Le Chatelier (PLC) effect and shear band formation in

an AA5754 alloy," *Acta Materialia,* vol. 55, p. 4151–4160, 2007.

[57] S. D. Mesarovic, "Dynamic Strain Aging and Plastic Instabilities," *J. Mech. Phys. Solids,* vol. 43, pp. 671-700, 1995.

VITA AUCTORIS

NAME:	Federico Ferrari
PLACE OF BIRTH:	Biella, Italy
YEAR OF BIRTH:	1993
EDUCATION:	University of Windsor, International M.A.Sc. in Automotive Engineering, Windsor, ON, Canada, 2017
	Politecnico di Torino, M.A.Sc. in Automotive Engineering, Turin, Italy, 2017
	Politecnico di Torino, B.Sc. in Automotive Engineering, Turin, Italy, 2015